

## General Disclaimer

### One or more of the Following Statements may affect this Document

- This document has been reproduced from the best copy furnished by the organizational source. It is being released in the interest of making available as much information as possible.
- This document may contain data, which exceeds the sheet parameters. It was furnished in this condition by the organizational source and is the best copy available.
- This document may contain tone-on-tone or color graphs, charts and/or pictures, which have been reproduced in black and white.
- This document is paginated as submitted by the original source.
- Portions of this document are not fully legible due to the historical nature of some of the material. However, it is the best reproduction available from the original submission.

NASA CR-170566

Reports of the Department of Geodetic Science and Surveying

Report No. 338

(NASA-CR-170566) ON THE GEODETIC APPLICATIONS OF SIMULTANEOUS RANGE-DIFFERENCING TO LAGEOS Final Report (Ohio State Univ., Columbus.) 229 p  
HC A11/MF A01 CSCI 08B G3/43 13600 N83-33287 Unclass

# ON THE GEODETIC APPLICATIONS OF SIMULTANEOUS RANGE-DIFFERENCING TO LAGEOS

by  
Erricos C. Pavlis

Prepared for  
National Aeronautics and Space Administration  
Goddard Space Flight Center  
Greenbelt, Maryland 20770

Final Report  
Research Contract NAS5-25888  
OSURF Project No. 712407

OSU

The Ohio State University  
Research Foundation  
Columbus, Ohio 43212

December, 1982





Reports of the Department of Geodetic Science and Surveying

Report No. 338

ON THE GEODETIC APPLICATIONS OF SIMULTANEOUS RANGE-  
DIFFERENCING TO LAGEOS

by

Erricos C. Pavlis

Prepared for

National Aeronautics and Space Administration  
Goddard Space Flight Center  
Greenbelt, Maryland 20770

Final Report  
Research Contract NAS5-25888  
OSURF Project No. 712407

The Ohio State University  
Research Foundation  
Columbus, Ohio 43212

December, 1982

## DEDICATION

To Despina,  
Daphne, and  
Constantine

## PREFACE

The Principal Investigator of this project is Professor Ivan I. Mueller, Department of Geodetic Science and Surveying, The Ohio State University. The Science Advisor is Dr. David E. Smith (Code 921, Geodynamics Branch), the Technical Officer is Mr. C. Stephanides (Code 942), and the Contracting Officer is Lillian E. Walker (Code 289), all of NASA/ Goddard Space Flight Center, Greenbelt, Maryland 29771.

This report was originally presented as a dissertation to the Graduate School of The Ohio State University in partial fulfillment of the requirements for the PhD degree.

## ABSTRACT

This investigation studies the possibility of improving the accuracy of geodetic results by use of simultaneously observed ranges to Lageos, in a differencing mode, from pairs of stations. Despite their complexity and expensive computational requirements, orbital models are still not accurate enough to achieve geodetic parameter accuracies comparable to those of laser measurements. Parameters of interest here are the baseline lengths and the coordinates of the pole. Simulation tests show that model errors can be effectively minimized by simultaneous range-differencing (SRD) for a rather broad class of network-satellite pass configurations. To generate the required quasi-simultaneous range events, we compare the methods of least squares approximation with monomials and Chebyshev polynomials and the cubic spline interpolation. The latter seems preferable in the case of uniform and dense sets of data.

Analysis of three types of orbital biases (radial, along- and across-track) shows that radial biases are the ones most efficiently minimized in the SRC mode. The degree to which the other two can be minimized depends on the type of parameters under estimation and the geometry of the problem. Sensitivity analyses of the SRD observation show that for baseline length estimations the most useful data are those collected in a direction parallel to the baseline and at a low elevation. Estimating individual baseline lengths with respect to an assumed but fixed orbit not only decreases the cost, but it further reduces the effects of model biases on the results as opposed to a network solution. Enforcing the simultaneity constraint ensures that the results are also free of possible biases introduced by inconsistent coordinate systems in which independent station determinations refer. Analogous results and conclusions are obtained for the estimates of the coordinates of the pole.

## ACKNOWLEDGMENTS

It is undoubtedly true that it takes hard work to carry out a project such as the one reported herein. The personal labor, however, would never be enough, and it is hard to imagine a successful completion without the guidance, help and encouragement of several people.

Of all most important is the support and patience of my family. Their continuous sacrifices during these years leave me no choice as to my next most important lifelong project: a full-time husband and father.

Of equal importance was the guidance, help, support and friendship of my mentor, Professor Ivan I. Mueller. Working with him has been one of the most educating and pleasing experiences. To him and to Professors Richard H. Rapp and D.P. Hajela, a special thanks for pointing out the weak points of the original manuscript rather than praising the good ones.

During my studies at Ohio State University I have had the luck of meeting and befriending a number of people from around the world. Their friendship and constructive criticism have helped make my stay here more enjoyable--above all, the esteemed members of the "500 Club": Dr. Kostas Katsambalos, Dr. Christopher Jekeli, Dr. Oscar Colombo and Dr. John Hannah. The long and often heated discussions with Dr. Yehuda Bock and Mr. Zhu Sheng-Yuan will always be remembered for their contribution in clarifying several issues on a variety of topics. Discussions on time with Dr. John McK. Luck have been most interesting and most timely! The help of Dr. Lenny A. Krieg in acquainting myself with the Ohio State computer facility is gratefully acknowledged.



My thanks go to the NASA/GSFC scientists Mr. Ron Kolenkiewicz, Ms. Barbara Putney, and Mr. Chris Stephanides for their support and their comments, and special thanks to JPL scientists Dr. E. Myles Standish, Jr., Dr. Theodore Moyer, Dr. Fred Krogh, and Dr. Henry Fliegel for their prompt responses to all my requests for data and information.

Thanks go also to NASA/Goddard Space Flight Center for the opportunity to work on such an interesting and educational project and for providing extensive financial support through Contract No. NAS5-25888. The financial support provided by The Ohio State University as a Graduate Teaching Associate is gratefully appreciated and so is the computer support of the Instruction and Research Computer Center. Acknowledged also is the financial support of the Wild-Heerbrugg Geodetic Fellowship (1980).

Last but not the least, my thanks to Mr. Irene Tesfai for her excellent workmanship in typing and editing the final form of this report.

## TABLE OF CONTENTS

	Page
DEDICATION.....	ii
PREFACE .....	iii
ABSTRACT .....	iv
ACKNOWLEDGMENTS .....	v
LIST OF FIGURES.....	xii
LIST OF ABBREVIATIONS.....	xiv
 Chapter	
1. INTRODUCTION.....	1
1.1 From Time Interval Measurement to Range Inference.....	1
1.2 Systems Accuracy; Some General Remarks.....	2
1.3 Scope and Philosophy of the Investigation.....	3
1.4 Outline of the Proposed Simultaneous Laser Range- Difference (SRD) Mode.....	5
2. THEORETICAL BACKGROUND.....	12
2.1 Reference Systems and Frames.....	12
2.2 The Lageos Orbital Model.....	17
2.2.1 Orbit Determination with the Method of Special Perturbations.....	20
2.2.2 Gravitational Acceleration from N Point Masses.....	23
2.2.3 Gravitational Acceleration from Terrestrial Nonsphericity.....	27
2.2.4 Solar Radiation Pressure Acceleration.....	30
2.2.5 Tidal Acceleration.....	34
2.2.6 Lageos Empirical Along-Track Acceleration.....	36
3. THE OBSERVABLE.....	39
3.1 Hardware Components.....	39

3.1.1	Laser Ranging Instrumentation.....	39
3.1.2	Laser Geodynamic Satellite (Lageos).....	41
3.2	Generation of Simultaneous Range-Differences.....	43
3.2.1	Description of the Original Set of Range Data.....	44
3.2.2	Selection of Ranging Data on Simultaneously Observed Satellite Passes.....	48
3.2.3	Functional Representation of the Data Selected for SRD Generation.....	50
3.2.3.1	Least Squares Approximation Using Monomials and Chebyshev Polynomials As Base Functions.....	54
3.2.3.2	Interpolation with Cubic Spline Functions..	62
3.2.3.3	Comparison of Least Squares Estimates and Cubic Spline Interpolants for the Range Function.....	69
4.	THE ESTIMATION PROCESS.....	83
4.1	Introduction.....	83
4.2	Differential Relations Between the Observable and the Parameters.....	87
4.3	Estimable Parameters.....	92
4.3.1	Information Required for the Determination of the Problem Parameters.....	93
4.4	Minimization of Model Biases by Use of SRD Observations....	99
4.4.1	Simulation Study for Bias Propagation Characteristics.....	102
4.4.2	Analysis of the Simulation Results.....	104
4.5	Sensitivity Analysis of SRD Observations.....	118
4.5.1	Introduction.....	118
4.5.2	Optimal Designs for Baseline Estimation.....	119
4.5.3	Optimal Design for the Estimation of the Motion of the Pole.....	123
4.6	Operational Approach for Parameter Estimation.....	134
4.6.1	Estimation of Baseline Lengths.....	134
4.6.2	Estimation of the Coordinates of the Pole.....	136
5.	NUMERICAL EXPERIMENTS AND RESULTS.....	142
5.1	Simulation Studies.....	145

5.1.1	Simulations for an Existing SLR Network .....	145
5.1.2	Simulations for a Proposed SLR Network .....	153
5.1.2.1	Baseline Recovery .....	153
5.1.2.2	Polar Motion Parameter Recovery .....	161
5.2	Experiments with Real Data .....	167
5.2.1	Preliminary Adjustment for Data Editing .....	167
5.2.2	Estimation of the 7943-7090 Baseline .....	175
6.	CONCLUSIONS AND RECOMMENDATIONS .....	182
6.1	Conclusions .....	182
6.2	Recommendations .....	187
	REFERENCES .....	189
APPENDIX A:	Derivation of the Variational Equation of State for the Case of Tidal Accelerations .....	196
APPENDIX B:	Systematic Corrections Applied to the Observations ..	199
APPENDIX C:	Further Development of the Differential Error Equations .....	205
APPENDIX D:	Residual Summaries for Ten SLR Stations for the August, 1980, Lageos Data .....	209

## LIST OF TABLES

Table	Page
1. Lageos Along-Track Acceleration Magnitude.....	38
2. Lageos Nominal Orbital Elements.....	42
3. Comparison of Monomial Fits Using $N$ and $\bar{N}$ .....	71
4. Distribution of Ground Truth Points, Sparse Data.....	71
5. Distribution of Ground Truth Points, Dense Data.....	73
6. Least Squares Approximation with Monomials, Dense Data.....	74
7. Least Squares Approximation with Monomials, Sparse Data.....	74
8. Least Squares Approximation with Chebyshev Polynomials, Dense Data.....	75
9. Least Squares Approximation with Chebyshev Polynomials, Sparse Data.....	75
10. R-Ratio Test Results ( $\alpha = 0.01$ ).....	77
11. Interpolation with Cubic Splines, Dense Data Sets.....	79
12. Interpolation with Cubic Splines, Sparse Data Set.....	79
13. Comparison of Recovery Errors from Two Cubic Splines for the Complete and the Restricted Dense Data Sets.....	81
14. Lageos Data Selection Summary.....	145
15. Overlapping Data Distribution for Eight Station Pairs.....	147
16. Polar Motion Component Recovery Error Summary.....	152
17. Baseline Recovery Error Summary.....	152
18. Coordinates for the Stations Used in the Simulations.....	154
19. Distribution of Ranges and SRD's for Each Baseline.....	154
20. Baselines Recovered from Network Adjustments.....	156
21. Baselines Recovered from Independent Adjustments.....	158
22. Summary Statistics for Baseline Recovery Errors.....	161
23. Polar Motion Component Values Used in the Simulations.....	163
24. Polar Motion Component Recovery Results, Complete Data Set Solution.....	164
25. Statistics for the Recovered Polar Motion Components Obtained from the Complete Data Set.....	164



Table	Page
26. Polar Motion Component Recovery Results, Restricted Data Set Solution .....	165
27. Statistics for the Polar Motion Components As Obtained from the Restricted Data Set .....	165
28. Numerical Values of Constants Used by GEOSPP .....	168
29. Numerical Orbit Integration Information for GEOSPP .....	169
30. A Priori CTS Station Coordinates .....	170
31. Residual Summary for the Complete Lageos Range Data Set Adjustment by GEOSPP .....	170
32. Station Coordinates and Standard Deviations Estimated by GEOSPP .....	172
33. Initial State Vector for Lageos As Obtained by GEOSPP from the Complete Lageos Range Data Set Adjustment .....	172
34. Baseline Lengths and Standard Deviations Estimated by GEOSPP .....	173
35. Observation Summary for Range Data from Station 7943 .....	175
36. Observation Summary for Range Data from Station 7090 .....	176
37. Station Coordinates and Baseline Length Estimates and Statistics Obtained from the Range Data Adjustment .....	177
38. Station Coordinates and Baseline Length Estimates and Statistics Obtained from the SRD Data Adjustment .....	177
39. Pass-by-Pass Residual Summary for Adjusted Range Data from Station 7090 .....	180
40. Pass-by-Pass Residual Summary for Adjusted Range Data from Station 7943 .....	180
41. Pass-by-Pass Residual Summary for Adjusted SRD Data from the 7090-7943 Station Pair .....	181
42. Residual Summary for Station 7063 .....	210
43. Residual Summary for Station 7090 .....	210
44. Residual Summary for Station 7091 .....	211
45. Residual Summary for Station 7092 .....	211
46. Residual Summary for Station 7096 .....	211
47. Residual Summary for Station 7114 .....	211
48. Residual Summary for Station 7115 .....	212
49. Residual Summary for Station 7120 .....	212
50. Residual Summary for Station 7907 .....	212
51. Residual Summary for Station 7943 .....	213

## LIST OF FIGURES

Fig.	Page
1. Simultaneous range-differencing .....	9
2. Relative geometry of barycentric and geocentric coordinate systems .....	26
3. Cylindrical shadow geometry .....	33
4. Range versus time graph for the sparse data set from station 7943 .....	52
5. Range versus time graph for the dense data set from station 7115 .....	53
6. Geometric interpretation of the best linear approximation .....	56
7. Range bias surfaces for the fixed station 1 .....	108
8. Radial bias surfaces for ranges from the four locations of station 2 .....	109
9. Latitudinal bias surfaces for ranges from the four locations of station 2 .....	110
10. Longitudinal bias surfaces for ranges from the four locations of station 2 .....	111
11. Radial bias surfaces for SRD's from four 2000 km baselines ...	112
12. Radial bias surfaces for SRD's from four 200 km baselines ....	113
13. Latitudinal bias surfaces for SRD's from four 2000 km baselines .....	114
14. Latitudinal bias surfaces for SRD's from four 200 km baselines .....	115
15. Longitudinal bias surfaces for SRD's from four 2000 km baselines .....	116
16. Longitudinal bias surfaces for SRD's from four 200 km baselines .....	117
17. Satellite pass - baseline geometry for simultaneous range differences .....	121
18. Sensitivity surfaces for the coordinates of the pole in the case of a station at $\lambda = 0^\circ$ , $\phi = 40^\circ$ .....	126
19. Sensitivity surfaces for the coordinates of the pole in the case of a station at $\lambda = -90^\circ$ , $\phi = 40^\circ$ .....	127

Fig.	Page
20. Sensitivity surfaces for the x-coordinate of the pole for the three 1000 km baselines near $\lambda \cong 0^\circ$ .....	129
21. Sensitivity surfaces for the y-coordinate of the pole for three 1000 km baselines near $\lambda \cong 0^\circ$ .....	130
22. Sensitivity surfaces for the x-coordinate of the pole for three 1000 km baselines near $\lambda \cong -90^\circ$ .....	131
23. Sensitivity surfaces for the y-coordinate of the pole for three 1000 km baselines near $\lambda \cong -90^\circ$ .....	132
24. The effect of nonuniform observing schedules in the estimation of the coordinates of the pole .....	140
25. Unbalanced data distribution effects in the estimation of time-dependent averages .....	141
26. Lageos groundtracks for the AG80 simulated data set .....	149
27. Network solution results, recovery errors versus baseline length .....	157
28. Independent solution results, recovery errors versus baseline length .....	160
29. Baseline network for polar motion monitoring .....	162
30. Lageos SRD Event Distribution for the Data Used in Determining the 7090-7943 Baseline .....	178

## LIST OF ABBREVIATIONS

AU	Astronomical Unit
CCR	Corner Cube Reflector
CES	Celestial Ephemeris System
CIS	Conventional Inertial System
CLRS	Compact Laser Ranging System
CPU	Central Processing Unit
CSTG	Commission on International Coordination of Space Techniques for Geodesy and Geodynamics
CTS	Conventional Terrestrial System
DE114	Development Ephemeris 114
DOC	Differential Orbit Correction
EDM	Electromagnetic Distance Measuring
EIH	Einstein-Infeld-Hoffman
Eq. E	Equation of Equinox
GPS	Global Positioning System
GSFC	Goddard Space Flight Center
IAU	International Astronomical Unit
JPL	Jet Propulsion Laboratory
Lageos	Laser Geodynamic Satellite
LE58	Lunar Ephemeris 58
LLR	Lunar Laser Ranging
NASA	National Aeronautics and Space Administration
NSSDC	National Space Science Data Center
rms	Root Mean Square
SAO	Smithsonian Astrophysical Observatory
SECOR	Sequential Collation of Ranges
SF	Spline Function
SGRS	Spaceborne Geodynamic Ranging System
SLR	Satellite Laser Ranging

SRD	Simultaneous Range-Differencing
TAI	International Atomic Time
TDB	Barycentric Dynamical Time
TLRS	Transportable Laser Ranging System
UTC	Universal Time Coordinated
VLBI	Very Long Baseline Interferometry



## 1. INTRODUCTION

### 1.1 From Time Interval Measurement to Range Inference

The laser systems which are deployed in satellite ranging are generally categorized as one type of electromagnetic distance measuring device (EDM). In a wider sense though, one can think of them as being one type of communications system. After all, in order to infer the distance defined by the instrument and the satellite, the transmitted signal must travel to the satellite and upon reflection return to the receiving system of the instrument. Assuming the velocity of the signal is known, the length of the signal path can then be computed, if the elapsed time is measured. The concept is remarkably simple; however, stringent accuracy requirements for the inferred distance demand that a great deal of calibration of internal errors and correcting for other systematic effects (e.g., atmosphere, retroreflector array biases, etc.) has to be done before the accuracy reaches acceptable levels. What this implies is that careful monitoring of the performance of every component of the instrument is required on a short as well as a long time basis, detailed recording of parameters descriptive of the environment, and, finally, tedious calculations to compute and apply the corrections. At times, much to the dismay of the scientist, even after all these corrections have been applied, the results do not reach the expected accuracy level. Human errors not excluded, the reason most of the time is the fact that the applied corrections

are in error themselves. Since none of the physical processes involved is known perfectly, we have to rely on laws and models based on observation in computing their effects on the observable.

Naturally, the errors inherent in these models will propagate into our computations. In addition to this, the parameters needed to evaluate these models are also obtained from observation (e.g., temperature, pressure, clock offsets, clock rates, etc.) and therefore carry their own uncertainties due to observational errors. Even without having to go into a detailed description of the various steps involved in computing the final value for the station-satellite distance, it should be by now obvious that an enormous number of factors have introduced uncertainties of different levels during this process. What is then provided to the analyst as an "observed range" is no more than a number out of some computer software package along with a rather subjective estimate for its accuracy.

## 1.2 Systems Accuracy; Some General Remarks

It is common practice to implicitly assume that the error spaces of the various factors affecting a system are nearly orthogonal and that the interactions between them are therefore negligible. Although our present experience has not yet made a strong case against such practice, most statisticians [Scheffé, 1959] and metrologists [Eisenhart, 1963] maintain that a system is best calibrated as a whole while in normal operation rather than in a piecemeal fashion or ideal conditions. We must clarify here that their definition of a system is the entity which consists of hardware and software components as well as operators and analysts. It is thus clear that quotations such as "our

present ranging capabilities to satellites" are rather meaningless unless they are supplemented with an explanation of the particular system we are referring to. Naturally, the satellite itself is a very important component, and even if everything else were to remain the same, changing the satellite can lead to order of magnitude changes in the system accuracy.

### 1.3 Scope and Philosophy of the Investigation

The scientist who is interested in a particular subset of parameters will usually blame the inadequate hardware if the expected level of accuracy is not finally achieved. To a certain extent this may be true; however, hardware improvements are hard to come by and in most cases are very expensive. One then has to reassess the accuracy requirements and seek alternative solutions as well. The areas where we can look for improvements are the instrument design, the experiments or mission design, and the method of analysis of the collected data.

This study addresses the third problem in connection with the estimation of interstation distances and variations in the coordinates of the pole from a geodetic satellite ranging system dedicated to geodynamics research: the Lageos system. As far as instrument design improvements are concerned, it is unlikely that a geodesist can contribute directly to any significant extent. It is important, however, that the geodesist has an understanding of a little more than its very basic principles since it is only thus that problem areas can be pointed out and subsequently looked at by the specialists. This knowledge will also help in communicating and exchanging information and ideas among the various science disciplines involved. If nothing else, it makes

it easier to foresee the miracles that the electronic gadgetry can or cannot achieve.

The design of the experiment is an area where the geodesist will contribute more than anyone else involved. It is also the area where the most disappointment will be suffered. Even when the proposed design is a truly optimal one for the particular problem, what is finally implemented rarely bears more than a vague resemblance to what was originally conceived. Geographical, economical, political and other similar factors will usually reshape the design at the expense of optimality. There is very little that one can do about this other than accept what is made available.

Finally, the data analysis is the area where the geodesist can really experiment and innovate with practically no other than economical limitations. The issue that this study addresses in that respect is whether a new method of analysis can be formulated which will minimize, if not completely eliminate, the effect the biases (inherent or introduced in the supplied data) have on the final results for the estimated parameters. The method proposed and investigated here is based on a linear transformation of the range data to range-difference data. The range-differencing here refers to observations made simultaneously from two ground stations to one satellite point as opposed to classical range-differencing of observations made from a single station to two consecutive satellite positions. To avoid confusion the proposed method will be hereinafter referred to as "simultaneous range-differencing" (SRD).

To summarize what has been said to this point, the scope of this investigation is the search for a new approach in analyzing range observations which can be less expensive and time consuming while it will still provide estimates for the parameters that are of a higher or at least comparable level of accuracy to those obtained otherwise. The philosophy of the investigation can probably be best summarized in the cliché "The more expensive is not necessarily the better."

#### 1.4 Outline of the Proposed Simultaneous Laser Range-Difference (SRD) Mode

Laser systems currently deployed in satellite tracking have recently been upgraded to accuracy levels where biases from systematic unmodeled effects prohibit us from extracting the full amount of information contained in the observations. Considering that the instrumentation quality improves at a faster pace compared to the available physical models, one can foresee that in the near future (when, for instance, NASA replaces all its lasers with third-generation models) the limiting factor for estimate accuracies will be the aforementioned biases. In light of these advances in the technological sector, it is only natural to look for new methods for the reduction of the observations in ways that the effect of the biases can be kept well below the noise level.

The spectrum of geodetic satellite positioning techniques has been vastly enriched in the rather short quarter century life of this discipline. It has though remained polarized between two basic concepts: the geometrical positioning and the dynamical positioning. Over the years a number of hybrid techniques have also appeared to fill



the gap between the two dominant constituents of the spectrum. In the early days, simultaneous direction observations to satellites were successfully utilized to determine interstation directions [Veis, 1967; Aardoom et al., 1967; Schmid, 1974] using the formalism of geometric satellite geodesy and camera observations to balloon satellites such as Echo, Pageos, etc. Ranging systems never really participated in these solutions except for SECOR and C-band radar [Mueller et al., 1973] with rather poor quality observations. Apart from the fact that laser systems were not as developed as they are today, the stringent requirement of the geometric solution for simultaneous observations from at least four and preferably more ground stations made the inclusion of laser ranging observations impossible. Still, geometric solutions are the only ones that do not rely on the dynamics of the satellite orbit and therefore the only ones which are not affected by their imperfections. Despite their large number of solve-for parameters and severe data distribution requirement to avoid critical configurations and ill-conditioning [Blaha, 1971; Tsimis, 1973], their contribution to geodesy is vast and important.

As models for the orbit dynamics improved, attention shifted rapidly to dynamic solutions and the geometric solution sustained a period of hibernation, only to be recently revived due to the development of the airborne laser ranging system by NASA [SGRS Workshop, 1979]. Full-fledged dynamic solutions are very expensive and involve thousands of unknowns with observations spanning several years and a number of satellites. Necessity, therefore, and the fact that the shorter the orbit the less time the orbital biases have to build up and corrupt

the solution, gave birth to hybrid semi-dynamical solutions (short-arc, translocation, etc.). These techniques have been extensively applied in the case of Doppler satellite tracking observations which is natural if one takes into account how popular Doppler equipment has become in the scientific as well as the commercial sector [Brown, 1976; Kouba, 1979].

In the case of laser observations, the equipment has been limited and mostly of observatory type, difficult to relocate and for most uses too far apart to allow for significant amounts of simultaneously observed satellite passes. Furthermore, truly simultaneous events would be impossible to obtain since there is always an unknown synchronization difference between the clocks of the various stations. The launch of Lageos, however, has improved tremendously the geometry of the problem, since due to its high altitude (~5900 km) it is now possible that even intercontinental stations can co-observe this satellite. As for the station mobility, the advent of TLRS I and the recent deployment of CLRS/TLRS II, as well as the international trend towards highly mobile and self-contained "observatories on wheels/wings," will soon allow for rapid deployment of instruments in almost any area that calls for it. Finally, when satellite time transfer becomes operational, it is hoped that global laser networks will be synchronized to better than 100 ns compared to today's ~1  $\mu$ s. Still, though, the use of laser ranging in a truly geometrical mode is highly unlikely due to its absolute dependence on weather conditions, a factor which is beyond our control (at least for the foreseeable future). That, however, has not stopped scientists from seeking alternate ways to improve the quality

of results obtained from the analysis of laser ranges to satellites.

One of the most notable attempts to take advantage of geometry to improve the estimation of interstation distances from satellite laser ranging observations is summarized in [Latimer and Gaposchkin, 1977]. Their method, scalar translocation, takes advantage of coobserved satellite passes over the baseline under estimation. With rather poor data they have reported results that tend to be almost an order of magnitude better in accuracy and compare very favorably to independent estimates of the same baselines. Their success prompted us to undertake the investigation of using not only the coobserved part of the satellite pass, but, in addition, of converting the ranges to range-differences in hopes that they will be less affected by biases in the orbital model, the reference system, and in the observations themselves. Since there are not data taken specifically for this type of reduction technique, we had to select passes which had been coobserved by chance and then generate simultaneous ranges from an interpolation of the recorded range observations. Using then the generated simultaneous ranges from the end points of each station pair, we determine the simultaneous range difference (see Fig. 1). These quasi-observables are then analyzed to obtain the minimum variance estimate of the baseline length.

It is noteworthy that after this proposed investigation had been accepted by NASA, scientists at the Goddard Geodynamics Branch studied through an error analysis the advantages of using coobserved satellite passes in baseline determinations [Christodoulidis and Smith, 1981], and their conclusions are in favor of this concept. Their

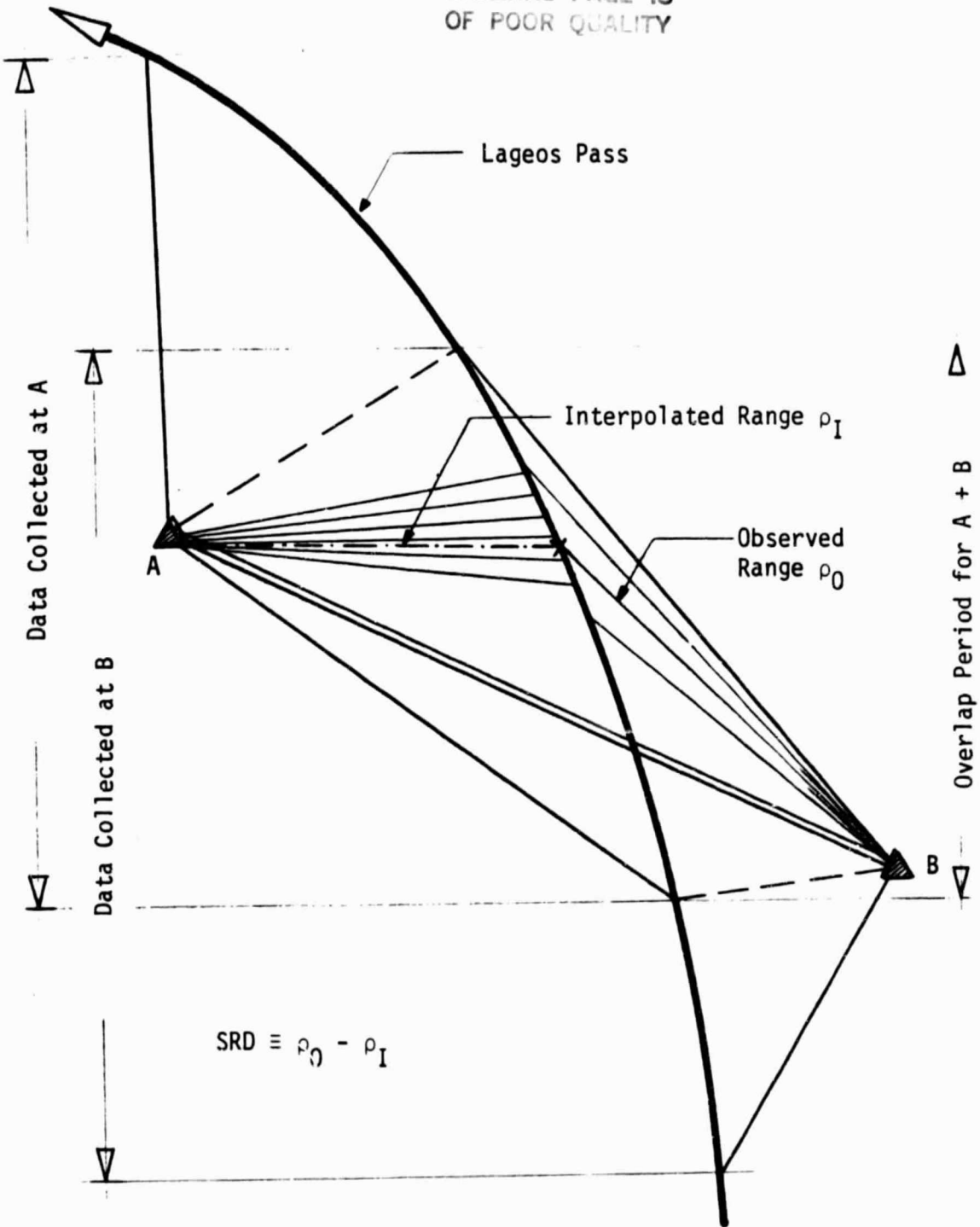


Fig. 1 Simultaneous range-differencing.

study indicates that even with the currently available instrumentation and physical models, a short arc of only five days with just six to eight passes coobserved by the baseline end stations can yield a  $2\sigma$  accuracy of better than one part in  $2 \times 10^7$  for baseline lengths ranging from 200 to 500 km.

With such encouraging results when only implicit use of the geometry was made (only coobservation of the same portion of the orbit was required), it seems that our effort to make explicit use of it (simultaneity--the same satellite position must be coobserved) is well justified. Aside from this fundamental difference in the use of geometry, this investigation goes beyond baseline estimation and addresses the equally important subject of polar motion estimation from the same type of observables.

As is well known and also discussed in this investigation, one cannot determine all station positions (and baselines therefrom) and the coordinates of the pole on the basis of the same satellite laser range data. To determine either of these types of parameters, the other should be known. The systematic errors in the latter do, of course, affect the estimation of the former. The choices here are rather limited. We could either fit some arbitrary functions to reduce the error growth--admittedly not a very attractive solution--or we can use the proposed simultaneous data reduction technique to minimize the effect of those unmodelled errors on the estimated parameters.

The presentation of the material follows the natural sequence in which the questions arise and the results are presented, interpreted and discussed in the final chapters. The second chapter summarizes the

theoretical foundations required in this study. It discusses the reference systems and frames as they are later used in the investigation and the orbital model for the satellite on which this study focuses most (Lageos). The third chapter is devoted to the observable, with a brief discussion on the instrumentation and an extensive investigation of techniques for generating quasi-simultaneous range-differences when lacking simultaneous ranging events. The fourth chapter deals with the estimation process and related topics such as the estimability of the parameters, the sensitivity of the observable in those parameters and the optimal network configurations for their estimation.

The fifth chapter is a summary presentation of numerical experiments performed during the course of study of the proposed technique, using mainly simulated data and some real data which were available. The report of the investigation concludes with a chapter summarizing our conclusions and listing our recommendations for future research in this area.

## 2. THEORETICAL BACKGROUND

### 2.1 Reference Systems and Frames

One of the basic tasks in designing and carrying out an experiment is the collection of a set of rules which will properly describe the space in which the experiment takes place. We call this set of rules the reference system.

In almost all cases these rules are abstract in nature and present no means by which one could materialize the system in practice. That is, however, the ultimate goal, to be able to realize the concepts contained in the rules. The means by which we achieve this constitute the reference frame.

The various reference systems and the reference frames bear a relationship much like that between two volumes of an encyclopedia. Although the covers are the same, the content is quite different. In our case the same reference system can be realized in different ways, each one being a distinct reference frame. The distinction derives from the different means by which the system is realized (stellar catalog, planetary ephemerides, quasar source catalog, etc.) as well as from the different numerical values adopted in each case. Even though the concept of a reference system may imply some sort of uniqueness, the realization in practice may have infinitely many variants. To remind ourselves of this arbitrariness we adopt the qualifier "conventional" reference systems and frames. We finally note that certain

assumptions and approximations made in the course of defining a system may render its validity as only an approximation of the ideal system and therefore in some cases the additional qualifier "quasi" needs to be used to indicate this.

The nomenclature adopted here follows closely that proposed in [Kovalevsky and Mueller, 1981] since that is the most complete, self-consistent and internationally accepted one today.

Although from the theoretical point of view one reference system would be sufficient for the description of the experiments, from a practical point of view we traditionally distinguish between space-fixed and earth-fixed systems. Both systems describe the same space continuum, though from a different point of view. The issue here is not the variety or number of systems to be involved, but rather the formalism from which the rules defining these systems will be drawn. Should we follow the classical Newtonian formalism or should we follow Einstein's geometro-dynamics (general theory of relativity).

Moritz [1979] suggests that a midcourse be sought. For all geodetic purposes, the classical formalism amended with small corrections to account for relativistic effects can serve as a sufficient approximation. It is acknowledged, however, that one place where the classical formalism will fail is the fourth coordinate of the continuum: time. The reason is twofold: Einstein's curved space-time has definitely discarded the (Newtonian) notion of a "universal" time, and, since time measurements today are the most accurate of all (less than one part in  $10^{13}$ ), there is no room for compromise or approximation. Each reference system has to have its own time scale associated with



it. This should come as no surprise, since as Minkowski [1908] himself put it, "Henceforth space by itself, and time by itself, are doomed to fade away into mere shadows, and only a kind of union of the two will preserve an independent reality." For these reasons we have chosen to follow the theory of geometrodynamics in the operational definition of the required Conventional (quasi-) Inertial System (CIS). The corresponding Conventional Terrestrial System (CTS) is also defined in a consistent way, the former through the geodesic equations (or equations of motion) of the satellite in the field generated by the surrounding bodies (Sun, Earth, Moon), and the latter by an adopted set of distances between a globally distributed set of stations--the CTS polyhedron. Since working with these distances is quite cumbersome, a set of coordinates for these terrestrial stations is used, consistent with the distances within the error of measurement [Bock, 1983].

If our experiments were confined to events and processes well defined within the frame of the CTS, then we would not need to discuss it further. But we do refer to processes and events occurring outside the CTS, and we therefore need to ascertain that the above definition provides for accurate connection with other frames. With the origins of the two systems coinciding at the center of mass of the earth, the problem to be solved is that of the orientation of the axes of the crust-fixed CTS with respect to another frame which is observable with respect to the available observations. For reasons explained in [Mueller, 1980] and investigated in [Leick, 1978], we feel that the appropriate system is the Celestial Ephemeris System (CES). The third axis of this system is called the Celestial Ephemeris Pole or simply

the Celestial Pole (C). The defining principle for C is that it should have "no periodic diurnal motion relative to the crust (not the mantle!) or the CIS" [Mueller, 1980]. The adoption of this axis and the geocenter constrains the remaining two axes to a plane that is perpendicular to C and contains the geocenter. The motion of C with respect to the CTS third axis is described by the (observationally determined) coordinates of the pole ( $x_p$ ,  $y_p$ ) and the connection between the two is accomplished through two well-established orthogonal rotations [Mueller, 1969]. A remaining third rotation accounts for the earth's (i.e., polyhedron's) sidereal rotation. This angle is modeled by a polynomial in time based on Simon Newcomb's expression for the right ascension of the fictitious mean Sun [Newcomb, 1898] and a linear-in-time component based on the mean sidereal spin rate of the earth. The true angle is obtained by correcting for the nutation in right ascension, known as the Equation of the Equinox (Eq. E) [Mueller, 1969]. A small correction must also be added (determined observationally again) to account for irregularities in the earth's spin rate. The resulting angle determines the instantaneous angular separation of two corresponding meridians of the CTS and the Celestial System, for example, the angle between their first axes.

The relative motions of these frames are relatively well known in theory [Mueller, 1969]. The numerical models, though, are incomplete and subject to continuous improvement as more observations become available and as their accuracies increase. In dealing with real data we have used the latest numerical models adopted by the IAU for use from 1984 onward [Kaplan, 1981]. In brief, the precession

formulation is that published in [Lieske, 1979], the nutation series are those derived by Wahr [1981], and the relationship defining the angular separation between the first axes of the CES and CTS (commonly known as the "Greenwich Apparent Sidereal Time") is taken from [Kaplan, 1981]. The CIS-referenced orbits of the major perturbing bodies considered in this investigation are taken from the JPL Development Ephemeris 114 (DE114) and the corresponding Lunar Ephemeris 58 (LE58) [Standish, 1981, private communication].

The time scales used in this investigation are the Universal Time Coordinated (UTC) [Mueller, 1969] for data tagging purposes and the Barycentric Dynamical Time (TDB) [Kaplan, 1981] for the integration of the orbit. Both time scales are related to the International Atomic Time (TAI) scale, and therefore the relationship between the two is also known [Moyer, 1981a; 1981b].

## 2.2 The Lageos Orbital Model

The orbital model for a satellite consists of a set of formulas that determine the accelerations the satellite experiences within the frame of reference. As such, all the accelerations in our case will be referred to the CIS. For the particular case of Lageos, the accelerations which will be included are the terrestrial, lunar and solar point-mass effects, the terrestrial nonsphericity effects, the effects due to solid earth tides, the solar radiation pressure effects and an along-track acceleration of well-established magnitude but of as yet undetermined cause [Smith et al., 1982]. Atmospheric drag effects are not included due to the high altitude of Lageos (~5900 km) and its very small cross-sectional area-to-mass ratio. All of the accelerations but the one due to the earth's nonsphericity are computed directly in the CIS frame. This deviation is due to the fact that the spherical harmonics that describe the earth's departures from a perfect point-mass body are given with respect to a body-fixed frame rather than an inertial one. To obtain an inertial expansion would mean to make those harmonics depend on time since they actually describe the anisotropic distribution of mass-density within the earth, which changes with time in an inertial frame due to the earth's rotational motions. For this particular acceleration then, the determination results from a two-step procedure where first we determine the inertial acceleration in the CTS and then we rotate it into the CIS to make it consistent with the rest of the model. This particular acceleration is the only one involving the transformation between the CIS and CTS frames.

The point-mass effects of the massive bodies in the solar system are determined partly on the basis of the geometrodynamical equations of motion, the Einstein-Infeld-Hoffman (EIH) formulation [Moyer, 1971], and partly on the basis of Newtonian theory. The former is used for the case of the solar, lunar and terrestrial effects, while the latter is reserved for the rest of the bodies in the solar system since their relativistic effects are too small to affect significantly Lageos' orbit [Moyer, 1982, private communication].

The determination of tidal accelerations is based on a series expansion of the tidally induced potential by each of the considered celestial bodies (primarily the Moon and the Sun), truncated to the second degree. A more sophisticated model where the accelerations are computed on the basis of the tidal constituents (such as the ones derived by Doodson [1921]) is not required, since our goal here is not to study the tides per se, but rather to include their effects on the motion of the satellite in order to obtain a more realistic model for the actual motion. This formulation assumes a static earth and the same elastic response behavior of the earth for all orders within the same degree of the expansion. Although a dependence of this response on the frequency of the sustained tidal wave has been established [Lambeck, 1980; Gaposchkin, 1981], for the purpose of the present study the simplified model is a sufficient approximation of the physical process. Since no special modeling of the ocean tides is included, it is justified to refer to our model as that for the solid-earth tides. Ocean tide effects are not modeled here since their effect is about an order of magnitude smaller than that of the solid-earth tides [Melchior, 1978]. As pointed out by

Musen [1973] though, both tides cause satellite perturbations with the same frequency spectrum and therefore aliasing is possible. In fact, aliasing effects are responsible for the discrepancy between satellite-derived and ground-data-derived values of the effective Love number  $k_2$  that characterizes the earth's elastic response to the applied tidal attractions [Melchior, 1978]. For this exact reason the value  $k_2 \cong 0.27$  is deemed more appropriate for use here rather than that of  $k_2 \cong 0.30$  which is generally accepted as the more accurate estimate today [Lambek, 1980].

For the solar radiation pressure we have adopted a simple model based on the Sun's mean flux and a cylindrical shadow model as that given in [Cappellari et al., 1976]. A more sophisticated model would require tedious computations, and it is rather doubtful that the end result would justify the required effort.

In the following sections we present the formulation for the computation of each individual acceleration and the corresponding variational equations. It should be mentioned here that the only unknowns in the orbital model are the position and velocity vectors of the satellite at the initial epoch of the integration. All other constants involved are assumed errorless although in practice one would solve for a number of them. For this reason, the variational equations which are presented here are only those that pertain to the unknowns; a more general set of equations can be found in [Cappellari et al., 1976]. The formulation is given in Cartesian rectangular coordinates since the special perturbation method of orbit determination has been chosen due to the complex accelerations involved.

### 2.2.1 Orbit determination with the method of special perturbations.

The determination of Lageos' orbit using the method of special perturbations [Cappellari et al., 1976] was dictated by the complexity of the orbital model and the stringent accuracy requirements. Although analytical methods can be more efficient and faster in orbit computations, when the modeled physical phenomena become complex, those methods simply cannot handle them as accurately as numerical techniques and in some cases cannot incorporate them at all. In case of Lageos, no special formulation of the problem (time regularization, change of dependent variables, etc.) is required since the orbit is almost circular and very stable; we therefore chose the Cartesian formulation and coordinate time as the independent variable.

A review of the relevant literature reveals that multistep numerical integration methods are the most efficient and accurate for problems such as the determination of orbits. Furthermore, the integration of the original second-order differential equations is to be preferred to that of the reduced first-order system, since the higher-order set has a much larger region of stability. Higher accuracy can be achieved--for a given stepsize--by increasing the order of the method; however, the higher the order, the less stable the process. We thus select an algorithm that permits variable order so that neither loss of accuracy nor instability can affect the solution. From the theoretical point of view the orbit of Lageos can be integrated with a fixed stepsize. Since, however, we use a variable order integrator, variable stepsize can result in some savings since as the order increases the stepsize is allowed to

increase too. A relative error test is used to determine whether to increase or decrease the stepsize and/or the order. The algorithm which fit our requirements and was conveniently available in computer coded form was that developed by Krogh [1969; 1970] of JPL. The structure of this method consists of a modified Adams-Bashforth predictor and an Adams-Moulton corrector of order one higher than the predictor. The mathematical formulation of these algorithms are given in [Krogh, 1969], and the user required information in [Krogh, 1970].

Denoting by capital letters vectors defined in the CIS frame of the integration and by  $t$  coordinate time TDB, we can write symbolically the Lageos orbit equations of motion as:

$$\ddot{\mathbf{R}} = \ddot{\mathbf{R}}_{PM} + \ddot{\mathbf{R}}_{NS} + \ddot{\mathbf{R}}_{TD} + \ddot{\mathbf{R}}_{SR} + \ddot{\mathbf{R}}_{AT} \quad (1)$$

where

- PM denotes point-mass effects
- NS denotes nonsphericity of the earth effects
- TD denotes solid-earth tidal effects
- SR denotes solar radiation pressure effects
- AT denotes Lageos ad hoc along-track acceleration

All of the above accelerations are functions of the satellite state vector and a number of model parameters (e.g., geopotential coefficients, etc.) which are assumed errorless in this study. Since the state vector at the initial epoch (initial conditions of the integration) is to be adjusted through the differential orbit correction (DOC) process to best fit the available observations, the variation in the initial conditions must be propagated to the epoch of observation state vector. This is



achieved by means of the transition matrix (or Jacobian of the state at the epoch with respect to the initial state) which is obtained through the integration of the variational equations of the state [Cappellari et al., 1976]:

$$\frac{d^2}{dt^2} \left( \frac{\partial \bar{R}}{\partial \bar{P}} \right) = \left( \frac{\partial \ddot{\bar{R}}}{\partial \bar{R}} \right) \left( \frac{\partial \bar{R}}{\partial \bar{P}} \right) + \left( \frac{\partial \dot{\bar{R}}}{\partial \bar{R}} \right) \frac{d}{dt} \left( \frac{\partial \bar{R}}{\partial \bar{P}} \right) + \left( \frac{\partial \ddot{\bar{R}}}{\partial \bar{P}} \right)^* \quad (2)$$

where  $\bar{P}$  denotes the vector of parameters of the DOC, in our case  $\bar{R}_0$  and  $\dot{\bar{R}}_0$ , the initial epoch state vector, and the \* on the last term indicates that the differentiation is carried explicitly with respect to  $\bar{P}$ . Equation (2) can be put in a more compact form if we define the following matrices:

$$\begin{aligned} A(t) &= \begin{bmatrix} \frac{\partial \ddot{\bar{R}}}{\partial \bar{R}} \\ \frac{\partial \ddot{\bar{R}}}{\partial \bar{P}} \end{bmatrix} & B(t) &= \begin{bmatrix} \frac{\partial \dot{\bar{R}}}{\partial \bar{R}} \\ \frac{\partial \dot{\bar{R}}}{\partial \bar{P}} \end{bmatrix} & C(t) &= \begin{bmatrix} \frac{\partial \ddot{\bar{R}}}{\partial \bar{P}} \end{bmatrix}^* \\ Y(t) &= \begin{bmatrix} \frac{\partial \bar{R}}{\partial \bar{P}} \end{bmatrix} & \text{and} & \dot{Y}(t) &= \begin{bmatrix} \frac{\partial \dot{\bar{R}}}{\partial \bar{P}} \end{bmatrix} \end{aligned} \quad (3)$$

We can then write (2) as

$$\ddot{Y} = A(t)Y + B(t)\dot{Y} + C(t) \quad (4)$$

Considering (1) we can write  $A(t)$  as

$$A(t) = \frac{\partial \ddot{\bar{R}}_{PM}}{\partial \bar{R}} + \frac{\partial \ddot{\bar{R}}_{NS}}{\partial \bar{R}} + \frac{\partial \ddot{\bar{R}}_{TD}}{\partial \bar{R}} + \frac{\partial \ddot{\bar{R}}_{SR}}{\partial \bar{R}} + \frac{\partial \ddot{\bar{R}}_{AT}}{\partial \bar{R}} \quad (5)$$

where each term is a 3 x 3 matrix. Except for the relativistic part of  $\ddot{\bar{R}}_{PM}$  and the  $\ddot{\bar{R}}_{AT}$  term in (1), no other acceleration depends on  $\dot{\bar{R}}$ . Since both these accelerations are extremely small, their contributions to the variational equations can be neglected with no loss of accuracy. The variational equations are quite insensitive to such small effects,

and in fact higher-order effects from the geopotential (for Lageos, above degree and order four) can also be neglected. This is important because the computation of these effects is very tedious and computer time consuming. With no velocity-dependent terms in the model, we can set  $\bar{B}(t)$  equal to the null matrix. In addition to this,  $C(t)$  can also be set equal to the null matrix because the accelerations do not depend explicitly on either  $\bar{R}_0$  or  $\dot{\bar{R}}_0$ , which are the only elements of vector  $\bar{P}$ . The variational equations that need to be integrated then take the simple form

$$\ddot{Y} = A(t) Y \quad (6)$$

with initial conditions (i.e.,  $Y(t = 0)$ )

$$Y_0 \equiv [I \mid \phi] \quad (7)$$

$I$  and  $\phi$  being the  $3 \times 3$  identity and null matrix respectively.

### 2.2.2 Gravitational acceleration from $N$ point masses.

In discussing the CIS system in Section 2.2, we pointed out that the chosen system will be realized in practice through the ephemerides of the bodies responsible for the gravitational field, as computed from the EIH formulation of their equations of motion. At this point, before we give the explicit EIH equations, we must note again that this formulation is only accurate to an order  $O(1/c^2)$ , and it assumes no masses beyond our solar system. For the particular case of Lageos, we can further simplify the formulation by ignoring the relativistic effects of all bodies except for the Earth, the Sun and the Moon. Furthermore, since Lageos' mass is insignificant compared to that of the other bodies involved, we can safely assume that it does not contribute

to the generation of the field, and therefore it behaves as a true massless particle. Deviations of the assumptions on the internal structure of the perturbing bodies are not a problem either, since they can be taken into account through additional perturbing accelerations. The EIH equations have been derived by Moyer [1971] in a body-system-barycentric coordinate system for the general case of motion of body  $i$  in the environment of  $N$  bodies:

$$\begin{aligned} \ddot{\bar{r}}_i = & \sum_{\substack{j=1 \\ j \neq i}}^N \frac{\mu_j (\bar{r}_j - \bar{r}_i)}{|\bar{r}_{ij}|^3} \left\{ 1 - \frac{4}{c^2} \sum_{\substack{\ell=1 \\ \ell \neq i}}^N \frac{\mu_\ell}{|\bar{r}_{i\ell}|} - \frac{1}{c^2} \sum_{\substack{k=1 \\ k \neq j}}^N \frac{\mu_k}{|\bar{r}_{jk}|} \right. \\ & + \frac{\dot{\bar{r}}_i^T \dot{\bar{r}}_i}{c^2} + 2 \frac{\dot{\bar{r}}_j^T \dot{\bar{r}}_j}{c^2} - 4 \frac{\dot{\bar{r}}_i^T \dot{\bar{r}}_j}{c^2} - \frac{3}{2c^2} \left[ \frac{(\bar{r}_i - \bar{r}_j)^T \dot{\bar{r}}_j}{|\bar{r}_{ij}|} \right]^2 + \frac{1}{2c^2} (\bar{r}_j - \bar{r}_i)^T \ddot{\bar{r}}_j \left. \right\} \\ & + \frac{1}{c^2} \sum_{\substack{j=1 \\ j \neq i}}^N \frac{\mu_j}{|\bar{r}_{ij}|^3} [(\bar{r}_i - \bar{r}_j)^T (4\dot{\bar{r}}_i - 3\dot{\bar{r}}_j)] (\dot{\bar{r}}_i - \dot{\bar{r}}_j) + \frac{7}{2c^2} \sum_{\substack{j=1 \\ j \neq i}}^N \frac{\mu_j \ddot{\bar{r}}_j}{|\bar{r}_{ij}|} \quad (8) \end{aligned}$$

where the required  $j$ -body accelerations are computed on a Newtonian basis from

$$\ddot{\bar{r}}_j = \sum_{\substack{k=1 \\ k \neq j}}^N \mu_k \frac{(\bar{r}_k - \bar{r}_j)}{|\bar{r}_{jk}|^3} \quad (9)$$

Equations (8) and (9) are the basis for the derivation of the equations of motion for Lageos. To obtain the acceleration of Lageos in the geocentered CIS frame, we use (8) to compute the Lageos acceleration with respect to the barycenter  $(\ddot{\bar{r}}_{PM}^B)_L$ , and in a second application, the acceleration of the geocenter with respect to the barycenter

$(\ddot{r}_{PM}^B)_G$ . The required acceleration  $\ddot{R}_{PM}^I$  for Lageos is obtained as their difference then:

$$\ddot{R}_{PM}^I = (\ddot{r}_{PM}^B)_L - (\ddot{r}_{PM}^B)_G \quad (10)$$

Since the first terms in (8) represent the Newtonian acceleration, we can collect them together to produce a more illustrative form of the final equations. All of the other terms are divided by the speed of light squared, and we will use the notation  $(\ddot{r}_{REL}^B)_L$  to indicate the sum of those terms, where the outer subscript indicates the event to which they refer, (L, Lageos; G, Geocenter). We can write (10) then as:

$$\begin{aligned} \ddot{R}_{PM}^I = & \mu_E \frac{(\bar{r}_E - \bar{r})}{|\bar{r}_E - \bar{r}|^3} + \mu_S \frac{(\bar{r}_S - \bar{r})}{|\bar{r}_S - \bar{r}|^3} + \mu_M \frac{(\bar{r}_M - \bar{r})}{|\bar{r}_M - \bar{r}|^3} \\ & - \mu_S \frac{(\bar{r}_S - \bar{r}_E)}{|\bar{r}_S - \bar{r}_E|^3} - \mu_M \frac{(\bar{r}_M - \bar{r}_E)}{|\bar{r}_M - \bar{r}_E|^3} + (\ddot{r}_{REL}^B)_L - (\ddot{r}_{REL}^B)_G \end{aligned} \quad (11)$$

where the vector quantities on the right-hand side of the equation are all referred to the solar system barycentric coordinate system, and the differentiation is performed with respect to coordinate time, TDB. The above equation is written for the three major perturbing bodies, the Earth, the Sun, and the Moon as indicated by the subscripts E, S, and M respectively. Nonsubscripted quantities refer to the Lageos. This notation is illustrated in Fig. 2.

For any other bodies of the solar system, only their Newtonian contributions are taken into consideration using the following expression [Cappellari et al., 1976]:



$$|\ddot{\bar{R}}|_{PM} = \sum_{i=1}^k \mu_i \left( \frac{\bar{R}_i - \bar{R}}{|\bar{R}_i - \bar{R}|^3} - \frac{\bar{R}_i}{|\bar{R}_i|^3} \right) \quad \text{ORIGINAL PAGE IS OF POOR QUALITY} \quad (12)$$

The contribution of  $\ddot{\bar{R}}_{PM}$  to the variational equations is based on the Newtonian terms only since the relativistic terms are too small to have any significant effect and the computation of their effect would unwarrantedly overcomplicate the numerical integration process. From [ibid.] again we have:

$$\frac{\partial \ddot{\bar{R}}_{PM}}{\partial \bar{R}} = - \left( \frac{\mu_E}{|\bar{R}|^3} + \sum_{i=1}^N \frac{\mu_i}{|\bar{R}_i - \bar{R}|^3} \right) I + 3 \left( \frac{\mu_E \bar{R} \bar{R}^T}{|\bar{R}|^5} + \sum_{i=1}^N \mu_i \frac{(\bar{R}_i - \bar{R})(\bar{R}_i - \bar{R})^T}{|\bar{R}_i - \bar{R}|^5} \right) \quad (13)$$

and

$$\frac{\partial \ddot{\bar{R}}_{PM}}{\partial \dot{\bar{R}}} = [\phi] \quad (14)$$

with  $I$  and  $\phi$  the  $3 \times 3$  identity and null matrices.

### 2.2.3 Gravitational acceleration from terrestrial nonsphericity.

The infinite spherical harmonics series which describes the geopotential in space is given in [Heiskanen and Moritz, 1967]:

$$\phi(r, \phi, \lambda) = \frac{\mu_E}{r} \left[ 1 + \sum_{n=2}^{\infty} \left( \frac{a_E}{r} \right)^n \sum_{m=0}^n [C_{nm} \cos m\lambda + S_{nm} \sin m\lambda] P_{nm}(\sin\phi) \right] \quad (15)$$

It is implicitly assumed in writing (15) that the coefficients  $C_{nm}$  and  $S_{nm}$  are referenced to the  $(r, \phi, \lambda)$  coordinate system. The acceleration induced on the satellite by  $\phi$  is equal to its gradient,  $\nabla\phi$ . Since the zero<sup>th</sup> term is considered in the point mass acceleration

computations, we must subtract it from (15) which leads us to the "non-spherical" part of  $\phi$ , the perturbing potential  $V$ . The derivation of  $\nabla V$  and subsequently  $\ddot{\mathbf{R}}_{NS}$  is given in [Cappellari et al., 1976]. Because of the fact that the coefficients  $C_{nm}$  and  $S_{nm}$  are coordinate system dependent, the acceleration  $\ddot{\mathbf{R}}_{NS}$  is obtained indirectly from the acceleration of Lageos in the body-fixed system to which these coefficients refer. This computation involves the CIS to CTS transformation, and it assumes that these coefficients refer to the CTS. It is possible though that this may not be the case. If this is true then the classical procedure must be revised and the harmonics must be transformed to the CTS. Formulas for such a transformation are given in [Kleusberg, 1980]. Assuming that this transformation has been applied, and denoting by  $\ddot{\mathbf{r}}_b$  the Lageos (inertial) acceleration in the CTS frame, then the acceleration in the CIS frame is

$$\ddot{\mathbf{R}}_{NS} = (\text{SNP})^T \ddot{\mathbf{r}}_b \quad (16)$$

where  $(\text{SNP})^T$  is the CTS to CIS transformation [Mueller, 1980]. The acceleration vector  $\ddot{\mathbf{r}}_b$  is obtained from  $\nabla V$  as [Cappellari et al., 1976]

$$\ddot{\mathbf{r}}_b = \begin{bmatrix} -\frac{xz}{r^2 p} & -\frac{y}{p^2} & \frac{x}{r} \\ -\frac{yz}{r^2 p} & \frac{x}{p^2} & \frac{y}{r} \\ \frac{p}{r^2} & 0 & \frac{z}{r} \end{bmatrix} \nabla V \quad (17)$$

where

$$(x, y, z) = (X, Y, Z) (\text{SNP})^T \quad (18)$$

$$r^2 = x^2 + y^2 + z^2 \quad (19)$$

and

$$p^2 = x^2 + y^2 \quad (20)$$

The coordinates X,Y,Z are CIS referenced, and the x,y,z, CTS referenced. The 3x3 matrix in (17) transforms from the spherical coordinates r,φ,λ to the Cartesian x,y,z coordinates.

The associated variational equations of state are given in [Cappellari et al., 1976] as

$$\begin{bmatrix} \frac{\partial \ddot{R}}{\partial \dot{R}} \\ \frac{\partial \ddot{R}}{\partial R} \end{bmatrix}_{NS} = (SNP)^T \begin{bmatrix} \frac{\partial \ddot{r}_b}{\partial \dot{r}_b} \\ \frac{\partial \ddot{r}_b}{\partial r_b} \end{bmatrix}_{iS} (SNP) \quad (21)$$

and

$$\begin{bmatrix} \frac{\partial \ddot{R}}{\partial \dot{R}} \\ \frac{\partial \ddot{R}}{\partial R} \end{bmatrix}_{NS} = [\phi] \quad (22)$$

with φ the 3x3 null matrix.

Even if the consistency of the coordinate systems has been assured though, there are still conditions under which the above equations will give erroneous results. The reason is that certain low-degree harmonics, namely, C<sub>20</sub>, C<sub>21</sub>, S<sub>21</sub>, C<sub>22</sub>, and S<sub>22</sub> are actually associated with the elements of the earth's inertia tensor [Heiskanen and Moritz, 1967; Nagel, 1976], and it can be shown [Nagel, 1976; Reigber, 1981] that through these harmonics one can orient the reference frame in which they are referred, with respect to the principal axes of inertia system as implied by these coefficients. The problem arises from the fact that since the earth is not a rigid body, its axis of figure (principal axis of maximum inertia) has body-fixed motions due to seasonal mass redistributions (free motion) and a diurnal motion due to the tidal bulge (forced motion). The free motion is rather small,



with an amplitude of at most 2m and a period close to the Chandlerian (~430 days), but the forced diurnal motion can reach amplitudes of  $\pm 60$  m! These facts have been known for some time [McClure, 1973; Nagel, 1976; Leick, 1978; Moritz, 1979], but a combination of improved measuring accuracies, more stringent requirements for accurate results, and more dense (frequent) observational records have almost reached the point that one cannot afford to continue ignoring them for much longer [Tapley, 1982].

In the present study we have adopted a time variant nature for the  $C_{21}$  and  $S_{21}$  coefficients, computing their values at each epoch on the basis of the adopted  $C_{20}$  value and the coordinates of the pole, using the formulation of Reigber [1981].

#### 2.2.4 Solar radiation pressure acceleration.

Photons emitted from a radiating source at a frequency  $\nu$  possess an energy  $h\nu$ , where  $h$  is Planck's constant. Since they travel in space with the speed of light, their momentum can be computed as the ratio of their energy to their speed. When a massive body travels through their continuum, the impinging photons transfer part of their momentum to the body upon impact. It is obviously impossible to know the exact number of photons that collide with a satellite, but we can determine the total force if we know the distribution of photons in the continuum, i.e., their flux. This flux, however, varies, and its instantaneous value can only be obtained through observation. For the sun, for instance, solar flares can significantly increase the flux, hence the photon count. Nevertheless, for the present study adopting a mean

flux is sufficient, since the effect on Lageos is quite small already.

To determine the acceleration of the satellite due to solar radiation pressure, we first determine the force exerted on the satellite. This force is proportional to the satellite's area of impact  $A$ , the solar flux  $S$ , and a radiation pressure coefficient  $C_R$ , and inversely proportional to the speed of light  $c$ , and the sun-satellite distance  $|\bar{R}_S - \bar{R}|$  squared. The radiation pressure factor  $C_R$  is dependent on the reflectance characteristics of the impact area. This radiation pressure coefficient has been sufficiently accurately determined for Lageos at 1.1729. The magnitude of the resulting acceleration on Lageos can be written, then, as [Cappellari et al., 1976]

$$\frac{F}{m} = \frac{S}{c} \frac{|\bar{R}_S|^2}{|\bar{R}_S - \bar{R}|^2} \frac{C_R A}{m} \quad (23)$$

where  $S$  is the mean solar flux at one astronomical unit (1 AU), and  $F$  is the force exerted on the spacecraft. For convenience  $S/c$  is denoted by  $P_S$ , the solar radiation pressure constant, and it gives the force exerted on a perfectly absorbing body ( $C_R=1$ ) at a distance of 1 AU from the sun. We have adopted the value of about  $4.626 \times 10^{-6}$  Newtons/ $m^2$  for  $P_S$ .

Since this acceleration is the result of a collision, its direction is opposite to that of the impinging photons, i.e., in the direction of  $\bar{R} - \bar{R}_S$ . We can then express the acceleration in the CIS coordinates as

$$\ddot{\bar{R}}_{SR} = P_S \frac{|\bar{R}_S|^2}{|\bar{R}_S - \bar{R}|^2} \frac{C_R A}{m} \frac{\bar{R} - \bar{R}_S}{|\bar{R} - \bar{R}_S|} \quad (24)$$

Because the satellite is not always exposed to solar radiation, its motion can eventually bring it within the earth's shadow; equation (24) must be applied only part of the time in the computation of an orbit. To check whether the satellite is in or out of this shadow, one can go to various degrees of sophistication, from the simple cylindrical shadow model to the complex conical one, discriminating between umbra and penumbra regions [Baker, 1967]. We adopt the simple cylindrical model and we introduce the eclipse factor  $\gamma$  with only two possible values:

$\gamma = 1$       the satellite is in sunlight

$\gamma = 0$       the satellite is in the shadow

To determine the value of  $\gamma$ , the following computational checks are performed at each step:

- (a) If  $\bar{R} \cdot \bar{R}_S \geq 0$ , then  $\gamma = 1$
- (b) If  $\bar{R} \cdot \bar{R}_S < 0$ , then compute  $\frac{|\bar{R} \times \bar{R}_S|}{|\bar{R}_S|} - a_E$

$$\text{If } D = \frac{|\bar{R} \times \bar{R}_S|}{|\bar{R}_S|} - a_E \geq 0, \text{ then } \gamma = 1$$

$$\text{If } D = \frac{|\bar{R} \times \bar{R}_S|}{|\bar{R}_S|} - a_E < 0, \text{ then } \gamma = 0$$

The logic behind this check is best explained in Fig. 3.

If one wants to be absolutely rigorous in the computation of  $\ddot{\bar{R}}_{SR}$ , then the earth is not the only body to consider. The lunar shadow should also be considered. Furthermore, the above formulation considers only the effects of direct solar radiation. If radiation pressure is a

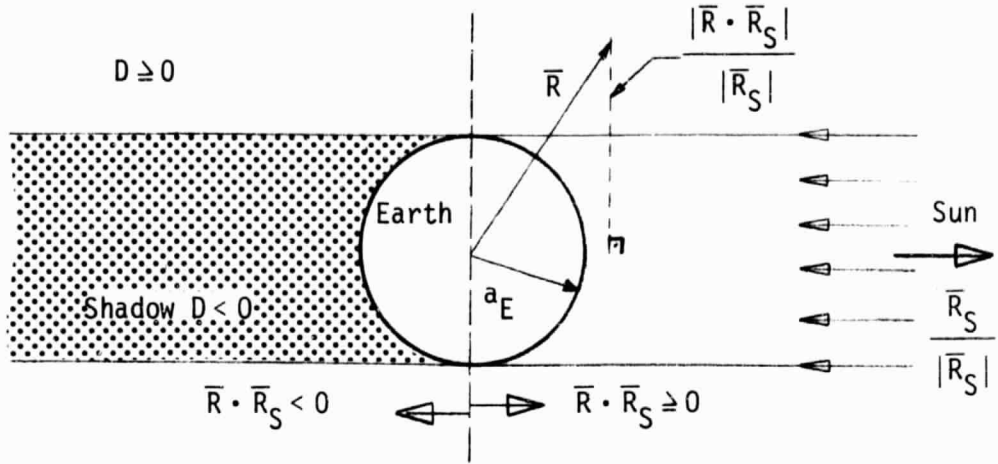


Fig. 3 Cylindrical shadow geometry.

major perturbation in the motion of a satellite (unlike Lageos,  $A/m \sim 0.007$ ), then in addition to direct effects, one must consider the effects of diffusely and specularly reflected visible radiation from the earth and also the opposing effect of promptly and delayed emitted infrared radiation from the body of the satellite itself [Baker, 1967].

The associated partial derivative of (24) that contributes to the variational equations of the state are given in [Cappellari et al., 1976] as

$$\left[ \frac{\partial \ddot{\mathbf{R}}_{SR}}{\partial \mathbf{R}} \right] = \gamma \frac{P_S}{m} \frac{|\bar{\mathbf{R}}_S|^2 C_R A}{|\bar{\mathbf{R}} - \bar{\mathbf{R}}_S|^3} \left[ \mathbf{I} - 3 \frac{(\bar{\mathbf{R}} - \bar{\mathbf{R}}_S)(\bar{\mathbf{R}} - \bar{\mathbf{R}}_S)^T}{|\bar{\mathbf{R}} - \bar{\mathbf{R}}_S|^2} \right] \quad (25)$$

and

$$\left[ \frac{\partial \ddot{\mathbf{R}}_{SR}}{\partial \dot{\mathbf{R}}} \right] = [\phi]$$

where  $\mathbf{I}$  and  $\phi$  denote the identity and null matrix respectively.

## 2.2.5 Tidal acceleration.

The attraction of the Sun and the Moon on the deformable Earth creates a time-varying (due to the relative motion of the bodies) potential field which in turn induces additional accelerations on an Earth-orbiting satellite. This tidal potential can be expanded on the Earth's surface as an infinite series, as we have already discussed, though only the second-degree term is of any significance in this study. According to A.E.H. Love [1911], the earth not being a perfectly elastic body, the actual response of the earth can be obtained from this potential as a fraction of it. The ratio of the induced potential to the tidal potential was designated by Love as  $k$ , a number whose value depends on the elastic properties of the earth. Further dependence of  $k$  on the frequency of the tidal waves has been established today, but for this study we will simply use the effective Love number  $k_2$  with a numerical value of 0.2748, consistent with satellite results when no modeling of the ocean tides is included.

The tidal potential on the earth's surface can be written then in the CIS frame as follows

$$U_{T_b} = \frac{\mu_b}{|\bar{R}_b|^3} a_E^2 P_2(\cos\theta) \quad (27)$$

where  $R_b$  is the distance between the centers of mass of the earth and the disturbing body  $b$ ,  $a_E$  is a mean radius for the earth,  $P_2$  is the Legendre polynomial of degree 2, and  $\theta$  is the angle defined by the direction of the geocentric radius of the evaluation point and the geocentric direction to the disturbing body. On the basis of (27) and using

Dirichlet's principle, we can obtain the potential  $U_{D_b}$  that perturbs the satellite's motion as

$$U_{D_b}(\bar{R}) = \frac{k_2}{2} \frac{\mu_b}{|\bar{R}_b|^3} \frac{a_E^5}{|\bar{R}|^3} \left[ 3 \left( \frac{\bar{R}_b}{|\bar{R}_b|} \cdot \frac{\bar{R}}{|\bar{R}|} \right)^2 - 1 \right] \quad (28)$$

where we have used the inner product between vectors to give a more manageable expression for  $P_2(\cos\theta)$ . From (28) and the fact that the tidal acceleration on the satellite is equal to  $\nabla U_{D_b}(\bar{R})$ , we obtain

$$\ddot{\bar{R}}_{TD_b} = \frac{3}{2} k_2 \frac{\mu_b}{|\bar{R}_b|^3} \frac{a_E^5}{|\bar{R}|^4} [1 - 5(\bar{u}_b \cdot \bar{u})^2] \bar{u} + 2(\bar{u}_b \cdot \bar{u}) \bar{u}_b \quad (29)$$

where  $\bar{u}_b$  and  $\bar{u}$  are unit vectors in the direction of the tide producing body  $b$  and the satellite respectively.

From (29) we can obtain the contribution of this acceleration to the variational equations as

$$\left[ \frac{\partial \ddot{\bar{R}}_{TD}}{\partial \bar{R}} \right]_b = \frac{3}{2} k_2 \frac{\mu_b}{|\bar{R}_b|^3} \frac{a_E^5}{|\bar{R}|^4} \left\{ [35(\bar{u}_b \cdot \bar{u})^2 - 5] \bar{u} \bar{u}^T + 2 \bar{u}_b \bar{u}_b^T + [1 - 5(\bar{u}_b \cdot \bar{u})^2] I - 10(\bar{u}_b \cdot \bar{u}) [\bar{u} \bar{u}_b^T + \bar{u}_b \bar{u}^T] \right\} \quad (30)$$

and

$$\left[ \frac{\partial \ddot{\bar{R}}_{TD}}{\partial \dot{\bar{R}}} \right]_b = [\phi] \quad (31)$$

where  $I$  and  $\phi$  are the  $3 \times 3$  identity and null matrix respectively. The derivation of this equation can be found in Appendix A.

The complete effects on the satellite are obtained through a summation of each body's effects over the number of bodies considered.

### 2.2.6 Lageos empirical along-track acceleration.

As more dense and accurate observations became available from Lageos, its orbit was determined with increasing accuracy to the extent that an unmodeled secular acceleration causing a mere 1.1 mm/day decrease of the semi-major axis could definitely be identified in all orbital fits [Smith and Dunn, 1980]. The mysterious acceleration, although small, alarmed scientists since its definitive existence jeopardized the long-term stability of Lageos' orbit and scientific interest was stirred up to attempt to give an explanation as to what is the physical cause for it. In most cases, the research has been concluded with a rejection of the assumed physical phenomenon as the possible cause, which in science is sometimes a more valuable contribution than finding the cause itself. Two most recent publications give an example of the diverse directions in which a solution has been sought.

Rubincam [1980] has examined a number of physical processes characteristic of the upper atmosphere and others such as gravitational resonance, gravitational radiation and terrestrial radiation, only to conclude that of all processes examined only drag due to charged and most likely neutral particles can be a plausible cause for the acceleration. If the relevant theories were further developed, then a more definitive answer could be given. For the time being though, his main argument for accepting this explanation is that it also helps solve the so-called "helium problem" [Chamberlain, 1978].

Szebehely [1981] on the other hand, keeping in line with his interest in the inverse problem of celestial mechanics, attempts to find the potential that would generate the unexplained acceleration. On the

basis of a circular orbit and two-body motion he shows that this potential is proportional to the spiral function of Lageos (i.e., the equation described by Lageos on its orbital plane) and inversely proportional to the square of its geocentric radius. One could then conceivably examine processes that are candidates for the solution of the problem and identify which of them could give rise to such a potential.

Since there is no definitive answer to the problem yet, we chose to model the unexplained acceleration in the same empirical way that the GSFC researchers do. From the full amount of available observations on Lageos, a set of monthly values of the magnitude of this acceleration has been compiled. We have adopted as definitive values those shown in Table 1, communicated to us by Mr. Ron Kolenkiewicz of GSFC, covering the period of time that was of interest to us. In a recent report [Dunn, 1982], the average value of this magnitude over the first five years of Lageos data has been reported to be  $2.86 \times 10^{-12} \text{ m/s}^2$ . This value can be used as a standard of comparison for the monthly variations of the effect.

The empirical model assumes that a restraining force is acting against the motion of the satellite, giving rise to an along-track (in the direction opposite to that of the velocity vector) acceleration  $\ddot{\mathbf{R}}_{AT}$ . One then can express this acceleration as

$$\ddot{\mathbf{R}}_{AT} = -\alpha \frac{\dot{\mathbf{R}}}{|\dot{\mathbf{R}}|} \quad (32)$$

where  $\alpha$  is the magnitude of the acceleration taken from Table 1 for the relevant time period. No contribution to the variation of the state is



Table 1. Lageos Along-Track Acceleration Magnitude

Time Period	Acceleration Coefficient $\alpha \times 10^{-12} \text{ m/s}^2$
October 1979	4.3
November	4.4
December	3.2
January 1980	1.6
February	0.4
March	0.8
April	3.8
May	4.3
June	3.2
July	3.5
August	3.4
September	3.3

computed due to the fact the effect is too small to bring any significant change in the variational partial derivatives.

### 3. THE OBSERVABLE

#### 3.1 Hardware Components

The operational principle of a laser ranging system was already mentioned in the introduction of this study. The range is inferred from the round-trip flight time of a pulse emitted from the station, reflected on the satellite and received back at the station. It is thus obvious that the system consists of two major components, the ground-based active instrumentation and the spaceborne satellite target.

##### 3.1.1 Laser ranging instrumentation.

The basic subcomponents of the ground-based part of the SLR system are the laser cavity, the timing equipment, the detection equipment, and the pointing system. Other secondary components are mini-computers, ancillary data collecting devices, calibration instruments, etc.

We will restrict ourselves here to describing the present capabilities of the available systems in terms of the observed ranges' accuracy and pointing out the sources of systematic errors affecting them. For a more detailed explanation of these errors consult [NASA, 1980].

From the laser cavity itself, the major source of error is the distortion of the wavefront. It can map into the range as high as 6.0 cm, but for the last (third) generation systems is no larger than 0.5 cm.

The receiver system contributes a much higher error which is a result of the photodetector, the discriminators and the delays from the various cables involved. Depending on the quality of the system, it varies between 1.5 - 8.0 cm. The timing system introduces systematic errors in the data for two reasons. The time interval counter frequency drift affects the measurement directly. The frequency standard that keeps absolute time and is used in determining the epoch of the measurement is also affected by similar factors, and it indirectly degrades the accuracy of the data by supplying biased epochs. The total effect is no larger than 1.0 cm though.

Finally, the calibration process itself, although by definition its purpose is to remove such errors from the measurements, can be in error too. In the older systems that calibration was performed through test measurements before and after a ranging session; the contribution to the error budget could be as high as 1.0 cm. New models which are capable of doing a real-time calibration have almost eliminated this error source [Silverberg, 1981a].

Although the above errors are systematic for a particular station, we cannot claim that they are systematic among stations. In fact it is more likely that they would be random in that sense. It may be that in some cases simultaneous range-differencing between two stations will result in a minimization of the above errors, but we cannot safely assume that this will be the case always.

### 3.1.2 Laser Geodynamic Satellite (Lageos).

The spaceborne segment of a satellite laser ranging system consists of a satellite which is equipped with corner cube reflectors (CCR) which reflect light at the incident direction. One such satellite which is dedicated to laser ranging is the Laser Geodynamic Satellite--Lageos (7603901). We describe this satellite only because as its name hints it has been launched to support geodynamics research and therefore it is the optimal target for such purposes.

The utility and merits of a target satellite such as Lageos are best summarized in [Johnson et al., 1976], the abstract of which we quote:

The fundamental concept of Lageos is a long-lived, dense, electrically and mechanically inert spherical satellite with its surface speckled with retroreflecting cube corners, designed such that range measurements between duly equipped laser ground stations and the satellite are possible with an ultimate accuracy of 2 cm when data from a single satellite pass are appropriately averaged. The Lageos concept requires that the satellite be placed in an orbit for which an ephemeris can be determined ultimately to 5 cm rms uncertainty for a 24-hour arc. These required satellite characteristics should allow the several geodynamic motions experienced by ground stations to be determined typically with 2 cm accuracy.

Lageos is a sphere of 0.59988 m diameter, with a mass of 407.821 kg, which results in a mass-to-area ratio of  $1.44 \times 10^3$  kg/m<sup>2</sup> and therefore small sensitivity in solar radiation pressure and aerodynamic drag forces. The outer shell of the sphere is made of aluminum with a matte exterior surface which results in Lageos appearing as a star of visual magnitude 12-13. The sphere contains a core drum made of beryllium copper to provide the desired weight.

The surface of the satellite is speckled with corner cube retro-reflectors arranged as uniformly as possible in eighteen "rows" or "rings" and two single CCR's at each end of the satellite's axis of symmetry. There is a total of 426 high quality, precision manufactured and tested CCR's [Fitzmaurice et al., 1977].

Following the basic concept of the Lageos system, its orbit was selected in such a way that perturbations caused by solar radiation pressure, drag, and high frequency poorly determined gravitational contributions were minimized. Nominal characteristics of the orbit, as determined on the basis of initial acquisition data obtained with the Baker-Nunn camera and laser system of SAO are given in Table 2 [Pearlman et al., 1976]. Lageos has ever since been consistently tracked with the international laser network maintained by NASA, SAO, and individual country agencies. Its ephemeris quality has improved considerably as improved ground instrumentation has been deployed and as the parameters for the force model have been obtained with similarly better accuracy. It is claimed [Lerch and Klosko, 1982] that we can now model

Table 2 Lageos Nominal Orbital Elements

Epoch	June 7.0, 1976
Inclination	109°8585
Eccentricity	0.003929
Apogee Height	5941.9 km
Perigee Height	5845.4 km
Period	225.4706 min
Semimajor Axis	12 271.790 km

the motion of Lageos over a month's time to better than 0.5 m. Nevertheless, it is natural to seek orbital models that have accuracies comparable to that of our observations which to date have reached the impressive 2-3 cm level. Once we achieve parity in that respect and subsequently maintain it, we can say that we have exploited the full potential of the Lageos system.

### 3.2 Generation of Simultaneous Range-Differences

The most tedious part of this investigation, aside from the writing, debugging and testing of the required orbital program, was the part pertaining to the generation of SRD's from the voluminous amount of laser ranging data provided by NASA/GSFC. The above statement though requires clarification, since the normally required effort is much less than what one might surmise from it. Most of the work involved can be characterized as "hunting" for suitable data. The fact that no specific campaign was ever devoted to the application of this new technique made data collected from stations coobserving the same pass hard to come by and only by coincidence. It must be noted here that this task was enormously facilitated by computer software kindly made available to us by Mr. Ron Kolenkiewicz of NASA/GSFC [Kolenkiewicz, 1980, private communication].

In the following sections we summarize the procedure that has been followed herein for the generation of the SRD's. We initially describe the range data set as originally obtained, the corrections that were already applied to the ranges and corrections which we had to apply in addition. For the sake of completeness, we describe the details of the

selection process, although this in effect amounts to an explanation of the NASA-supplied software. Finally, since we would eventually need to interpolate the selected observations in order to generate the SRD's, we have investigated three popular approximation techniques, truncated power series, Chebyshev polynomials, and cubic splines, in order to determine which would suit our purpose best. This by no means should be taken as an exhaustive treatment of the problem since it is a research topic in its own right and one can probably spend several years testing various approximation methods each with its own merits and drawbacks as well.

An investigation into the required relativistic corrections in the measured ranges and the corresponding SRD's showed that this correction is for all practical purposes negligible for the latter. The formulation and derivation of these corrections along with the station dependent tidal corrections are given in Appendix B.

### 3.2.1 Description of the original set of range data.

Prior to the discussion of this section's topic, some clarification on terminology is in order, as far as the types of data encountered in laser ranging is concerned. We will refer to the data collected at the individual laser stations as "raw data." Besides the observation itself, each raw data set contains a great amount of ancillary data that is required in the preprocessing of each observation. Raw data are not useful to an analyst unless the person is familiar with the operational details of the NASA- or SAO-supported networks of stations. Instead, we obtain the "preprocessed data" which comprise the actual observations

with certain corrections applied, and with other corrections having been computed but not applied. The latter are included in the disseminated data set with appropriate indicators that inform the analyst of what has been included already in terms of corrections and what yet remains to be applied. Such practice is particularly helpful in case someone would prefer to compute the corrections anew with different models or revised constants. The quality of the raw data depends heavily on the quality of the laser and timing instrumentation at each station. The preprocessed data, though, go through a number of processing stages and their quality is determined not only by that of the input raw data, but additionally by the integrity of those processes which they undergo. It is rather unfortunate that no scrupulous account has yet been published for either of these two stages of data handling. For both, the initial in situ processing of the collected data, and for the subsequent further refinement at the central computational center of NASA at GSFC, the documentation is outlined in a single short document [Carpenter, 1978] distributed to project investigators or obtained on request.

The gist of this document is that there are in general four corrections which need be applied (and are) to the observed ranges: fixed threshold to peak (return) signal offset, instrumental calibration correction, atmospheric refraction correction, and satellite center-of-mass offset correction. Some other corrections might be done additionally to compensate for peculiarities of individual instruments (e.g., mount axis offset correction for X-Y type mounts). The first correction is obtained from the output of the waveform digitizer and the registered



travel time of the pulse. The internal calibration correction is determined from ground-target ranging results collected just prior and immediately after a satellite ranging session. For the latest generation of laser instrumentation these two corrections are determined and applied in real time [Silverberg and Malevich, 1978; Silverberg, 1981a]. The atmospheric refraction correction is computed from a formula given in [Marini and Murray, 1973] using the pertinent information collected at the station during the tracking session and transmitted along with the raw data to the computing center. The center of mass offset correction is determined for each satellite before its launch. It is meant to refer the observed range to the point which is considered the center of mass of the vehicle and to which the computed orbit state vectors refer. For spherically symmetric satellites, such as Lageos, the correction is a constant (0.24 m for Lageos), but for satellites with complicated figures (e.g., those which carry solar paddles) and whose center of mass location depends on the relative position of moving parts (such as the paddles), the computation of the correction depends on several factors and sometimes it can only be approximately known. This is one more reason why satellites such as Lageos are ideal for the precise positioning required in geodynamics research.

When all the corrections have been applied, the data collected over each satellite pass are fitted to a polynomial to identify blunders and edit suspect observations. Nominally, a fifteenth-degree polynomial is used; however, for passes where less than 60 ranges are accepted, the degree of the polynomial is reduced to one-fourth the number of acceptable data points. The editing is performed by comparing the difference

between the observed range and that computed from the fit to the rms deviation of the fit. Data points which differ by more than three times this standard deviation are edited and the process repeated. Carpenter [1978] assures us that for relatively well-distributed data points, this process converges quickly and indeed edits only spurious data. It is not the goal of this investigation to examine the correctness of these subtasks, but it is worth noting that the so-called  $3\sigma$  rule has been contested on various occasions [Uotila, 1973 and 1976], and the implicit assumption that the analyzed data errors are normally distributed (for the rule to have any meaning at all) is made rather out of convenience than on the basis of some theoretical justification. At any rate, discussions at the meetings of the parties involved indicate an awareness of the problems in data preprocessing, and it is safe to say that major revisions can be expected in the near future in several aspects of this task.

The corrected ranges and the applied corrections are archived at the National Space Science Data Center (NSSDC) from which copies may be obtained upon request. It is this type of data that we have obtained for the numerical tests of this investigation. The format in which the data have been encoded on the magnetic tapes for transmittal is commonly known as the "Lageos binary format" [Putney, 1980], and it replaces the previously used (similar) Geos format.

### 3.2.2 Selection of ranging data on simultaneously observed satellite passes.

The distributed preprocessed ranging data are obtained on magnetic tapes, arranged in files, one for each month of the period covered. Within each file, the data are arranged in chronological order. For each set of monthly data, a catalog is constructed showing the stations which have collected observations over that month and the number of observations collected. The catalog contains also a pass-by-pass breakdown of the data and the beginning and ending epochs for each station having observed a certain pass. On the basis of this catalog and the known geographical location of the observing stations, the station pairs which are likely to have sufficient numbers of observations on the same portion of a satellite pass are determined.

If the number of coobserved satellite passes and the distribution of the observations seem promising, the next step is the actual determination of the overlapping observational periods and the number of observations collected by each station of the pair over those periods. This is accomplished by examining the data with the OVERLAP software. Due to either equipment or data failures, occasionally a pass is interrupted by gaps due to the missing or edited data. These gaps result in an uneven data distribution over the pass and can cause problems at a later stage, when simultaneous ranges are to be interpolated. To alleviate this problem, the software checks the duration of these gaps in the selected passes, and if they are larger than an allowed value, the pass is broken down into subsets of data. A 30-second maximum gap has proven reasonable as it does not cause problems in the interpolation, and at

the same time it does not result in extremely small subsets that would be hard to interpolate due to insufficient data points. At this point the results of the overlap analysis are examined as to the data content and distribution; periods with less than ten data points are rejected and so are the data from station pairs that have no significant total amount of observations over the whole month.

The remaining identified periods are now used to select the actual observations out of the original data set. At this stage, the distribution of the selected data within the overlap period for each of the paired stations is determined. In almost all cases, and for obvious reasons, the station with the largest number of observations also has the best distribution. It is important to know this detail, because only for one of the stations need the ranges be interpolated at the epochs that the alternate station has observed. We therefore choose to interpolate the ranges from the station with the best data distribution in order to keep approximation errors as small as possible. The end product of the selection process is two files, one containing the selected observations, and one containing a data-station directory. Included in the directory are the endpoint epochs for each batch of data constituting a pass or a portion of it, the identification numbers of the stations coobserving the pass, and an indicator that determines for which of the stations the ranges will be interpolated and for which the actual observations will be used.

### 3.2.3 Functional representation of the data selected for SRD generation.

We discuss here three different approaches for the approximation of the station-satellite distance at a number of given epochs, on the basis of observations of this distance at other instances spanning the approximated interval. One restriction in our choice from available methods is the arbitrary distribution of the observed ranges over the satellite pass. Having no control at all over this factor, we have but to eliminate outright the possibility of using some very simple, efficient and accurate methods such as the Chebyshev approximation [Dahlquist and Björk, 1974] or, for that matter, any other method which requires that the given base points correspond to a particular set of values of the free variable. Of the remaining viable methods, we have chosen to study two which either by virtue of their simplicity or their accuracy properties have attained widespread popularity among those who analyze experimental measurements. These methods are the least squares approximation and the cubic spline interpolation. There is a vast literature for both topics; one, however, is almost obliged to refer to the classical text of Davis [1975] for the first, and the concise but practical treatise of Späth [1974] for the second. As far as the least squares method is concerned, we have investigated the application of the method with two different sets of base functions: monomials and Chebyshev polynomials. To test the three methods in the absolute as well as the relative sense, the following experiment was performed.

We chose two sets of ranges, each set distributed over an interval of about 15 minutes, typical of the overlapping periods encountered in

this study. One set is chosen to have a high data density, with observations being made at a rate of about 1 pps. The other set is one of very sparse data, with observations about 20 seconds apart on the average. The sparse data set was collected at the Orroral (7943) SLR station in Australia, while the dense one comes from the Goldstone (7115) SLR station in California. Figs. 4 and 5 are the plots of these ranges versus time. The vertical bars indicate the actual data points. From these two sets of ranges, we selected a number of data points evenly distributed over the entire pass to form a "ground truth" data set. These selected ranges were eliminated from the original data sets. The remaining observations were subsequently used in the approximation process, using all three different methods. The results are then used to approximate the station-satellite distance at the "ground truth" points previously selected. Comparing the true values with the interpolated ones provides a criterion for the integrity of the method. The performance of each method in a regional, as well as a global sense is examined, and finally the results of the three methods are intercompared, taking into account also the complexity (or simplicity) of each method, its efficiency and the computational time that it requires.

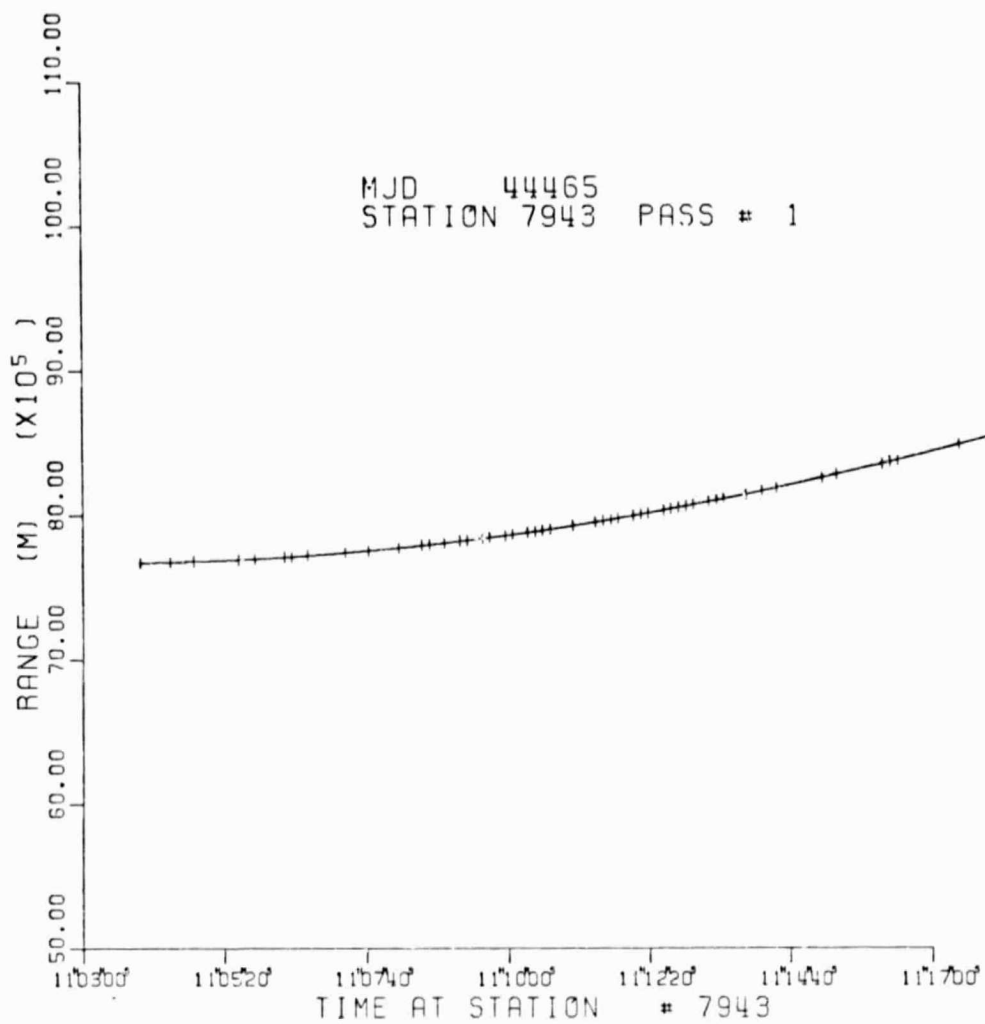


Fig. 4 Range versus time graph for the sparse data set from station 7943.

ORIGINAL PAGE IS  
OF POOR QUALITY

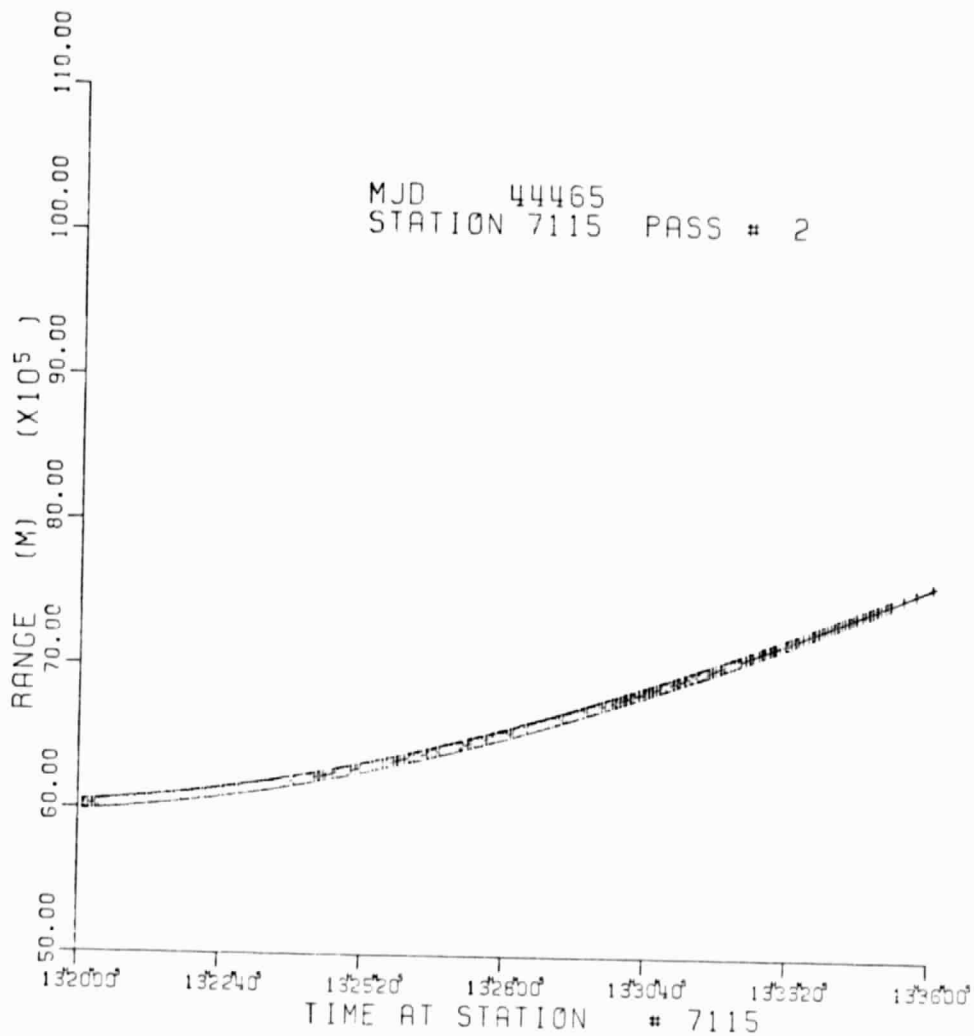


Fig. 5 Range versus time graph for the dense data set from station 7115.



3.2.3.1 Least squares approximation using monomials and Chebyshev polynomials as base functions. The existence and uniqueness of an  $n^{\text{th}}$ -degree polynomial that takes given values on a set of  $n + 1$  points of a closed interval  $[a, b]$  is guaranteed by the well-known theorem of polynomial interpolation [Davis, 1975]. The representation theorems of interpolation theory provide the tools for determining this polynomial in various ways. Lagrange's and Newton's formulae are the more often quoted solutions for this problem. It is equally well known, though, that as the number of given points increases (the degree of the polynomial increases, too) insurmountable problems arise from the computational aspect of this polynomial. Furthermore, even if the numerical problems could be overcome, the resulting polynomial will exhibit such strong oscillations between the fiducial points that it would be impossible to use it as a reliable approximation in those intervals. Despite, therefore, Weierstrass uniform approximation theorem and Walsh simultaneous interpolation and uniform approximation theorem, in practice we must find a working alternative free of the aforementioned drawbacks. One such alternative that we study in this section is the application of "best approximation," best in some sense soon to be defined.

A natural requirement for any type of approximant to a function  $f$  is that it should be "close" to  $f$ . As soon as we define the notion of "closeness" quantitatively, we have established a criterion for determining the best approximant of  $f$  in that sense. For the specific problem encountered in this investigation, we can restrict ourselves to the theory as applied for normed linear spaces of finite dimension [Davis, 1975]. We chose to work with the 2-norm, since in that case its

interpretation as the geometric distance between two elements of the space is simple and intuitively appealing. For an element  $x$  of the  $n$ -dimensional real space  $R^n$ , the 2-norm is defined as

$$\|x\| = \left( \sum_{i=1}^n x_i^2 \right)^{\frac{1}{2}} \quad (33)$$

where  $x_i$  ( $i=1, \dots, n$ ) are the components of  $x$ . If  $x, y$  are two elements of a metric space  $R^n$ , and  $d$  denotes the distance function in  $R^n$ , then enforcing

$$d(x, y) = \|x - y\| \quad (34)$$

to hold for all  $x, y \in R^n$ , makes  $R^n$  a normed linear space.

An alternate and more appropriate way of obtaining a normed linear space is to start with an inner product space. The inner product is a "two-slot machine" similar to the distance function, possessing linearity, symmetry, homogeneity and positivity, and denoted by  $\langle \cdot, \cdot \rangle$ . If we force in an inner product space the following equality to hold

$$\|x\| = \sqrt{\langle x, x \rangle} \quad (35)$$

then we obtain a normed linear space. Depending on the definition of the inner product, we obtain different norms for the resulting normed linear space. As they are all results of the more primitive concept of an inner product, we call them "induced norms."

We have already chosen to work with the 2-norm, and it is easy to see from (33) and (35) that the inner product should be defined as

$$\langle x, x \rangle = \sum_{i=1}^n x_i^2 \quad (36)$$

to be consistent with the rest of our formulation. We can now define the best approximation in terms of closeness under the 2-norm:

Definition: The best approximation of  $y$  by a linear combination of  $(x_1, \dots, x_k)$  is  $a_1x_1 + \dots + a_kx_k$  if the following inequality holds for every choice of the constants  $A_1, \dots, A_k$ :

$$e = \|y - (a_1x_1 + \dots + a_kx_k)\| \leq \|y - (A_1x_1 + \dots + A_kx_k)\| \quad (37)$$

The quantity  $e$  is called the error norm, and it is obvious from the above definition that the best approximation is the one which minimizes  $e$ . Since the  $x_1, \dots, x_k$  span a subspace  $R^k$ , which contains the approximant  $a_1x_1 + \dots + a_kx_k$ , the above inequality can be illustrated as a projection of  $y$  onto this subspace  $R^k$ . The error  $e$  then can be viewed as the perpendicular distance from  $y$  to  $R^k$ , and the approximant as the projection of  $y$  onto  $R^k$ , as shown in Fig. 6.

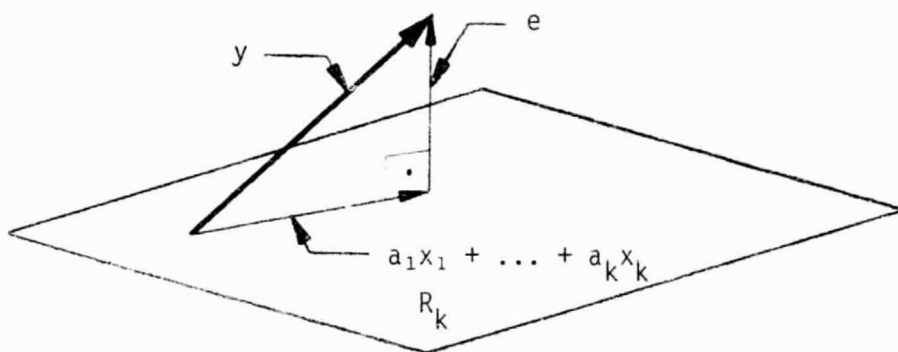


Fig. 6 Geometric interpretation of the best linear approximation.

It can be shown that for a given inner product, solving the projection problem is equivalent to solving the best approximation problem. If the solution to either problem exists, then it is unique. Furthermore, we can guarantee the existence of the solution (therefore its uniqueness, too) by choosing  $x_1, \dots, x_k$  to be linearly independent and

$k \geq n$ . We can now construct the projection of  $y$  onto  $R^k$  and thereby obtain at the same time the best approximation under the 2-norm, better known as least squares approximation.

Let  $x_1, \dots, x_k$  be a spanning set for  $R^k$ . By means of the Gram-Schmidt orthogonalization process we can form an orthogonal basis  $e_1, \dots, e_k$  for  $R^k$ . We are seeking the projection  $s$  of  $y$  onto  $R^k$  so that  $(y-s) \perp R^k$  or equivalently  $(y-s) \perp e_i$  for all  $e_i$  in  $R^k$ . Since  $\{e_i\}$  are a basis for  $R^k$  and  $s$  is an element of  $R^k$ , we can find  $\{c_i\}$  constants so that

$$s = \sum_{i=1}^k c_i e_i \quad (37)$$

The error vector  $y-s$  being orthogonal to all  $e_i$  satisfies

$$\langle y-s, e_i \rangle = 0 \quad i=1, \dots, k \quad (38)$$

or

$$\langle y, e_i \rangle = \langle s, e_i \rangle \quad i=1, \dots, k \quad (39)$$

and by (37):

$$\langle y, e_i \rangle = c_i \|e_i\|^2 \quad (40)$$

which leads to

$$c_i = \frac{\langle y, e_i \rangle}{\|e_i\|^2} \quad (41)$$

The projection  $s$  is therefore fully determined and by the equivalence theorem the representation (37) is the best approximation of  $y$  in the least squares sense.

If we want to determine  $s$  in terms of the original spanning set  $\{x_i\}$ , then we modify (38), (39) and (40) accordingly:

$$\langle y-s, x_i \rangle = 0 \quad i=1, \dots, k \quad (42)$$

$$\langle y, x_i \rangle = \langle s, x_i \rangle \quad i=1, \dots, k \quad (43)$$

and since now

$$s = \sum_{i=1}^k c_i x_i \quad (44)$$

we get

$$\langle y, x_i \rangle = \sum_{\ell=1}^k c_\ell \langle x_\ell, x_i \rangle \quad i=1, \dots, k \quad (45)$$

The last equation can be written in matrix form as

$${}_k[\langle y, x_i \rangle]_1 = {}_k[G_{ij}]_k {}^k[c_j]_1 \quad (46)$$

where

$$G_{ij} = \langle x_j, x_i \rangle \quad (47)$$

and it can be easily verified that the matrix  $G$  is symmetric. Equation (46) is the normal equation of the problem. It is also known as the Gramian of  $\{x_i\}$  with respect to the adopted inner product. The solution of (46) yields the sought for coefficients  $\{c_i\}$  and the required inverse of  $G$  is guaranteed by the linear independence of the basis elements  $\{x_i\}$ .

Two different sets of basis elements  $\{x_i\}$  have been used in this study. The set of monomials

$$M(t) = t^\ell \quad \ell=0, \dots, k-1 \quad (48)$$

and the Chebyshev polynomials  $T_\ell(t)$  defined as

$$\begin{aligned} T_0(t) &= 1 & \vdots \\ T_1(t) &= t & \vdots \end{aligned}$$

$$T_{\ell}(t) = 2t T_{\ell-1}(t) - T_{\ell-2}(t) \quad \ell=2, \dots, k-1 \quad \vdots \quad (49)$$

The former result in the widely used "polynomial fit" to the given data, while the latter, due to certain properties they have, show a superiority from the computational point of view that becomes increasingly more evident as the degree of approximation (the dimension of  $R^k$ ,  $k$ ) increases. In theory the two fits (for the same degree  $k$ ) should be equivalent, since  $T(t)$  are linear combinations of  $M(t)$  and vice versa, and therefore span the same space  $R^k$ . The former have the interesting property of being orthogonal with respect to summation though, when the summation is carried over specific points in the interval  $[-1, 1]$ :

$$\sum_{\ell=0}^m T_i(t_{\ell}) T_j(t_{\ell}) = \begin{cases} 0, & i \neq j \\ \frac{m+1}{2}, & i = j \neq 0 \\ m+1, & i = j = 0 \end{cases} \quad (50)$$

where  $\{t_{\ell}\}$  are the zeros of  $T_{m+1}(t)$  defined as

$$t_{\ell} = \cos\left(\frac{2\ell+1}{m+1}\frac{\pi}{2}\right) \quad \ell=0, 1, \dots, m \quad (51)$$

This property is the basis for the excellent from all aspects Chebyshev interpolation [Dahlquist and Björk, 1974; Snyder, 1966], when we can choose the distribution of the given data. It seems, however, that for a dense distribution of data sums of products of  $T_{\ell}(t)$ 's, such as those encountered in the formation of the normal equations (46), tend to behave in much the same way. The growth of the off-diagonal elements of the  $G$  matrix is slower in this case (with respect to the degree  $k$ ) compared to a fit with monomials  $M_{\ell}(t)$ . Furthermore, the loss of significance (due to the finite nature of the computer) is much less serious

here than it is for the classical monomial fit. We can thus use higher-degree Chebyshev expansions than polynomial ones without the risk of divergence and thereby absurd results due to an ill-conditioned normal matrix.

The question then arises as to what should be the choice of the degree  $k$ . Obviously, for a convergent fit the error will decrease as the degree increases. The oscillation of the resulting approximant will also increase though, and we must find a way of stopping at some optimum degree before that and the loss of significance make the approximant worthless. Since some of the criteria that we have studied are based on statistical concepts, we first have to introduce such concepts to our approximation process, which so far is of a purely mathematical nature. The simplest way of doing this is to modify our definition of the inner product (36) by including a weight function  $w(x_i)$  which is assumed to be positive definite:

$$\langle x, x \rangle_w = \sum_{i=1}^n w(x_i) x_i^2 \quad (52)$$

The meaning of  $w(x_i)$  can be that of assigning various degrees of importance to each  $x_i$  in a relative sense. One natural choice in the least squares approximation is to gauge importance against the amount of information contained in each observation for the parameters of the problem. To do this we must have some measure of the level of observational errors, and this can be achieved statistically by defining their distribution. If the distribution is the normal, which is usually the case, then it is fully defined through its first two moments, the mean

$\mu$  and the variance  $\sigma^2$ . This being the case, it can be shown [Rao, 1973] that the Fisher information measure of each observation on the  $\mu$  parameter of its distribution is

$$\mathcal{J}(\mu) = \frac{1}{\sigma^2} \quad (53)$$

ORIGINAL PAGE IS  
OF POOR QUALITY

$\mathcal{J}(\mu)$  is a function that complies with the requirements of the weighting function, and from its definition it seems that it is one fit for this purpose. The weights are therefore determined as

$$w(x_i) = \frac{1}{\sigma_i^2} \quad (54)$$

where in our case we have used  $\sigma_i^2 = \sigma^2$  ( $i=1, \dots, n$ ), since we have no means to discriminate between the observations. In matrix notation, the inner product can now be expressed by the following quadratic form:

$$\langle x, x \rangle_w = x^T W x \quad (55)$$

where

$$W = \text{diag} [w(x_i)] \quad (56)$$

If one can further make the assumption that the errors are distributed independently, then  $W$  is the inverse of their variance matrix  $\Sigma$ , and in this case the approximation is more appropriately called "minimum variance estimation" [Rao, 1973]. We can now, in light of the above discussion, speak of statistical properties of the approximant, and in fact we should also change our terminology, substituting estimation for approximation, estimator for approximant, and residuals for errors. This generalization of the process of approximation opens the way for use of various tests of significance, devised and applied in the



theory of linear statistical inference [Rao, 1973; Pollard, 1977]. In the tests that we have performed with the two selected sets of data we have looked at possibilities such as the convergence of the root mean square error of the fit (rms of fit), the rms of the recovered values at the ground truth points, and the significance of the change of the weighted sum of squares of the residuals between successive fits.

3.2.3.2 Interpolation with cubic spline functions. Despite the fact that theoretically one can always determine an interpolatory polynomial for the station-satellite range function, we have already seen that the large number of data points makes its computational aspects awkward and its qualitative and quantitative value questionable. To avoid the erratic behavior of the polynomial in between data points, we must keep its degree low. If, however, low-degree polynomials are fitted to the data, then we must tolerate the fact that they only approximate the function, that they do not reproduce the function at the fiducial points, and additionally, that some filtering of the high frequencies in the data is unavoidable. An alternative that exhibits the described low-degree-polynomial behavior and the reproducibility of the function at the fiducial points is the use of spline functions [Späth, 1974].

Spline functions (SF's) are curves consisting of low-degree polynomials each of which is defined over the closed interval  $[t_i, t_{i+1}]$  of two successive fiducial points. These elements of the SF are connected at these nodal points in such a way that their derivatives (to maximal order) exist. Since the SF passes through all nodal points, it

reproduces the interpolated function at these points exactly; and furthermore the use of low-degree polynomials suppresses the undesired oscillations between these nodal points. Provided that some boundary conditions are specified for the behavior of the SF at the endpoints of the interpolated interval, the existence and uniqueness of the SF is guaranteed [Späth, 1974].

As is the case with least squares approximation, the boundary conditions for the SF determine an "optimality" criterion which the resulting SF satisfies. A natural cubic spline  $s(t)$ ,  $t \in [a, b]$ , for instance, is determined with the boundary condition

$$s''(a) = s''(b) = 0 \quad (57)$$

and it is shown in [Späth, 1974] that  $s(t)$  minimizes the following integral

$$I(f) = \int_a^b [f''(t)]^2 dt \quad (58)$$

where  $f(t)$  is the interpolated function. Equivalently, one can say that the above SF is the solution to the variational problem

$$I(f) = \int_a^b [f''(t)]^2 dt = \text{a minimum} \quad (59)$$

with the aforementioned boundary conditions supplemented by the additional constraints that the resulting function passes through the given nodal points. Even though splines are interpolatory in nature, with a reformulation of the problem they can be "fitted" to the data in some optimal sense--most naturally the least squares sense. So one can conceivably solve the problem of approximation and filtering simultaneously

with this option [Späth, 1974]. Since in our case the weighting function for the observed nodal values is not known a priori, we refrain from using smoothing splines. In what follows, we summarize the computational aspects of cubic splines as we have applied them in this investigation.

We are given the values of the station-satellite range  $r_i$  at  $n$  epochs,  $t_1 < t_2 < \dots < t_n$ . We seek to determine the constituents  $f_i$  ( $i=1, \dots, n-1$ ) of the cubic spline  $s(t)$ , each  $f_i$  being a cubic polynomial, under the constraint that  $s(t)$  is twice differentiable at the  $n$  epochs  $t_1, \dots, t_n$ . Each of the  $f_i$ 's is defined on the corresponding range  $[t_i, t_{i+1}]$ . We adopt the following form for  $f_i$ :

$$f_i(t) = a_{i,1} (t-t_i)^3 + a_{i,2} (t-t_i)^2 + a_{i,3} (t-t_i) + a_{i,4} \quad (60)$$

so we will have four unknown coefficients for each of the  $n-1$   $f_i$ 's,  $4(n-1)$  total. To exploit the constraints for derivative continuity and existence, let us first establish the following notation for brevity:

$$\begin{aligned} \Delta t_i &= t_{i+1} - t_i & \Delta r_i &= r_{i+1} - r_i \\ r_i &= f_i(t_i) & r_{i+1} &= f_i(t_{i+1}) \\ r'_i &= f'_i(t_i) & r'_{i+1} &= f'_i(t_{i+1}) \\ r''_i &= f''_i(t_i) & r''_{i+1} &= f''_i(t_{i+1}) \end{aligned} \quad (61)$$

We can now write the following set of equations for each of the  $n-1$  intervals  $[t_i, t_{i+1}]$ :

$$r_i = a_{i,4} \quad (62)$$

$$r_{i+1} = a_{i,1} \Delta t_i^3 + a_{i,2} \Delta t_i^2 + a_{i,3} \Delta t_i + a_{i,4} \quad (63)$$

$$r'_i = a_{i,3} \quad (64)$$

$$r'_{i+1} = 3a_{i,1} \Delta t_i^2 + 2a_{i,2} \Delta t_i + a_{i,3} \quad (65)$$

$$r''_i = 2a_{i,2} \quad (66)$$

$$r''_{i+1} = 6a_{i,1} \Delta t_i + 2a_{i,2} \quad (67)$$

After some algebra, (62), (63), (66), and (67) can be solved for the four unknown coefficients  $\{a_{ij}, j=1, \dots, 4\}$ :

$$a_{i,1} = \frac{1}{6\Delta t_i} (r''_{i+1} - r''_i) \quad (68)$$

$$a_{i,2} = \frac{1}{2} r''_i \quad (69)$$

$$a_{i,3} = \frac{\Delta r_i}{\Delta t_i} - \frac{1}{6} \Delta t_i (r''_{i+1} + 2r''_i) \quad (70)$$

$$a_{i,4} = r_i \quad (71)$$

Substituting (68) - (71) into equations (64) and (65) we obtain for the first derivatives

$$r'_i = \frac{\Delta r_i}{\Delta t_i} - \frac{1}{6} \Delta t_i (r''_{i+1} + 2r''_i) \quad i=1, \dots, n-1 \quad (72)$$

and

$$r'_n = \frac{\Delta r_{n-1}}{\Delta t_{n-1}} + \frac{1}{6} \Delta t_{n-1} (2r''_n + r''_{n-1}) \quad (73)$$

From the continuity constraints for the first derivative we must force the following equality to hold at the nodes:

$$f'_i(t_{i+1}) = f'_{i+1}(t_{i+1}) \quad i=1, \dots, n-2 \quad (74)$$

Substituting from (64) and (65) we get the explicit constraint in terms of the coefficients  $\{a_{ij}\}$ :

$$3a_{i,1} \Delta t_i^2 + 2a_{i,2} \Delta t_i + a_{i,3} - a_{i+1,3} = 0 \quad (75)$$

We now substitute from (68) - (71) for the  $\{a_{ij}\}$  in terms of the second derivatives  $r_i''$ , etc. and obtain the following working expression:

$$\Delta t_i r_i'' + (2\Delta t_i + 2\Delta t_{i+1})r_{i+1}'' + \Delta t_{i+1} r_{i+2}'' = 6 \left( \frac{\Delta r_{i+1}}{\Delta t_{i+1}} - \frac{\Delta r_i}{\Delta t_i} \right) \quad (76)$$

$i = 1, \dots, n-2$

Obviously this expression cannot be written for the first and last nodal points, for there are neither prior (for the first) nor posterior (for the last) information on which the estimation of the  $r_1''$  and  $r_n''$  can be based. We therefore need to provide this information through the boundary conditions. In this case the first and last equations of the (76) system are modified appropriately. When written in matrix form, (76) is as follows:

$$\begin{bmatrix} 2(\Delta t_1 + \Delta t_2) & \Delta t_2 & & & 0 \\ \Delta t_2 & 2(\Delta t_2 + \Delta t_3) & \Delta t_3 & & \\ & \Delta t_3 & \ddots & \ddots & \Delta t_{n-2} \\ 0 & & \ddots & \Delta t_{n-2} & 2(\Delta t_{n-2} + \Delta t_{n-1}) \end{bmatrix} \begin{bmatrix} r_2'' \\ r_3'' \\ \vdots \\ r_{n-2}'' \\ r_{n-1}'' \end{bmatrix} = \begin{bmatrix} 6 \left( \frac{\Delta r_2}{\Delta t_2} - \frac{\Delta r_1}{\Delta t_1} \right) - \Delta t_1 r_1'' \\ 6 \left( \frac{\Delta r_3}{\Delta t_3} - \frac{\Delta r_2}{\Delta t_2} \right) \\ \vdots \\ 6 \left( \frac{\Delta r_{n-2}}{\Delta t_{n-2}} - \frac{\Delta r_{n-3}}{\Delta t_{n-3}} \right) \\ 6 \left( \frac{\Delta r_{n-1}}{\Delta t_{n-1}} - \frac{\Delta r_{n-2}}{\Delta t_{n-2}} \right) - \Delta t_{n-1} r_n'' \end{bmatrix} \quad (77)$$

ORIGINAL PAGE IS  
OF POOR QUALITY

For the system (77) to have a unique solution the coefficient matrix must be invertible. This matrix is symmetric, tridiagonal, with positive diagonal elements, and diagonally dominant. None of the primary determinants vanish therefore, and in fact they are all positive. The matrix is thus positive definite, and its Cayley inverse exists (unique inverse). For the particular case of SLR data interpolation, the second derivatives at the two end points are not known explicitly, and so we must look for an alternative set of boundary conditions. Since the observed range is a slowly varying function, we can safely assume that  $r_1''$  and  $r_n''$  are related linearly to  $r_2''$  and  $r_{n-2}''$  respectively.

$$\begin{aligned} r_1'' &= \sigma r_2'' \\ r_n'' &= \tau r_{n-1}'' \end{aligned} \tag{78}$$

where  $\sigma, \tau$  are constants which we must choose. The new set of boundary conditions (78) requires that the first and last of the equations (77) be changed to

$$\begin{bmatrix} (2+\sigma)\Delta t_1 + 2\Delta t_2 & \Delta t_2 & & & \\ \vdots & \vdots & & & \\ & & \vdots & & \\ & & \Delta t_{n-2} & 2\Delta t_{n-2} + (2+\tau)\Delta t_{n-1} & \\ & & & & \vdots \end{bmatrix} \begin{bmatrix} r_2'' \\ \vdots \\ r_{n-1}'' \end{bmatrix} = \begin{bmatrix} 6 \left( \frac{\Delta r_2}{\Delta t_2} - \frac{\Delta r_1}{\Delta t_1} \right) \\ \vdots \\ 6 \left( \frac{\Delta r_{n-1}}{\Delta t_{n-1}} - \frac{\Delta r_{n-2}}{\Delta t_{n-2}} \right) \end{bmatrix} \tag{79}$$

Finally, the choice we have made for  $\sigma$  and  $\tau$  is to set them equal to unity. The rationale behind this is that the derivatives of a polynomial become in general smoother as their order increases, and since we have a smooth function to begin with, there cannot possibly be a significant change in its second derivative over the few seconds that the two nodes are apart. Besides this, as shown in [Späth, 1974], the variation of the boundary conditions results in insignificant variations in the interior intervals and therefore a stable interpolation spline will be obtained for any reasonable choice of these conditions. The final form of (79) is therefore ( $\sigma=\tau=1$ ):

$$\begin{bmatrix} 3\Delta t_1 + 2\Delta t_2 & \Delta t_2 & & & 0 \\ \Delta t_2 & 2(\Delta t_2 + \Delta t_3) & \Delta t_3 & & \\ & \cdot & \cdot & \cdot & \Delta t_{n-2} \\ 0 & & & \Delta t_{n-2} & 2\Delta t_{n-2} + 3\Delta t_{n-1} \end{bmatrix} \begin{bmatrix} r''_2 \\ r''_3 \\ \vdots \\ r''_{n-1} \end{bmatrix} = \begin{bmatrix} 6 \frac{\Delta r_2}{\Delta t_2} - \frac{\Delta r_1}{\Delta t_1} \\ 6 \frac{\Delta r_3}{\Delta t_3} - \frac{\Delta r_2}{\Delta t_2} \\ \vdots \\ 6 \frac{\Delta r_{n-1}}{\Delta t_{n-1}} - \frac{\Delta r_{n-2}}{\Delta t_{n-2}} \end{bmatrix} \quad (80)$$

Solution of (80) yields the required second derivatives  $r''_i$  ( $i=2, \dots, n-1$ ) for the determination of the  $4(n-1)$  coefficients ( $a_{ij}$ ) through (68) - (71). At this point the spline  $s(t)$  is fully determined by the  $n-1$  cubic polynomials  $f_i(t)$  ( $i=1, \dots, n-1$ ) with the general expression (60). Values of the interpolated function can be obtained

from  $s(t)$  for any  $t_2 < t < t_{n-1}$ . We can use the interpolated values at the ground truth points to get an idea of how well  $s(t)$  approximates the range function.

3.2.3.3 Comparison of least squares estimates and cubic spline interpolants for the range function. We present and compare in this section the results obtained from a number of tests we performed with the SLR data collected during two passes of satellite Lageos over the Australian station at Orroral (7943) and the U.S. Station at Goldstone (7115). In all cases, except for spline interpolation, the domain of the function has been transformed to  $[-1, 1]$  through the following equation

$$\tau(t) = \frac{2t - (t_B + t_E)}{t_E - t_B} \quad (81)$$

where  $t_B$ ,  $t_E$  are the actual epochs of the first and last observations available. The above transformation greatly improves the conditioning of the normal equations, since raising  $\tau$  to high powers can now result only in losing some significance if  $\tau$  is very small. If  $t$  could be larger than one, then we ran the risk of exceeding the exponent magnitude limit of our computer.

With reference to the conditioning of the normals, we have also found helpful the scaling of the matrix in what is commonly termed "correlation form" in statistics. This technique results in making uniform the range of values of the elements of the matrix, thereby improving its numerical properties. The scaling is done by means of the square roots of the diagonal elements. We denote the original system of normal equations by



$$Nx = U \quad (82)$$

Then let

$$C = \text{diag} (n_{ii}^{-\frac{1}{2}}) \quad (83)$$

with  $|C| \neq 0$  since  $N$  is positive definite. We put

$$\bar{N} = CNC \quad (84)$$

and therefore

$$\bar{N}^{-1} = C^{-1}N^{-1}C^{-1} \quad (85)$$

Pre- and post-multiplying (85) by  $C$  we obtain

$$C\bar{N}^{-1}C = CC^{-1}N^{-1}C^{-1}C \quad (86)$$

or

$$N^{-1} = C\bar{N}^{-1}C \quad (87)$$

from which we obtain in combination with (82)

$$x = C\bar{N}^{-1}C U \quad (88)$$

Although this procedure does not alleviate numerical problems completely, it seems to improve the solution, especially in the case of a good distribution of data, as can be verified from Table 3. When the base functions are the Chebyshev polynomials, then the original normals are already uniform, and we see no change in the results of the two solutions.

The quality of the approximation depends not only on the global behavior of the approximant, but on the local as well. A generally good fit therefore can give poor results in some regions where the data distribution is worse than in the rest of the data set. When the differences between the observed ranges and the approximated at the ground truth points are examined, it is helpful to know whether we are working in a dense region or a sparse one. We have determined the time intervals

Table 3 Comparison of Monomial Fits Using N and  $\bar{N}$

Test Case	Dense Data					Sparse Data				
	Degree of Fit	Normal Eqs Used	RMS Fit (m)	Mean Error (m)	Recovery RMS (m)	CPU Time (s)	RMS Fit (m)	Mean Error (m)	Recovery RMS (m)	CPU Time (s)
16	N		0.24	0.01	0.12	1.3	3.5	-0.60	2.36	0.13
	$\bar{N}$		0.22	-0.01	0.08	1.3	0.5	0.10	0.59	0.15
19	N		7.21	0.23	6.37	1.7	1619.9	-406.20	1570.30	0.18
	$\bar{N}$		7.39	-0.50	4.61	1.7	1498.9	0.25	14.04	0.18

ORIGINAL PAGE IS  
OF POOR QUALITY

Table 4 Distribution of Ground Truth Points, Sparse Data

Station No. : 7943		<----- T ----->		
Observation Epoch		<---- T <sub>L</sub> ----><-- T <sub>R</sub> -->		
YYMMDD	HHMMSS.SSSS	T <sub>L</sub>	T <sub>R</sub>	T
800814	110626.8209	7.50	15.00	22.50
800814	110719.3610	37.54	22.53	60.07
800814	110842.0612	7.50	15.00	22.50
800814	110934.5613	15.00	7.50	22.50
800814	111019.5615	15.02	7.50	22.52
800814	1111 4.5216	22.46	22.46	44.92
800814	111134.4617	7.48	7.49	14.97
800814	1112 4.4618	15.00	7.50	22.50
800814	111219.4319	7.47	15.00	22.47
800814	111256.9021	7.47	7.50	14.97
800814	111319.4022	15.00	7.50	22.50
800814	111356.8823	22.48	15.00	37.48
800814	111526.8828	15.00	45.02	60.02
800814	111626.9931	7.50	59.96	67.46
800814	112019.1846	7.50	15.00	22.50

to the nearest observation prior to and after each of the ground truth points for both data sets. The epoch of these observations and these time intervals are displayed in Tables 4 and 5, where  $T_L$  is the interval in seconds to the nearest preceding observation, and  $T_R$  is the interval to the nearest succeeding one.

In all tests we have used expansions starting from degree five all the way up to 20. The summaries which are discussed here display only partial results which are enough to indicate the performance of each method. From Table 6 it is obvious that even for the dense pass the approximation with monomials starts diverging after degree 16. This is also true for the other pass, as can be seen from Table 7. The results for solutions up to degree 14 are identical for monomials and Chebyshev polynomials. From thereon though, while the former diverge, the latter converge with no major problems. The results given in Tables 8 and 9 can be compared to those of Tables 6 and 7 respectively to verify this. Only the recovered range data quality becomes poorer at higher degrees for the sparse data set, and this is caused by the distribution of the data, rather than instabilities in approximation technique. The denser pass shows a very good recovery even at those high degrees.

The computational time is about ten percent higher for the Chebyshev solutions compared to the monomials, but the increased stability and quality of the solution seems to be well worth it. It is therefore recommended that if one has to choose between these two solutions one should always go with the Chebyshev expansion rather than the monomials. The question that arises next is how to decide which is the lowest degree that gives a satisfactory representation of the data. Using the

ORIGINAL PAGE IS  
OF POOR QUALITY

Table 5 Distribution of Ground Truth Points,  
Dense Data

Station No. : 7115 Observation Epoch		<----- T -----> <---- T <sub>L</sub> ----><-- T <sub>R</sub> -->		
YYMMDD	HHMMSS.SSSS	T <sub>L</sub>	T <sub>R</sub>	T
800814	131626.0577	1.00	1.00	2.00
800814	131653.0577	1.00	1.00	2.00
800814	131714.0577	1.00	1.00	2.00
800814	131735.0577	1.00	1.00	2.00
800814	1318 2.0577	1.00	1.00	2.00
800814	1320 9.0577	1.00	1.00	2.00
800814	132032.0578	1.00	1.00	2.00
800814	132052.0578	1.00	1.00	2.00
800814	132113.0578	1.00	1.00	2.00
800814	132134.0579	1.00	1.00	2.00
800814	132156.0579	1.00	1.00	2.00
800814	132217.0580	1.00	2.00	3.00
800814	132240.0581	1.00	2.00	3.00
800814	1323 4.0581	1.00	1.00	2.00
800814	132325.0582	1.00	1.00	2.00
800814	132345.0583	1.00	1.00	2.00
800814	1324 9.0584	2.00	1.00	3.00
800814	132436.0585	3.00	2.00	5.00
800814	132518.0586	3.00	1.00	4.00
800814	132547.0588	3.00	1.00	4.00
800814	132623.0589	1.00	1.00	2.00
800814	132652.0591	1.00	1.00	2.00
800814	132720.0592	6.00	1.00	7.00
800814	132745.0594	2.00	1.00	3.00
800814	132811.0595	2.00	1.00	3.00
800814	132833.0597	1.00	1.00	2.00
800814	132854.0598	1.00	1.00	2.00
800814	132915.0599	1.00	1.00	2.00
800814	132939.0601	1.00	1.00	2.00
800814	1330 4.0602	1.00	2.00	3.00
800814	133038.0604	1.00	1.00	2.00
800814	1331 5.0606	1.00	1.00	2.00
800814	133137.0609	3.00	1.00	4.00
800814	1332 9.0611	2.00	1.00	3.00
800814	133247.0614	7.00	3.00	10.00
800814	133329.0617	2.00	2.00	4.00
800814	133427.0622	4.00	1.00	5.00
800814	133528.0627	14.00	14.00	28.00

Table 6 Least Squares Approximation with Monomials, Dense Data

Station: 7115 Date: 800814 Obs. Approx.: 754 Obs. Recov.: 38					
Degree of Fit	RMS of Fit (m)	Average Recovery Error (m)	RMS of Recovery Errors (m)	Average Serial Correlation for Recovered Obs.	CPU Time (ms)
6	5.373	-0.477	5.316	0.947	353
8	0.249	-0.014	0.130	0.923	496
10	0.220	-0.016	0.079	0.893	634
12	0.220	-0.014	0.084	0.860	803
14	0.219	-0.013	0.089	0.818	1064
15	0.219	-0.015	0.081	0.801	1177
16	0.220	-0.010	0.084	0.785	1315
17	0.323	0.024	0.133	0.770	1436
18	0.505	-0.162	0.334	0.751	1581
20	35.919	-1.033	9.041	0.709	1859

Table 7 Least Squares Approximation with Monomials, Sparse Data

Station: 7943 Date: 800814 Obs. Approx.: 41 Obs. Recov.: 15					
Degree of Fit	RMS of Fit (m)	Average Recovery Error (m)	RMS of Recovery Errors (m)	Average Serial Correlation for Recovered Obs.	CPU Time (ms)
6	1.350	0.110	1.012	0.859	43
8	0.381	0.082	0.458	0.806	57
10	0.340	0.051	0.472	0.777	70
12	0.339	0.045	0.473	0.730	91
14	0.336	0.032	0.474	0.645	121
15	0.332	0.082	0.561	0.573	135
16	0.460	0.096	0.592	0.484	150
17	18.399	-1.435	5.586	0.412	166
18	272.217	-57.402	222.250	0.355	182
20	68626.4	>10 <sup>5</sup>	48583.9	0.277	210

ORIGINAL PAGE IS  
OF POOR QUALITY

Table 8 Least Squares Approximation with Chebyshev Polynomials,  
Dense Data

Station: 7115 Date: 800814 Obs. Approx.: 754 Obs. Recov.: 38					
Degree of Fit	RMS of Fit (m)	Average Recovery Error (m)	RMS of Recovery Errors (m)	Average Serial Correlation for Recovered Obs.	CPU Time (ms)
15	0.219	-0.016	0.082	0.801	1296
16	0.219	-0.014	0.086	0.785	1433
17	0.219	-0.015	0.084	0.770	1580
18	0.218	-0.015	0.084	0.751	1731
19	0.218	-0.015	0.084	0.730	1898
20	0.218	-0.015	0.087	0.709	2064

Table 9 Least Squares Approximation with Chebyshev Polynomials,  
Sparse Data

Station: 7943 Date: 800814 Obs. Approx.: 41 Obs. Recov.: 15					
Degree of Fit	RMS of Fit (m)	Average Recovery Error (m)	RMS of Recovery Errors (m)	Average Serial Correlation for Recovered Obs.	CPU Time (ms)
15	0.313	0.070	0.531	0.573	140
16	0.319	0.015	0.458	0.484	156
17	0.319	0.011	0.455	0.412	173
18	0.318	0.386	1.592	0.355	191
19	0.318	0.642	2.561	0.294	209
20	0.317	-0.762	2.964	0.276	230

Note: CPU times above refer to the Amdahl V8 computer of The Ohio State University Instruction and Research Computer Center.

statistics on the recovered ground truth data gives some indication of the quality of the fit. It is, however, conditional on the selection, distribution and number of such points within the available data. It is, therefore, a very local test and does not provide a measure of the global performance of the estimator. The weighted sum of squares of the residuals, on the other hand, has this property, and it is a standard procedure in this type of problem to test the significance of the change of this statistic between solutions based on the same data. Hamilton [1964] derives the R-test to test the null hypothesis

$H_0$ : the  $k^{\text{th}}$  degree fit is as good as the  $(k+1)^{\text{th}}$  degree fit based on the variance ratio F-test.

The test statistic is the following:

$$R = \frac{(V^T PV)_k}{(V^T PV)_{k+1}} \quad (89)$$

where the subscript indicates the fit from which the residual norm has been computed. The theoretical value is obtained as

$$\mathcal{R}_{1, (n-k-1), \alpha} \equiv \frac{1}{n-k-1} F_{1, n-k-1, \alpha} + 1 \quad (90)$$

with significance level  $100\alpha\%$ . The hypothesis is rejected at this level if  $R > \mathcal{R}$ . The test must be used carefully, and one should make certain that the process has reached a stable convergence before one applies the test. Furthermore, the hypothesis to be tested should actually be a "chain-type" one, in the sense that we test from the highest degree down to the lowest one where we find that we must reject the hypothesis. For example, if we test in sequence

- $H_{01}$ : a 19th-degree fit is as good as a 20th
- $H_{02}$ : an 18th-degree fit is as good as a 19th
- ⋮
- $H_{07}$ : a 13th-degree fit is as good as a 14th
- ⋮

and we find that  $H_{07}$  is rejected while all previous hypotheses were supported by our results, then we can say that a 14th-degree fit is as good as any of the higher-degree fits at the tested significance level. Carrying out this test for the two test data sets, we have found that for the dense data set the lowest degree acceptable fit is for degree ten, and for the sparse data set it is degree seven. The test statistics are given in Table 10.

Table 10 R-Ratio Test Results ( $\alpha = 0.01$ )

Data Set Degree	Dense Data				Sparse Data			
	$V_{TPV}^T$	$R_{99\%}$	$H_0$		$V_{TPV}^T$	$R_{99\%}$	$H_0$	
5	232.05				2.6828			
6	217.67	1.0661	1.0080	R	0.7477	3.5881	1.329	R
7	3.0217	72.036		R	0.0662	11.2946		R
8	0.4679	6.4580		R	0.0596	1.1107		A
9	0.3745	1.2494		R	0.0557	1.0700		A
10	0.3646	1.0272		R	0.0474	1.1740	1.252	A
11	0.3644	1.0006		A	0.0473	1.0023		A
12	0.3635	1.0023	1.0080	A	0.0471	1.0040	1.230	A

Note: A - Accept, R - Reject



We have finally examined the statistical independence of the estimated range values at the ground truth points. Even if we assume that the available data are contaminated with uncorrelated random errors, the recovered ranges have approximation errors that are quite strongly correlated. The closer these points are to each other, the higher the correlation between every successive pair. The level of correlation drops as the degree of the fit is increased or as the data set becomes sparser. We have computed the average value of this serial correlation for each of the fits, and it is listed along with the other statistics in Tables 6 and 7 for fits with monomials, and Tables 8 and 9 for fits with Chebyshev polynomials. The choice of base functions has no effect whatsoever on this correlation. For the two fits that have been selected on the basis of the  $\chi^2$  test, the corresponding correlation levels are 83% for the seventh-degree fit on the sparse data set and 89% for the 10th-degree fit on the dense data set. Since a significant level of correlation is seen even between every fourth or fifth observation, one would have to include a full weight matrix in any subsequent use of these ranges if a meaningful result is sought. This, however, would make the use of such data very cumbersome and increase the computational effort beyond reason.

A way to circumvent this difficulty, without compromising on the assumed statistics of the estimates, is to use the cubic spline interpolation. Results for the two data sets are given in Tables 11 and 12. Since the splines fit exactly at the data points, the rms of the fit is identically zero and cannot be used as an indicator of the quality of the fit. We can use  $\chi^2$  though the recovered ground truth data statistics

Table 11 Interpolation with Cubic Splines - Dense Data Sets

Test	Observ. Approx.	Observa- tions Recovered	Average Recovery Error (m)	RMS of Recovery Errors (m)	CPU Time (ms)
I	754	38	-0.032	0.210	125
II	754	37	-0.007	0.147	125

Table 12 Interpolation with Cubic Splines - Sparse Data Set

Test	Observ. Approx.	Observa- tions Recovered	Average Recovery Error (m)	RMS of Recovery Errors (m)	CPU Time (ms)
I	41	15	-0.202	0.944	25

to compare with the least squares estimates. Because splines are very sensitive to data distribution, we have recomputed the statistics for the dense pass after deleting the last entry, which as can be seen from Table 5 is isolated and does not conform with the rest of the test points. This results in a significant improvement of the statistics. One should justify this in the sense that uniformity must exist if one wants to obtain results of some quality. At any rate, it is apparent that the results here show a higher rms error by a factor of two compared to the least squares estimates, but at the same time the computational effort is about three times smaller. In addition to that, because the interpolation over each interval is done using a different constituent of the spline, interpolates from different intervals are totally uncorrelated. One way to show this is the following experiment.

We have recomputed the spline curve for the dense data set, only this time we truncated the data set to data collected prior to  $13^{\text{h}}32^{\text{m}}00^{\text{s}}$ , and thus we are not recovering the last five ranges of the ground truth data. If this is done for the least squares estimator, the errors for the recovered ranges change, because the fit is done using information from all data points simultaneously. In the case of the spline curve though, only local information is used, and as can be seen from Table 13 the errors of recovery are identical at the common points for both the complete  $(\rho_0 - s_C(t))$  and the shortened  $(\rho_0 - s_S(t))$  data sets.

It can now be safely assumed that the interpolation errors for the cubic spline are uncorrelated, and therefore the error characteristics of the interpolated ranges are not altered by this process. For a uniform dense distribution of the base points in the region where the ranges are interpolated, the mean value of the recovery errors is below the centimeter level, and their fluctuation does not indicate a dispersion significantly different from that of the original data (cf. Table 11). It is very simple to check the quality of the interpolated ranges by examining the time intervals  $T_L$  and  $T_R$ . When these intervals are significantly different from their average value over the entire pass, then it might be wise to delete that range from the data set or at least give it a smaller weight in subsequent use. One cannot form strict rules to follow for this procedure; it is more easily solved on a case-by-case basis, and the action taken depends largely on the experience and judgment of the investigator. For the purpose of this study, we feel that the right approach is to delete such ranges completely.

ORIGINAL PAGE IS  
OF POOR QUALITY

Table 13 Comparison of Recovery Errors from Two Cubic Splines  
for the Complete and the Restricted Dense Data Sets

Station No. : 7115 Observation Epoch		<----- T -----> <---- T <sub>L</sub> ----><-- T <sub>R</sub> -->			Recovery Error $p_0 - S_c(t)$ $p_0 - S_r(t)$	
YYMMDD	HMMSS.SSSS	T <sub>L</sub>	T <sub>R</sub>	T	(m)	(m)
800814	131626.0577	1.00	1.00	2.00	0.1000	0.1000
800814	131653.0577	1.00	1.00	2.00	0.1191	0.1191
800814	131714.0577	1.00	1.00	2.00	-0.0708	-0.0708
800814	131735.0577	1.00	1.00	2.00	-0.0515	-0.0515
800814	1318 2.0577	1.00	1.00	2.00	0.1370	0.1370
800814	1320 9.0577	1.00	1.00	2.00	0.0818	0.0818
800814	132032.0578	1.00	1.00	2.00	0.0878	0.0878
800814	132052.0578	1.00	1.00	2.00	-0.1059	-0.1059
800814	132113.0578	1.00	1.00	2.00	-0.1053	-0.1053
800814	132134.0579	1.00	1.00	2.00	-0.0250	-0.0250
800814	132156.0579	1.00	1.00	2.00	-0.0225	-0.0225
800814	132217.0580	1.00	2.00	3.00	-0.0624	-0.0624
800814	132240.0581	1.00	2.00	3.00	-0.0514	-0.0514
800814	1323 4.0581	1.00	1.00	2.00	-0.0791	-0.0791
800814	132325.0582	1.00	1.00	2.00	-0.1289	-0.1289
800814	132345.0583	1.00	1.00	2.00	-0.0216	-0.0216
800814	1324 9.0584	2.00	1.00	3.00	-9.1772	-0.1772
800814	132436.0585	3.00	2.00	5.00	0.0008	0.0008
800814	132518.0586	3.00	1.00	4.00	0.0384	0.0384
800814	132547.0588	3.00	1.00	4.00	0.0733	0.0733
800814	132623.0589	1.00	1.00	2.00	0.2133	0.2133
800814	132652.0591	1.00	1.00	2.00	0.0625	0.0625
800814	132720.0592	6.00	1.00	7.00	-0.3168	-0.3168
800814	132745.0594	2.00	1.00	3.00	-0.1194	-0.1194
800814	132811.0595	2.00	1.00	3.00	-0.0176	-0.0176
800814	132833.0597	1.00	1.00	2.00	0.1412	0.1412
800814	132854.0598	1.00	1.00	2.00	-0.0258	-0.0258
800814	132915.0599	1.00	1.00	2.00	-0.2227	-0.2227
800814	132939.0601	1.00	1.00	2.00	0.0429	0.0429
800814	1330 4.0602	1.00	2.00	3.00	0.1807	0.1807
800814	133038.0604	1.00	1.00	2.00	0.1012	0.1012
800814	1331 5.0606	1.00	1.00	2.00	-0.1256	-0.1256
800814	133137.0609	3.00	1.00	4.00	0.4690	0.4690
800814	1332 9.0611	2.00	1.00	3.00	-0.0813	--
800814	133247.0614	7.00	3.00	10.00	-0.2887	--
800814	133329.0617	2.00	2.00	4.00	-0.0889	--
800814	133427.0622	4.00	1.00	5.00	0.0831	--
800814	133528.0627	14.00	14.00	28.00	-0.9416	--

The ease by which spline interpolation can be applied in our problem and the properties that we have found it to possess encouraged us to use it as the most suitable method for interpolating the quasi-simultaneous ranges required for determining the station-satellite-station range differences.

## 4. THE ESTIMATION PROCESS

### 4.1 Introduction

The motions of the satellite and the observing stations in space have been described in the second chapter in terms of models that depend on a number of parameters. Some of these parameters are obtained from theories based on very long (time-wise) records of observations and therefore carry a great deal of confidence in them (e.g., precession, nutation). A considerable number of these parameters, though, are only approximately known, and part of the reason for requiring an adjustment of the observations is the improvement of their numerical values. The other more obvious reason, of course, is the smoothing of the errors inherent in every measurement process. In short, the adjustment process determines the unknown parameters based on the information contained in the discrepancies between the measured values of the observables and those computed from the assumed model. The operator that relates the corrections in the parameters to these discrepancies is the design matrix of the problem. In the usual case where there are redundant observations available, the row space of the design matrix has a dimension larger than that of its column space. Its rank then is determined by the dimension of its column space. If its columns are linearly independent, then the rank is equal to their number, the dimension of the column space, and the problem will have a unique solution. In the event,

though, that two or more of its columns are linearly dependent, the design matrix is rank deficient, its deficiency determined by the number of interdependent columns. When this happens, the problem does not admit a unique and unbiased estimate for the parameters. Special techniques must be employed in order to obtain even a unique estimate, preferably one with a minimum bias too [Rao, 1973]. Other techniques which are applicable in such a case, although with different properties from the previous one, have been reviewed in [Pavlis, 1979].

The fact that the relationship between observations and parameters may be a nonlinear one, as is the case here, further complicates the process. Although extensive literature exists for the linear model, that for the nonlinear one is very much restricted and hardly ever addresses the validity of extending statistical concepts established for the first for use in cases involving the second. Technically, the solution is most usually obtained by means of a Newton-Gauss iterative procedure [Pope, 1974]. Starting from some approximation to the solution, the nonlinear relationship is expanded as a Taylor series retaining terms up to those including the first derivative. Assuming continuity and boundness for the original nonlinear function, the iteration might converge to the sought-for solution [Pope, 1972]. The convergence can be established by examining the percent change in the weighted sum of squares of the residuals between successive iterations. This test quantity can also be used to detect a divergent problem or an oscillating one. Possible explanations for these cases can be found, for instance, in [Hamilton, 1964; Pope, 1972; Uotila, 1975].

Even when the problem has converged because of the nonlinearity, one cannot be sure that the solution is the one that corresponds to the infimum of the weighted sum of squares of the residuals. It is always possible, depending on the starting approximate solution and the nature of the particular function involved, to converge to a local minimum. To assure the global convergence one would have to use several and widely differing starting approximations and establish that the algorithm always converges to the same minimum. This can hardly ever be accomplished in practice due to the large number of observations involved, but then again one has in most cases a very good idea of what values the parameters take on, and therefore in practice such dismal cases are scarce [Hamilton, 1964].

What is very real, however, is the fact that the DOC process as applied herein, and almost everywhere else, is neither a least squares adjustment nor a minimum variance one in the standard statistical sense of these terms [Rao, 1973]. The required partial derivatives in the Taylor expansion are determined in part numerically from the integration of the variational equation of state rather than from some well-defined analytical expression. It is then possible, even probable, that incorrect modeling or omission of the effect of dominant forces in the orbital model will result in an incorrect or strongly biased solution. The fact that the solution is obtained by means of the formulas for either of the aforementioned statistical adjustment procedures is not enough justification to call the result unbiased. Since we never know all the mechanisms that govern the orbit of the satellite perfectly, we are not entitled to use the term unbiased even in the cases when all the unknown



parameters entering the mathematical expressions of these mechanisms are being determined from the observations themselves. The best that we can probably have is a "conditionally unbiased" estimate of these parameters, the condition being that the assumed model reflects reality to a degree that exceeds the effect of computer round-off errors in the final result. Obviously, with the limited knowledge of the model, it is to our advantage to use the available observations in ways that will minimize the effect of this deficiency in the resulting solution, which is one of the objectives of this investigation. Nevertheless, the conditional unbiasedness of the results still holds, and it would be unrealistic to advocate the opposite just because technically the same mathematical formulas are used in both adjustment algorithms.

We finally want to address here an issue that some might object to, that is, the use of quantities (the simultaneous range-differences) as observations in the estimation which are not really observed, but rather inferred from observed quantities (the ranges). If we wanted to avoid this question but still be able to use the observed ranges in a differencing mode, we would have to modify our mathematical model in a way that the difference of simultaneous ranges and the parameters satisfy condition equations involving both. This mathematical mode, known as "combined model" [Uotila, 1967], will result in a solution that is identical with that obtained from the simpler model where the "pseudo-observed" SRD's are written as a function of the parameters alone (observation equations model).

#### 4.2 Differential Relations Between the Observable and the Parameters

Let  $\bar{F}$  be a vector function in  $\bar{X}$ , continuously differentiable. A first-order approximation of  $\bar{F}$  over a differentially small region about  $\bar{X} = \bar{X}_s$  can be obtained by expanding  $\bar{F}$  in Taylor series and retaining terms up to and including the first derivative:

$$\bar{F}(\bar{X}) \approx \bar{F}(\bar{X}_s) + \left[ \frac{\partial \bar{F}(\bar{X}_s)}{\partial \bar{X}} \right] (\bar{X} - \bar{X}_s) \quad (91)$$

Using (91) we can linearize the SRD function in order to be able to adjust them in the DOC process.

Let  $\bar{S}$  denote the vector of Cartesian CES referred coordinates of the satellite at the instant of an observation  $\delta\rho$ , and  $\bar{G}_1, \bar{G}_2$ , the corresponding coordinate vectors of the observing stations in the same system. We can express  $\delta\rho$  as

$$[\delta\rho_i] = [(\bar{S}_i - \bar{G}_2)^T (\bar{S}_i - \bar{G}_2)]^{\frac{1}{2}} - [(\bar{S}_i - \bar{G}_1)^T (\bar{S}_i - \bar{G}_1)]^{\frac{1}{2}} \quad (92)$$

where  $i$  is the number of observations. We can now identify  $[\delta\rho_i]$  as  $\bar{F}(\bar{X})$ , and  $\bar{X}$  as the vector containing the station and satellite positions along with several other parameters relating to the orbital model and the CIS to CES and CTS to CES transformations.

The relationship between these frames of reference is expressed through the orthogonal rotations for precession (P), nutation (N), earth rotation ( $\theta$ ), and polar motion (C) as

$$\bar{S}_i = [NP]\bar{R}_i \quad (\text{CIS} \rightarrow \text{CES}) \quad (93)$$

$$\bar{G}_j = [C\theta]^T \bar{U}_j \quad (\text{CTS} \rightarrow \text{CES}) \quad (94)$$

Because of the similarity of the two terms in (92), we need only form the partial derivatives for the first term; the ones for the second can

then be readily obtained by changing the index in the  $\bar{G}_j$  vector. The partial derivatives for  $\delta\rho_j$  can then be formed by differencing these two partials. From the above the only elements of the transformations that will be treated as unknown are contained in the matrices C and  $\Theta$ . From [Mueller, 1969],

$$C \approx \begin{bmatrix} 1 & 0 & x \\ 0 & 1 & -y \\ -x & y & 1 \end{bmatrix} \quad (95)$$

and

$$\Theta = \begin{bmatrix} \cos\theta & \sin\theta & 0 \\ -\sin\theta & \cos\theta & 0 \\ 0 & 0 & 1 \end{bmatrix} \quad (96)$$

where x,y are the coordinates of the celestial pole with respect to a local tangent plane coordinate system with its origin at the North CTS pole, its x-axis on the  $\lambda=0^\circ$  meridian, and its y-axis on the  $\lambda=270^\circ$  meridian, and  $\theta$  is the angle of rotation between the first axis of the CTS (origin of longitudes) and the first axis of the instantaneous CES. The x and y will be considered as parameters of the problem to be determined in the adjustment. We can also include the rate of change of  $\theta$  as a parameter in hopes of determining "length-of-day" variations; however, for reasons explained in [Van Gelder, 1978], this is best determined from observations with alternate techniques such as VLBI (Very Long Baseline Interferometry), rather than SLR.

The orbit is adjusted in terms of corrections to the initial approximation of the satellite's orbital elements at a fixed epoch. The instantaneous discrepancies at the epochs of observation are related

to these parameters through the transition matrix  $Y$ , obtained from the integration of the variational equation of state as formulated in Section 2.2.1, equation (6). This enables us to write:

$$d\bar{R}_i = Y [d\bar{R}_0; \dot{d}\bar{R}_0]^T \quad (97)$$

where  $[\bar{R}_0; \dot{\bar{R}}_0]^T$  is the initial epoch satellite - state vector.

Working with one range  $\rho_{ij}$  at a time, where

$$\rho_{ij} = [(\bar{S}_i - \bar{G}_j)^T (\bar{S}_i - \bar{G}_j)]^{\frac{1}{2}} \quad (98)$$

and letting  $\bar{T}_{ij}$  denote  $\bar{S}_i - \bar{G}_j$  for brevity, we use the chain rule of differentiation to obtain:

$$\begin{aligned} d\rho_{ij} = & \left[ \left( \frac{\partial \rho_{ij}}{\partial \bar{T}_{ij}} \right) \left( \frac{\partial \bar{T}_{ij}}{\partial \bar{U}_j} \right) \right] d\bar{U}_j + \left[ \left( \frac{\partial \rho_{ij}}{\partial \bar{T}_{ij}} \right) \left( \frac{\partial \bar{T}_{ij}}{\partial \bar{S}_i} \right) \left( \frac{\partial \bar{S}_i}{\partial \bar{R}_i} \right) \right] \left[ \left( \frac{\partial \bar{R}_i}{\partial \bar{R}_0} \right); \left( \frac{\partial \dot{\bar{R}}_i}{\partial \dot{\bar{R}}_0} \right) \right] \left[ \begin{array}{c} d\bar{R}_0 \\ \dot{d}\bar{R}_0 \end{array} \right] \\ & + \left[ \left( \frac{\partial \rho_{ij}}{\partial \bar{T}_{ij}} \right) \left( \frac{\partial \bar{T}_{ij}}{\partial \bar{G}_j} \right) \left( \frac{\partial \bar{G}_j}{\partial x} \right) \right] dx + \left[ \left( \frac{\partial \rho_{ij}}{\partial \bar{T}_{ij}} \right) \left( \frac{\partial \bar{T}_{ij}}{\partial \bar{G}_j} \right) \left( \frac{\partial \bar{G}_j}{\partial y} \right) \right] dy \end{aligned} \quad (99)$$

Using now (93) and (94) and the definitions for  $C$ ,  $\Theta$ , and  $\bar{T}_{ij}$ , the required partial derivatives for evaluation of (99) are determined explicitly:

$$\frac{\partial \rho_{ij}}{\partial \bar{T}_{ij}} = \frac{1}{\rho_{ij}} \bar{T}_{ij}^T \quad (100)$$

$$\frac{\partial \bar{T}_{ij}}{\partial \bar{U}_j} = - {}_3[C\Theta]_3^T \quad (101)$$

$$\frac{\partial \bar{T}_{ij}}{\partial \bar{S}_i} = {}_3[I]_3 \quad (102)$$

$$\frac{\partial \bar{S}_i}{\partial \bar{R}_i} = {}_3[NP]_3 \quad \text{ORIGINAL PAGE IS OF POOR QUALITY} \quad (103)$$

$$\left[ \begin{array}{c} \left( \frac{\partial \bar{R}_i}{\partial \bar{R}_0} \right) \\ \left( \frac{\partial \bar{R}_i}{\partial \dot{\bar{R}}_0} \right) \end{array} \right] = {}_3[Y]_6 \quad (104)$$

$$\frac{\partial \bar{T}_{ij}}{\partial \bar{G}_j} = -{}_3[I]_3 \quad (105)$$

$$\frac{\partial \bar{G}_j}{\partial x} = \begin{bmatrix} -U_{j3} \cos \theta \\ -U_{j3} \sin \theta \\ U_{j1} \end{bmatrix} \quad (106)$$

$$\frac{\partial \bar{G}_j}{\partial y} = \begin{bmatrix} -U_{j3} \sin \theta \\ U_{j3} \cos \theta \\ -U_{j2} \end{bmatrix} \quad (107)$$

Expressions (100) through (107) can be substituted in (99) to obtain the explicit first-order differential of  $\rho_{ij}$  with respect to the parameter vector  $[\bar{U}_j^T \ ; \ \bar{R}_0^T \ ; \ \dot{\bar{R}}_0^T \ ; \ x \ ; \ y]^T$ . Writing the resulting equation for  $j=1$  and  $j=2$ , and subtracting the two, we obtain the differential

$$d\delta\rho_i = d\rho_{i2} - d\rho_{i1} \quad (108)$$

which corresponds to the SRD of equation (92).

Assuming now that our initial approximation for the unknown parameters is close to their true values, we can use this differential expression (108) in connection with the Taylor expansion (91), where the following equalities are identified:

$$\bar{X} = [\bar{U}_j^T \ ; \ \bar{R}_0^T \ ; \ \dot{\bar{R}}_0^T \ ; \ x \ ; \ y]^T \quad (109)$$

$$\bar{F}(\bar{X}) = [\delta\rho_i + e_i] \quad (110)$$

with  $e_j$  denoting errors to be estimated during the adjustment. Note that in practice there will be a number of x,y parameter pairs in a problem since these represent averages of the coordinates of the pole over a predetermined time interval (e.g., five-day averages). With  $\bar{X}_s$  being the initial approximation to the parameters, and letting  $\bar{\beta} = \bar{X} - \bar{X}_s$ , we get:

$$\bar{\beta} = [d\bar{U}_j^T \ ; \ d\bar{R}_0^T \ ; \ d\bar{R}_0^T \ ; \ dx \ ; \ dy]^T \quad (111)$$

We will use the notation  $A_i$  to indicate the  $i$ th row of the design matrix which consists of the partial derivatives with respect to the parameters  $\bar{X}$  (arranged in precisely the same order). In addition, we let  $\bar{r}$  denote the residuals, estimates of the errors  $\bar{e}$ , and  $\bar{d}$ , the discrepancy vector:

$$\bar{d} = \bar{r}(\bar{X}_s) - [\delta\rho_i] \quad (112)$$

We can now write the linearized mathematical model in terms of the established notation, which results in the set of observation equations to be adjusted:

$$[r_i] = [A_{ij}][\beta_j] + [d_i] \quad (113)$$

The explicit expressions for the elements  $A_{ij}$  of the design matrix are further developed in Appendix C.

### 4.3 Estimable Parameters

The concept of "estimability" or "estimable parameters" was first introduced by R.C. Bose [1947] in an attempt to expand the applicability of the well-known theorem of Gauss-Markov [Rao, 1973]. In [ibid.] the estimability of the parameters or parametric functions in an estimation problem is examined through the rank of the design matrix of the experiment. Because of the fact that a matrix can become "algorithmically" rank deficient due to ill-conditioning [Forsythe and Moler, 1967], there has been some confusion in the past as to the status of geodetic parameters estimated from dynamic space techniques.

The truth of the matter is that the status of a parameter in this respect is determined by the underlying physical reality and not by the numerical entries of a matrix or their interrelationship. The scientific interest in this subject is reflected by some rather extensive literature, the most recent ones being [Van Gelder, 1978; Grafarend and Livieratos, 1978; Grafarend and Heinz, 1978; Pavlis, 1979]. None of these investigations, though, has looked at this issue from the physical point of view. The estimability of a parameter should be determined by two simple factors. Either the observations contain information about the parameter, or the model contains information, or both.

It is a trivial exercise to show that range measurements and linear measurements in general contain only scale information and are independent of the coordinate system that is used in the parametrization of the problem. On the other hand, the physical model describing the dynamics of the satellite contains information that is enough to define a particular coordinate system. If the harmonic coefficients for the

geopotential are assumed known, then the satellite orbit becomes sensitive to the coordinate system in which these coefficients are referenced. It is only a peculiarity of the physical figure of the Earth that two out of the three principal moments of inertia are nearly equal [Heiskanen and Moritz, 1967], namely, the equatorial moments; the definition of the origin of longitudes, therefore, is a very weak one. This is, in fact, the reason why in dynamic solutions with only metric measurements the longitude of one of the participating stations is kept fixed. This is not the only solution to overcome a case of pure ill-conditioning, but it is the most popular and the simplest to apply.

It is thus obvious that there is no rank deficiency in the dynamic problem of satellite geodesy conditional on the fact of a finite expression for the geopotential, but rather an extreme ill-condition due to the aforementioned reasons. With that in mind we can further investigate the interaction between parameters of interest to determine which of them are separable in a simultaneous adjustment. This can be best accomplished by examining the information required for their determination.

#### 4.3.1 Information required for the determination of the problem parameters.

The goal of this investigation is primarily the determination of interstation baseline distances and variations in the coordinates of the celestial pole. The former are obtained from the estimated station coordinates, while the latter are determined as additional rigid body rotations of the station network with respect to the satellite orbit, in addition to the modeled rotations included in the transformation



between the CTS and the CIS systems. The estimation will be based on simultaneous range-differences reduced in a long-arc dynamic mode solution. We examine here the complete observation equation with parameters, the station positions, the coordinates of the pole, and the initial state vector of the satellite to determine which of them are separable and therefore design experiments in which those parameters of primary interest will be estimable.

For the sake of brevity, the form of the observation equations used in this section is the "body-fixed" form presented in Appendix C. In the following, the prefix  $\Delta$  will denote differences of coordinates,  $W$  will denote the variational partials matrix rotated in the CTS system with  $W(j)$  denoting the  $j$ th column of that matrix. Subscripts will refer to station positions and superscripts to satellite positions. The letters  $X$ ,  $Y$  and  $Z$  will denote CTS coordinates, and coordinate differences are always taken between a satellite position and that of the observing station, i.e.,

$$\Delta X_2^1 = X^1 - X_2 \quad (113)$$

We write here two observation equations, each from a different pair of stations to a different satellite position. The parameter list is in the following order:

- (1) Station coordinates  $X, Y, Z$  for each of the stations,
- (2) Satellite state vector at initial epoch, and
- (3)  $x, y$  coordinates of the pole.

With three parameters for each of the four stations, six for the state vector, and two for the pole, there are twenty parameters in total, and



the design matrix  $A$  given in equation (114) will have twenty columns. In identifying linear dependencies between the parameters, we will use the notation  $A(j)$  for the  $j^{\text{th}}$  column of  $A$ . We can separate  $A$  into three submatrices according to the three major groups of parameters as previously stated:

$$A = [A_G \ ; \ A_S \ ; \ A_P] \quad (115)$$

with  $A_G$  consisting of the partials with respect to ground station coordinates,  $A_S$ , partials with respect to the satellite state vector, and  $A_P$ , partials with respect to the coordinates of the pole. From the definition of these groups and (114), we can state that there are no linear dependencies between columns of the design matrix within the same group. We concentrate, therefore, in finding the dependencies, if any, between columns of the design matrices among different groups. We are investigating here whether it is possible to find a set of constants  $\{c_1, \dots, c_{20}\}$ , not all zero, such that the following equality holds:

$$c_1 A(1) + c_2 A(2) + \dots + c_{20} A(20) = 0 \quad (116)$$

At first glance it would seem as if the columns of the  $A_S$  submatrix can be written as combinations of those of  $A_G$ . This is not so, though, since the  $W$  matrix is different from one observation to the next; and therefore its elements  $w_{ij}$  which are used in forming  $A_S$  differ too (which is obvious by the different superscripts in (114)). In the case of  $A_P$  and  $A_G$ , however, one can easily write the following relationships between their columns for the first observation:

$$(-Z_2)A_G(4) + (X_2)A_G(6) + (-Z_1)A_G(1) + (X_1)A_G(3) = A_P(1,1) \quad (117)$$

$$(-Y_2)A_G(6) + (Z_2)A_G(5) + (-Y_1)A_G(3) + (Z_1)A_G(2) = A_P(1,2) \quad (118)$$

and for the second:

$$(-Z_4)A_G(10) + (X_4)A_G(12) + (-Z_3)A_G(7) + (X_3)A_G(9) = A_p(2,1) \quad (119)$$

$$(-Y_4)A_G(12) + (Z_4)A_G(11) + (-Y_3)A_G(9) + (Z_3)A_G(8) = A_p(2,2) \quad (120)$$

Observing now the location of zero elements in  $A_G$ , we can combine the above in one equation that shows the existing sought for set of constants C to be:

$$C = \begin{bmatrix} -Z_1 & Z_1 & -Y_1+X_1 & -Z_2 & Z_2 & -Y_2+X_2 & -Z_3 & Z_3 & -Y_3+X_3 & -Z_4 & Z_4 & -Y_4+X_4 \\ 0 & 0 & 0 & 0 & 0 & 0 & -1 & -1 \end{bmatrix} \quad (121)$$

so that:

$$AC^T = [\phi] \quad (122)$$

The zero elements of C correspond to the columns of A which constitute the submatrix  $A_S$ . Dependencies between  $A_S$  and  $A_p$  do not exist, for if they did we would come to the contradiction that  $A_p$  which is a linear transformation of  $A_G$  can be written as a transformation of  $A_S$  and at the same time  $A_S$  can be independent of  $A_G$ .

We come to the conclusion, therefore, that we cannot separate the station parameters and the ones for the pole in a simultaneous adjustment. Theoretically, this dependence would be broken if (122) did not hold even for just one row of A. If that is the case, we assumed that x,y are known for the first (say) observation, and we set the corresponding partials  $A(1, 19)$ ,  $A(1, 20)$  equal to zero. The problem is that if we were to check the column independence of the resulting A matrix using (122), we would find that the result differs from zero only slightly. That means the corresponding parameters have extremely strong correlations, and the normal equations will be algorithmically singular. If the above is repeated for several rows of A, the condition of the

normal equations is improved, but one must realize that in this case the station coordinates are being determined from these first observations, the rest of them contributing very little due to the confounding between the two groups of parameters.

Conceivably, we could assume that the coordinates of the pole are known from previous solutions, for a sufficiently long period of time so that data available over that period can be used for the estimation of station positions alone. With our present capabilities in laser ranging, it would be required that data over more than a month's interval be used for this purpose, in order to achieve sufficiently accurate station positions for subsequent estimation of the global motions of this network. Objections that one can raise against this practice is the bulk of computations that need to be repeated in every solution and the fact that the coordinates of the pole estimated in each of these solutions refers to the CTS defined by the simultaneously estimated station positions. That is to say, every solution defines a new CTS. This is obviously the most undesirable of the two side effects of a simultaneous solution. It would therefore be more meaningful to do a separate solution for the stations from that for the coordinates of the pole. Adopting the resulting CTS at some epoch, we could then monitor the rotations of the defining network of stations with respect to the celestial pole by means of independent solutions in which the station positions are not allowed to adjust.

#### 4.4 Minimization of Model Biases by Use of SRD Observations

We have already seen that the adjustment of satellite ranging data is based on a model that involves hundreds or thousands of parameters, none of which is perfectly known. Moreover, it is practically impossible to include all of them as unknown parameters of the problem. We therefore resort to the option of adopting a fixed value for a number of them. Such a practice obviously biases the results of the adjustment since the adopted values differ from the ever unknown true values of the fixed parameters. From the description of the ranging model it should be clear that the most parameters which are held fixed are those involved in the determination of the satellite orbit (e.g., geopotential coefficients). Their errors affect the quality of the orbit directly, and when the model value for the range is computed from this orbit to compare it to the observed one, the errors propagate into the discrepancy vector and thereby in the solved for parameters. We will see now how these biases can be diminished if we take advantage of the simultaneity of the observations and use them in the simultaneous range-difference mode.

Assume that we have two sets of range data in which each observation from the first is taken at the same time to the same satellite position as the corresponding one from the second set. If we were to difference these data sets we would obtain the SRD data as we have described them in Chapter 3. The linearized observation equations for these two data sets can be written as

$$\begin{aligned} r_1 &= A_1\beta + d_1 \\ r_2 &= A_2\beta + d_2 \end{aligned} \tag{123}$$

and the solution for the parameters  $\beta$  is

$$\beta = -(A_1^T \Sigma_1^{-1} A_1 + A_2^T \Sigma_2^{-1} A_2)^{-1} (A_1^T \Sigma_1^{-1} d_1 + A_2^T \Sigma_2^{-1} d_2) \quad (124)$$

We have considered here the case of common parameters  $\beta$  for both data sets since the data are taken on the same satellite arc, and as we mentioned above the major source of bias is the computed satellite orbit.

The discrepancy vector  $d$  can be written out in terms of its components as

$$d_i = F_i(\beta_0) - \rho_i^0 \quad (125)$$

where  $F_i(\beta_0)$  is the model computed range and  $\rho_i^0$  the one observed. If the fixed parameters were fixed at their true values, then the computed range would have a different value,  $\rho_i^C$ . That would, of course, be the desired value also, although this is practically impossible. The term  $F_i(\beta_0)$  then has two components, one being  $\rho_i^C$  and the other being the bias  $b_i$ :

$$F_i(\beta_0) = \rho_i^C + b_i \quad (126)$$

Using (126) in (124) and denoting with  $N$  the matrix of normal equations, the resulting expression for the solved for parameters  $\beta$  becomes

$$\beta = -\{N^{-1}[A_1^T \Sigma_1^{-1}(\rho_i^C - \rho_i^0)_1 + A_2^T \Sigma_2^{-1}(\rho_i^C - \rho_i^0)_2] + N^{-1}[A_1^T \Sigma_1^{-1} b_1 + A_2^T \Sigma_2^{-1} b_2]\} \quad (127)$$

The first term in (127) represents the proper adjustment in the parameters  $\beta$  based on the information in the observations, while the second is the bias term in  $\beta$  due to errors in the adopted values of the nonadjusting parameters of the model. A secondary and much less serious effect of the erroneous model parameters is the error in the elements

of the design matrices  $A_1$  and  $A_2$  which in general are functions of these parameters. These errors, however, are more important in computing the covariance matrix of the adjusted parameters than in estimating  $\beta$ .

We will now derive the corresponding adjustment equations for the SRD mode. Since the order in which the observations have been arranged is not important in the adjustment, we may assume that the two data sets are already in correspondence, i.e.,

$$\rho_{1i} \leftrightarrow \rho_{2i} \quad \text{in the sense that:} \quad \delta\rho_i = \rho_{2i} - \rho_{1i} \quad (128)$$

From (123) and (128) then it follows that the linearized observation equations for the SRD mode are:

$$A\beta + d = r \quad (129)$$

with

$$\begin{aligned} A &= [A_2 - A_1], \\ d &= d_2 - d_1, \text{ and} \\ r &= r_2 - r_1 \end{aligned} \quad (130)$$

The minimum variance adjustment estimate for the solved for parameters will then be

$$\beta = -\{[(A_2^T - A_1^T)(\Sigma_1 + \Sigma_2)^{-1}(A_2 - A_1)]^{-1} (A_2^T - A_1^T)(\Sigma_1 + \Sigma_2)^{-1}(d_2 - d_1)\} \quad (131)$$

where we have used  $\Sigma_1 + \Sigma_2$  as the variance-covariance matrix of the SRD pseudo-observations as obtained through error propagation on the basis of (128).

Writing the discrepancy vector in its components again, we obtain the following:

$$d \equiv d_2 - d_1 = (\rho_2^C - \rho_1^C) - (\rho_2^O - \rho_1^O) + (b_2 - b_1) = \delta\rho^C - \delta\rho^O + (b_2 - b_1) \quad (132)$$

Denoting by  $\bar{N}$  the matrix of normal equations in (131) and considering (132) we can write



$$\beta = -\{\bar{N}^{-1}[(A_2^T - A_1^T)(\Sigma_1 + \Sigma_2)^{-1}(\delta\rho^C - \delta\rho^O)] + \bar{N}^{-1}[(A_2^T - A_1^T)(\Sigma_1 + \Sigma_2)^{-1}(b_2 - b_1)]\} \quad (133)$$

for the estimate of the parameters' adjustment from SRD observations. The last term in (133) is again the bias term, only this time it involves the difference of the bias in each of the computed ranges. Naturally, the two bias components  $b_1$  and  $b_2$  do not always have the same sign or magnitude, so we cannot outrightly set the last term to zero. We will examine though the behavior of this difference in comparison to its individual components by means of a simulation study.

#### 4.4.1 Simulation study for bias propagation characteristics.

The computation of  $\delta\rho^C$  is based on the coordinates of the observing stations and those of the satellite at the epoch of the observation. We will introduce known biases in the satellite coordinates and then examine how these biases and to what extent they affect the computed ranges  $\rho_1^C$  and  $\rho_2^C$ , as well as the corresponding SRD's  $\delta\rho^C$ . To simplify the computations, we will assume a spherical earth model and a satellite orbiting at the mean altitude of Lageos on a circular orbit. These assumptions are well justified since they are not too far from the real situation, and we are only after order of magnitude of the biases rather than exact numbers. We have computed the biases on the intersection points of a  $1^\circ \times 1^\circ$  grid covering the area around the observing stations and then plotted the results to ease their evaluation. It is common to state orbital errors in three directions, the radial, the along-track and the across-track, but we have chosen to use the radial, latitudinal, and longitudinal directions. This simplifies the computations without altering the results, and it also has the advantage that the bias-surface

plots are applicable for a much wider class of orbits, while otherwise we would have to restrict ourselves to those having the same inclination with Lageos as well as the same mean orbital altitude. Although we have tested several station configurations in terms of absolute position on the earth's surface, as well as relative to each other, we will present and discuss here only two cases which are representative of the complete set. In case A the observing stations are 2000 km apart (chord distance between them), while in case B we decreased the distance to 200 km. For both cases we have taken the first station to be at latitude  $40^\circ$  N and longitude  $0^\circ$ , while the second occupies four different positions so that the azimuth of the great circle arc connecting the two is  $0^\circ$ ,  $30^\circ$ ,  $60^\circ$ , and  $90^\circ$  counting clockwise positive from the meridian of the first station.

The satellite coordinates at the grid points are computed from the spherical coordinates  $r, \phi, \lambda$  using

$$\begin{aligned} X &= r \cos\phi \cos\lambda \\ Y &= r \cos\phi \sin\lambda \\ Z &= r \sin\phi \end{aligned} \tag{134}$$

and the biases in  $X, Y, Z$  are obtained from the adopted values in the  $r, \phi, \lambda$  system using the following transformation which follows from differentiation of (134):

$$\begin{bmatrix} \Delta X \\ \Delta Y \\ \Delta Z \end{bmatrix} = \begin{bmatrix} X/r & -XZ/p & -Y \\ Y/r & -YZ/p & X \\ Z/r & p & 0 \end{bmatrix} \begin{bmatrix} \Delta r \\ \Delta\phi \\ \Delta\lambda \end{bmatrix} \tag{135}$$

where we have used the following substitutions

$$\begin{aligned} p &= \sqrt{X^2 + Y^2} \\ \sin\phi &= Z/r & \cos\phi &= p/r \\ \sin\lambda &= Y/p & \cos\lambda &= X/p \end{aligned} \quad (136)$$

The values of  $\Delta r$ ,  $\Delta\phi$ , and  $\Delta\lambda$  used in the simulations are

$$\begin{aligned} \Delta r &= 2.00 \text{ m} \\ \Delta\phi &= 0''01 \\ \Delta\lambda &= -0''02 \end{aligned}$$

These values were arbitrarily chosen; their order of magnitude though reflects the present level of stability in the satellite orbit defined and maintained reference frames.

#### 4.4.2 Analysis of the simulation results.

Using equation (135) we have separated the biases into their components  $\Delta X_\phi$ ,  $\Delta X_\lambda$ ,  $\Delta X_r$ , etc. so that we can study individually the propagation characteristics of each one of them and their effects on the computed ranges and SRD's.

This arrangement resulted in three sets of biases (the radial, the latitudinal, and the longitudinal) for each station configuration considered. These biases are, of course, three-dimensional functions that depend on the absolute as well as the relative positions of the observing stations and the observed satellite points. An optimal way of displaying their features and characteristics is to create contour plots in the regions of interest. This is what is presented and discussed in this section. The contour plots which are discussed here are based on the results of the simulations described in Section 4.4.1.

The quantity which is plotted is the bias in the range/SRD due to the biases introduced in the orbit. In all cases this bias is plotted

in centimeters. The following example will clarify the use of these "bias surface" contour plots.

From Fig. 7(a) we find that when station 1 is ranging to Lageos at a point with subsatellite coordinates  $\phi = 37^\circ$  N and  $\lambda = 10^\circ$  E, the bias in the computed range due to the 2.00 m radial bias in the orbit used will be 1.98 m or 198 cm. Fig. 8(a) shows that when the same satellite point is observed from station 2, the bias in this case is about 1.88 m. When the two ranges though are subtracted to create an SRD observation, the resulting bias is only 10 cm (!), as can be verified from Fig. 11(a).

Inspection of the bias surface contour plots leads to a number of interesting remarks. The radial bias surface is bell shaped with its apex on the observing station's radius. The latitude and longitude bias surfaces exhibit an antisymmetry, the former with respect to a line of almost constant latitude (equal to that of the observing station), and the latter with respect to the station's meridian. The form of these three surfaces depends on the absolute position of the station only in the case of the latter two, and in this case the one for latitude depends only on the latitude of the station. In any event, their shape changes very slowly and since a coobserving pair of stations should not be more than about 2000 km apart (in case of Lageos), for all practical purposes we can assume the corresponding surfaces to be the same. Finally, as far as the smoothness of these surfaces is of concern here, we can see from their contour plots that at least in the vicinity of the observing stations the radial bias surface is by far the most flat of the three, the other two exhibiting considerably stronger gradients.

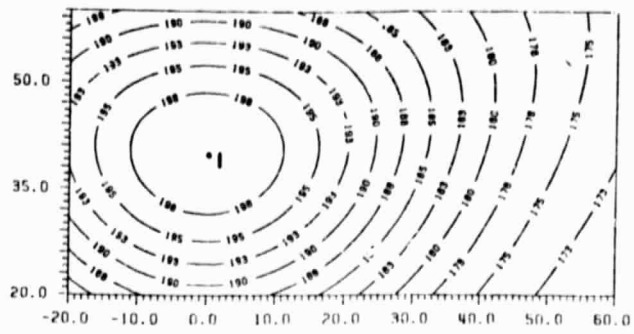
The bias surfaces for the range differences are computed exactly as the differences of the true SRD values from the biased ones. They represent therefore the difference surface of the corresponding range bias surfaces. On the basis of this observation and the previous discussion on the propagation characteristics of the various biases, it should come as no surprise that radial biases are almost completely eliminated when we use the SRD mode. Compare, for instance, the contour levels between Figs. 7(a) and 11(a). In addition to this we also note that the level to which this bias can be eliminated depends on the distance between the two stations as well as the relative location of the satellite track and the interstation baseline. The closer the stations, the smaller the remaining bias in the SRD's, as one can verify from Figs. 11 and 12. Since the two surfaces are nearly the same in the vicinity of the stations, their difference will be smallest in the area between the two stations and close to their baseline. If one now considers the fact that as the interstation distance increases, the area in which simultaneous observations are possible "shrinks" towards the point amid the two stations, it becomes obvious that the SRD mode has a clear advantage over simple ranging in the case of radial bias in the satellite orbit.

The situation is quite the opposite in the case of latitude and longitude biases. Since the range bias surfaces in this case have different signs in different areas, it is possible that for some areas the biases will increase in the SRD mode while they will still decrease in others. This is indeed what happens in the area in between the two stations as Figs. 7(b), 9 and 13 show for the latitudinal bias, and Figs. 7(c), 10 and 15, for the longitudinal case. If, however, the length of

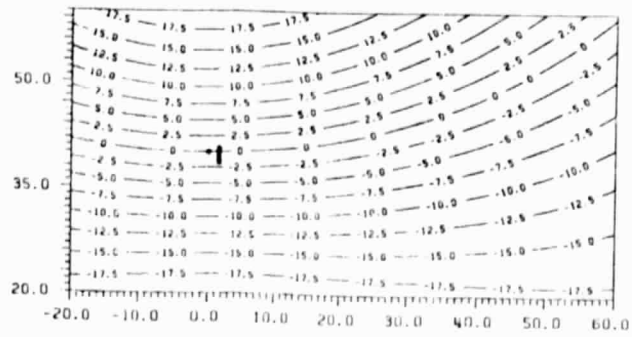
the interstation distance is decreased so that most of the coobservable satellite positions lie outside the critical area, then the SRD mode will again be biased to a much more limited extent than the ranging mode. This is illustrated by the 200 km baseline example in Figs. 14 and 16 which should be compared to the range bias surfaces shown in Figs. 7(b) and 7(c). We do not have to go to the extreme of using only very short baselines since the high altitude of Lageos allows for a rather extensive area of coobservable satellite positions even when the interstation distance is quite long. With a spherical approximation, the radius of Lageos observability around a station is about  $60^\circ$ . That means an area that is almost one-third of the total of the globe. Hence even with longer baselines, the SRD mode can be considerably less affected by biases in the latitude and longitude directions compared to the ranging mode if the data are collected in a region that excludes the immediate vicinity of the baseline.

In general, all three types of biases will affect the computed range differences, and we thus have to select our data in a way that all of them will be minimized simultaneously. Since the radial bias is minimized independent of the satellite position, the guidelines are set by the requirements we mentioned above for the minimization of the latitudinal and longitudinal biases.

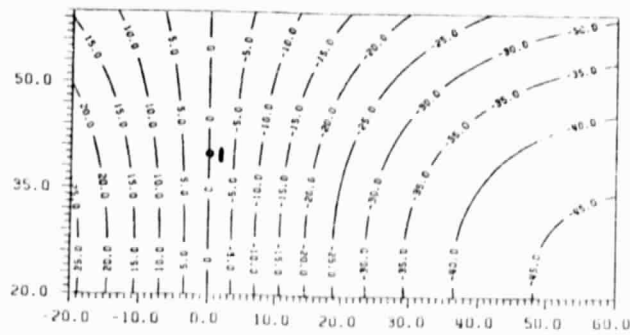
ORIGINAL PAGE IS  
OF POOR QUALITY



(a) radial



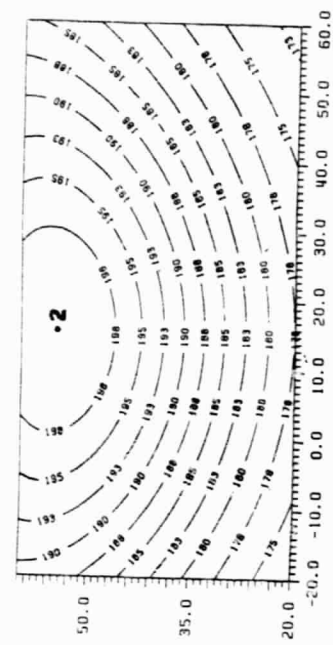
(b) latitudinal



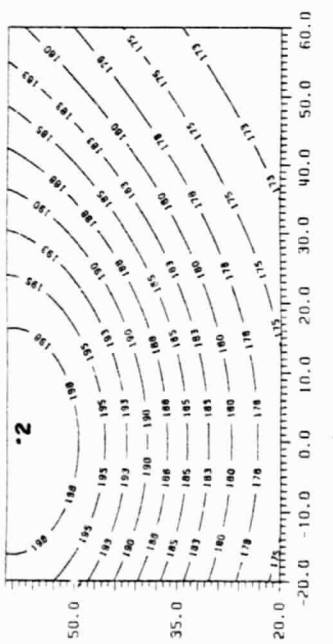
(c) longitudinal

Fig. 7 Range bias surfaces for the fixed station 1.

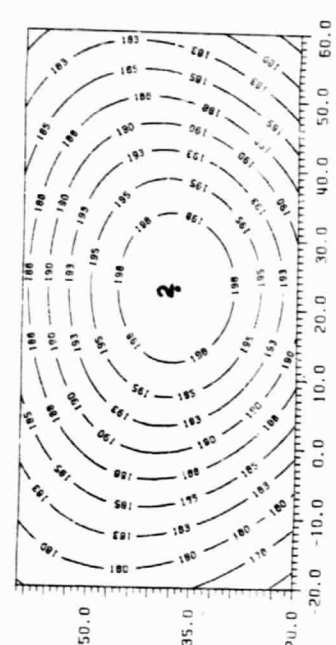
ORIGINAL PAGE IS  
OF POOR QUALITY



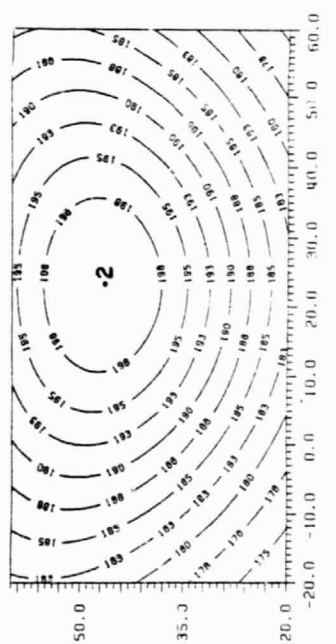
(a) 0° azimuth



(b) 30° azimuth



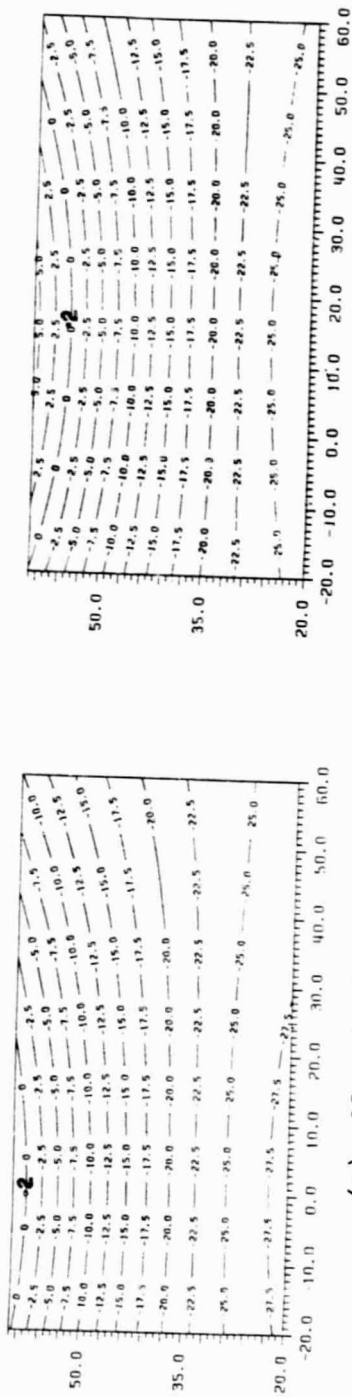
(c) 60° azimuth



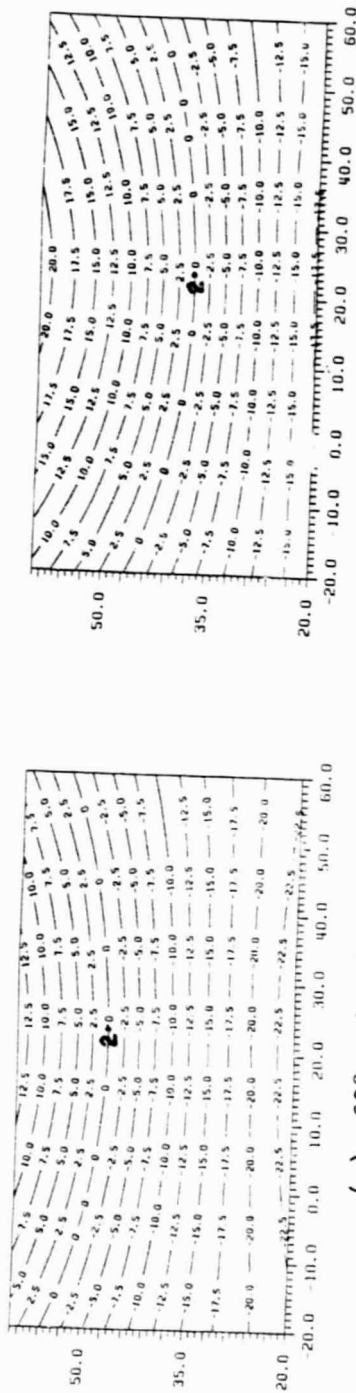
(d) 90° azimuth

Fig. 8 Radial bias surfaces for ranges from the four locations of station 2 (values in centimeters).





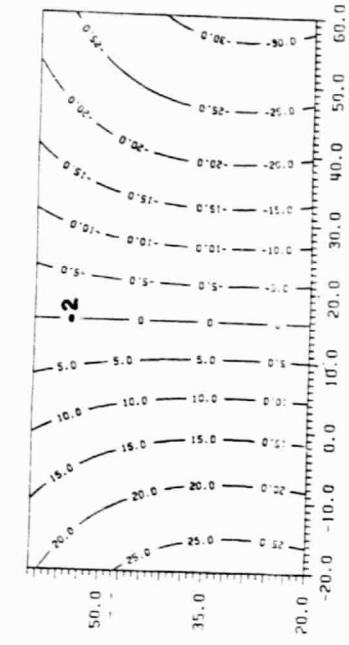
(b) 30° azimuth



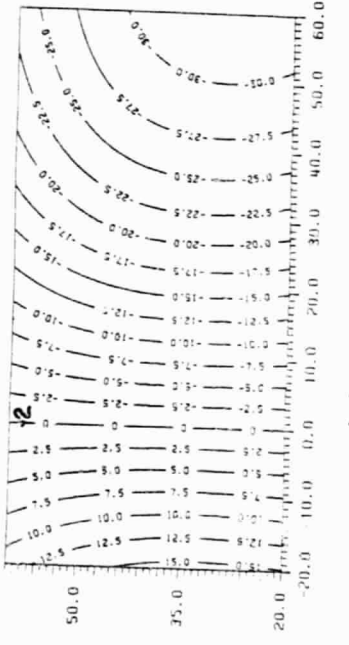
(d) 90° azimuth

Fig. 9 Latitudinal bias surfaces for ranges from the four locations of station 2 (values in centimeters).

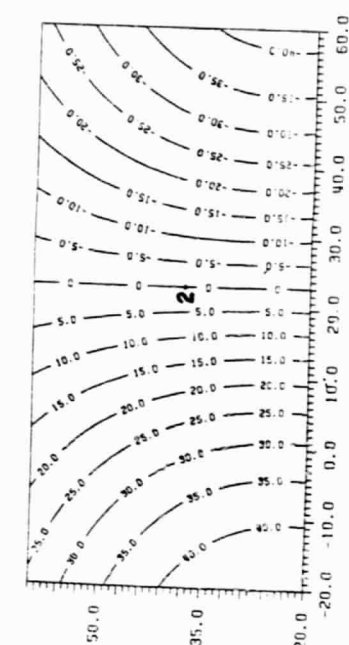
PRINTED AT THE  
OF POOR QUALITY



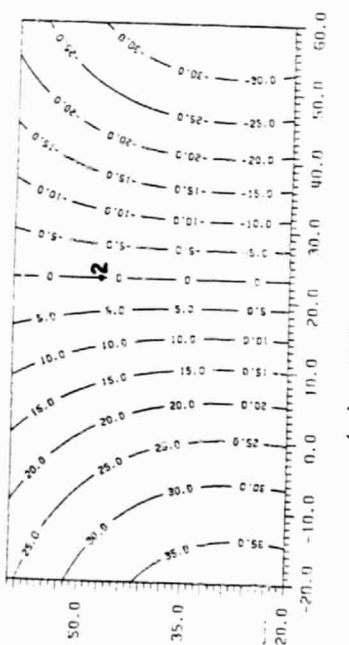
(a) 0° azimuth



(b) 30° azimuth



(c) 60° azimuth



(d) 90° azimuth

Fig. 10 Longitudinal bias surfaces for ranges from the four locations of station 2 (values in centimeters).

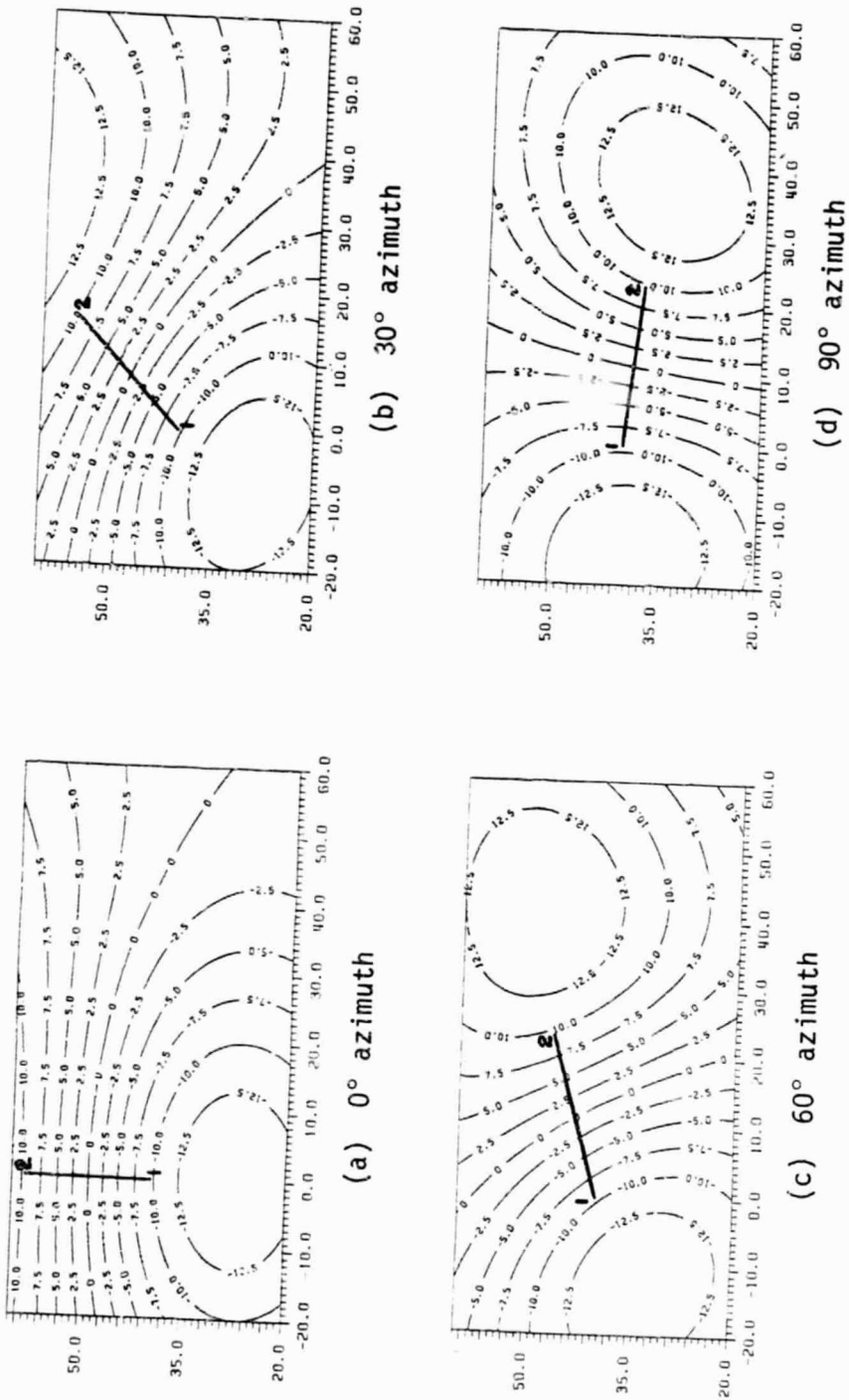
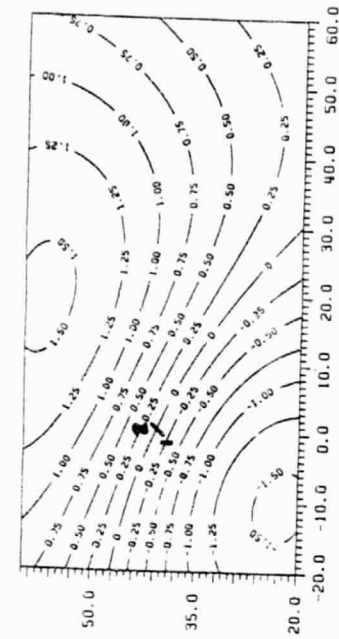
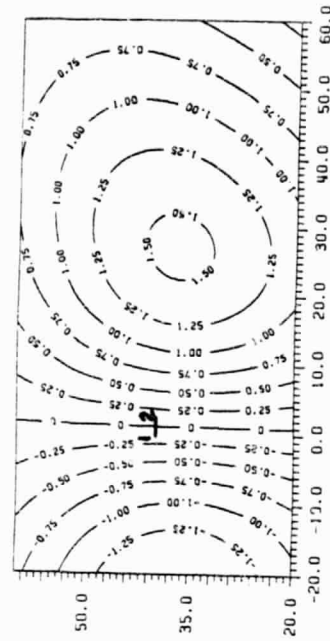


Fig. 11 Radial bias surfaces for SRD's from four 2000 km baselines  
(values in centimeters).

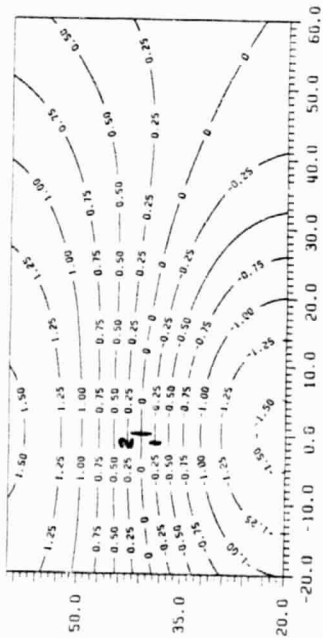
ORIGINAL PAGE IS  
OF POOR QUALITY



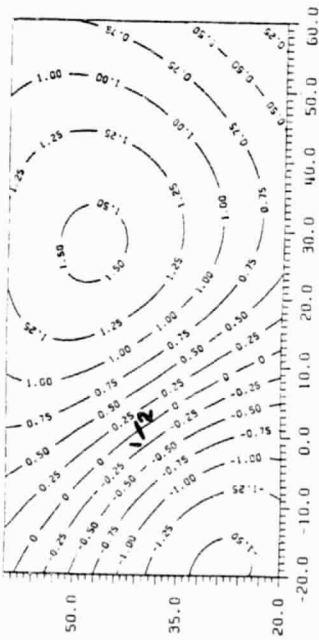
(a) 0° azimuth



(b) 30° azimuth



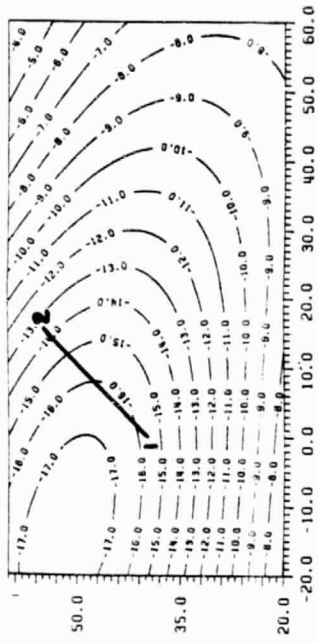
(c) 60° azimuth



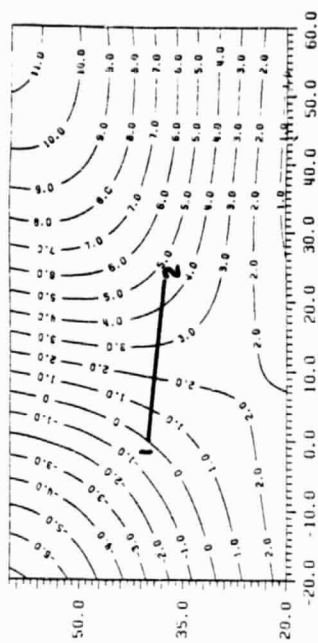
(d) 90° azimuth

Fig. 12 Radial bias surfaces for SRD's from four 200 km baselines  
(values in centimeters)

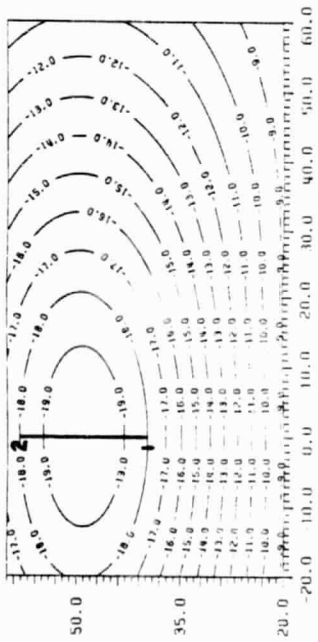
ORIGINAL PAGE IS  
OF POOR QUALITY



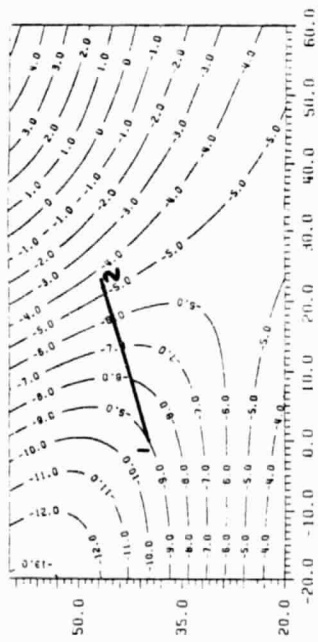
(a) 0° azimuth



(b) 30° azimuth



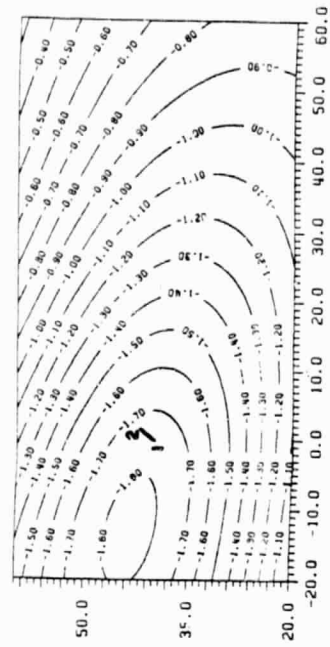
(c) 60° azimuth



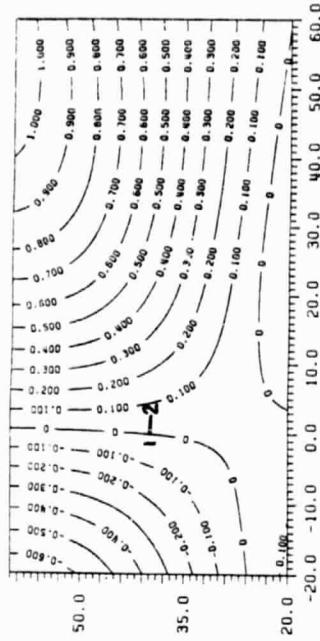
(d) 90° azimuth

Fig. 13 Latitudinal bias surfaces for SRD's from four 2000 km baselines (values in centimeters).

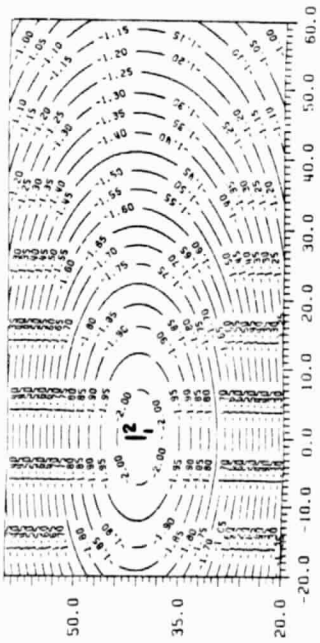
ORIGINAL PAGE IS  
OF POOR QUALITY



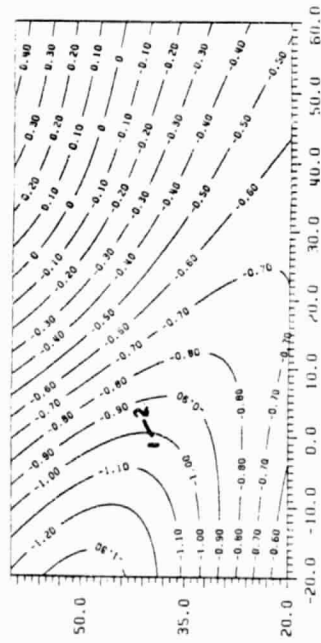
(b) 30° azimuth



(d) 90° azimuth

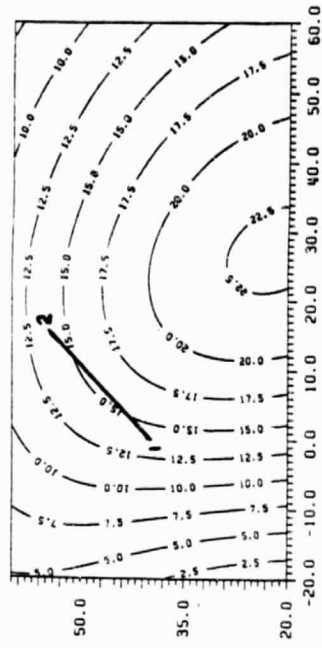


(a) 0° azimuth

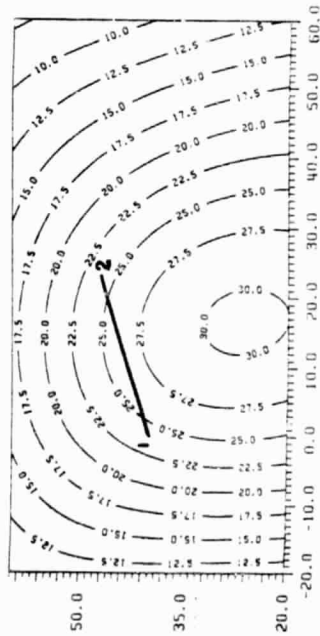


(c) 60° azimuth

Fig. 14 Latitudinal bias surfaces for SRD's from four 200 km baselines (values in centimeters).

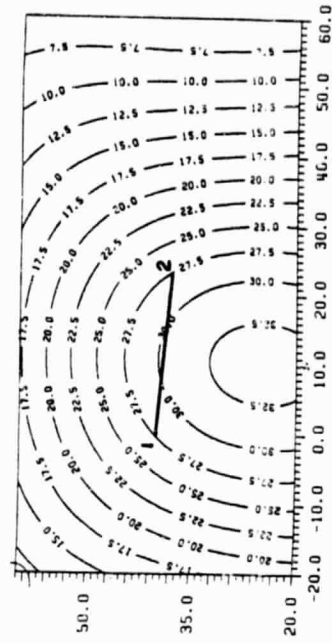


(a) 0° azimuth



(b) 30° azimuth

(c) 60° azimuth



(d) 90° azimuth

Fig. 15 Longitudinal bias surfaces for SRD's from four 2000 km baselines  
(values in centimeters).

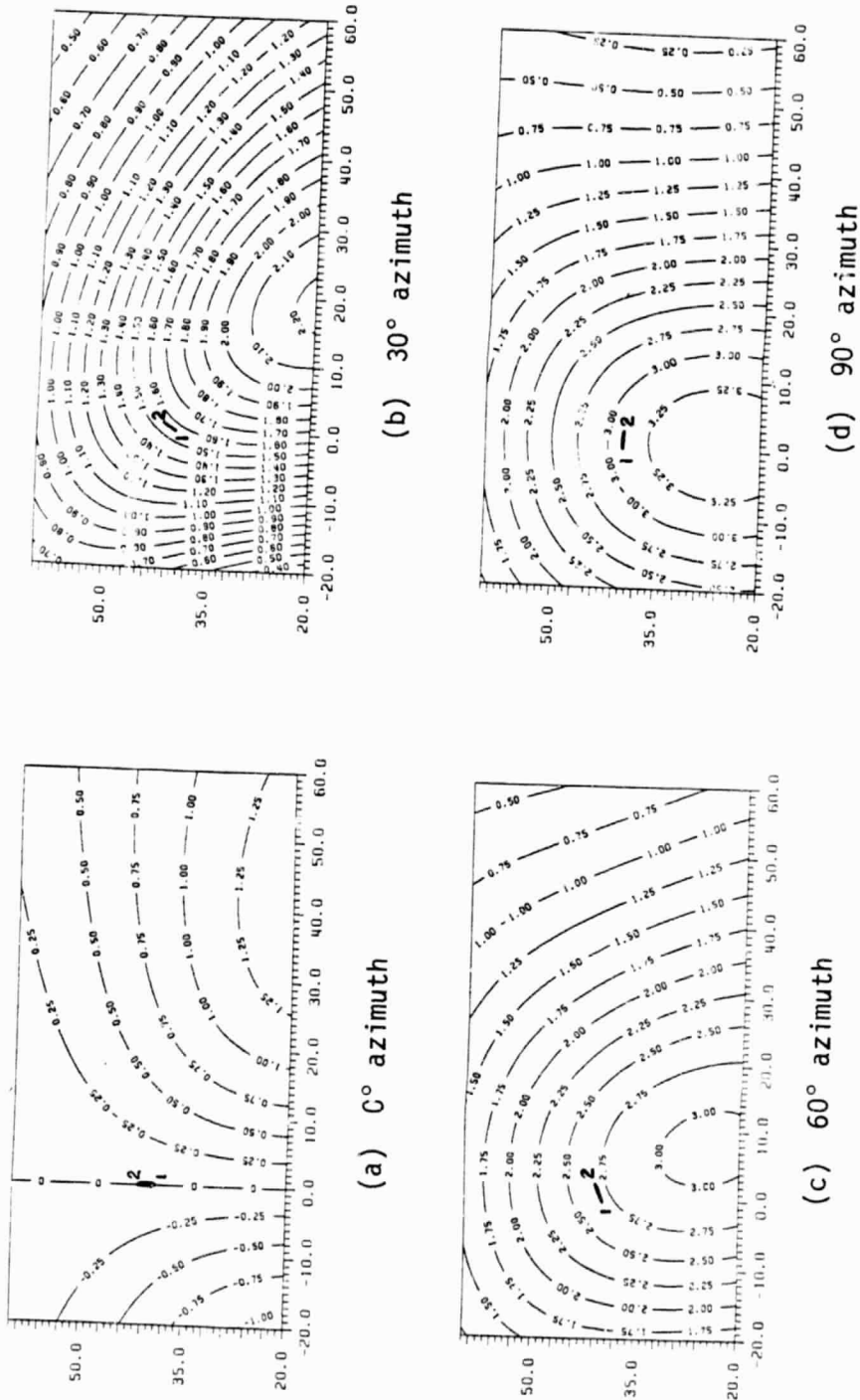


Fig. 16 Longitudinal bias surfaces for SRD's from four 200 km baselines  
(values in centimeters).



## 4.5 Sensitivity Analysis of SRD Observations

### 4.5.1 Introduction.

In designing an experiment the minimization of bias effects without overparametrizing the problem is an important factor, but it is neither "the" major factor nor the only one to be considered. A more important and challenging issue is the selection of the proper data that would yield the most accurate parameter estimates with the least amount of computations. Not all of the available observations will contain the same amount of information about the parameters in general. That does not mean that we should not use these observations, but if the computations are tedious and expensive in terms of required computer time, then we might want to weigh the benefits from the use of these observations against the increased computation effort and cost.

Optimization of a design in classical geodetic networks has been a popular topic with a very rich literature. In the case of space system networks, though, the problem becomes extremely complex and practically intractable on an observation-by-observation basis due to the possible thousands or even hundreds of thousands of observations connecting the space subset and ground subset of network vertices. We have to resort, therefore, to a geometrical analysis of "categories" of observations rather than a one-by-one examination. Since the observations are collected from individual satellite passes over the network stations, it seems natural to use the segregated observations over each pass as an entity whose optimal position relative to the network is sought. Optimality again is judged by the contribution of information about the problem parameters. Going from individual observations to individual passes

reduces the amount of work tremendously. Further savings can be achieved by classifying the passes according to their direction (e.g., North-South, East-West, etc.) and the maximum elevation that the satellite reaches with respect to the station's zenith (e.g., overhead passes, horizon passes, etc.). We therefore end up having to deal with only a small number of categories of observations which is a much more manageable problem than what we originally started with.

#### 4.5.2 Optimal designs for baseline estimation.

Our primary interest here is to find optimal estimates of the interstation chord distances (baselines). An extensive investigation for the range observable has been published in [Pavlis, 1979]. Since ranges and SRD's contain the same type of information, the conclusions of that study are valid for our problem too. Some of the most important results are the constancy of the relative precision of the system over a wide range of baseline lengths, the accuracy dependence of the estimated baseline on the orientation of the pass relative to its direction, and the independence of that estimate from biases in the adjustment's parameter estimates.

The first result is important from the point of view that we are not restricted to use baselines of equal length throughout our design. The last one is of importance also, especially in cases where due to insufficient data or unfavorable distribution a desired unbiased estimate for all or some of the parameters cannot be found. The usual practice in this case is to apply prior information (if available) and use the Bayesian adjustment process, whereby we deflate the variance of some of the parameters in exchange for the unbiasedness of the solution [Pavlis,

1979]. In our study, for instance, we have already seen that the station position and the coordinates of the pole are inseparable parameters. When the one is being estimated, the other must be kept constrained to already known values, and it is, of course, desired that the estimates be least affected by any bias introduced by the constraints.

The relative orientation between baselines and satellite passes will be reexamined here, since the peculiarities of the SRD observations shed more light on the relationship between observables and parameters. The results of the aforementioned study are still valid, that is, satellite passes parallel to the estimated baseline should be preferred to those which cross it at almost a right angle. Since the SRD's, though, are the differences of ranges emanating from the endpoints of the baseline and directed to the same satellite position, they can be expressed as functions of the baseline length directly. From Fig. 17 and some elementary geometry we see that if  $d$  is the length of baseline 1-2, and  $\delta$  is the observed range difference  $S_1-S_2$ , then

$$AB = d \cos \omega \quad (137)$$

where from the triangle  $\widehat{ISD}$  we find

$$\omega = \alpha + \psi \quad (138)$$

From the triangle  $\widehat{ICE}$  we obtain

$$AB = CE = C_1 \cos \psi \quad (139)$$

and since

$$SC = S_2 \Rightarrow C_1 = S_1 - S_2 \quad \text{or} \quad C_1 = \delta \quad (140)$$

Therefore

$$AB = \delta \cos \psi \quad (141)$$

which, upon substitution in (137), yields

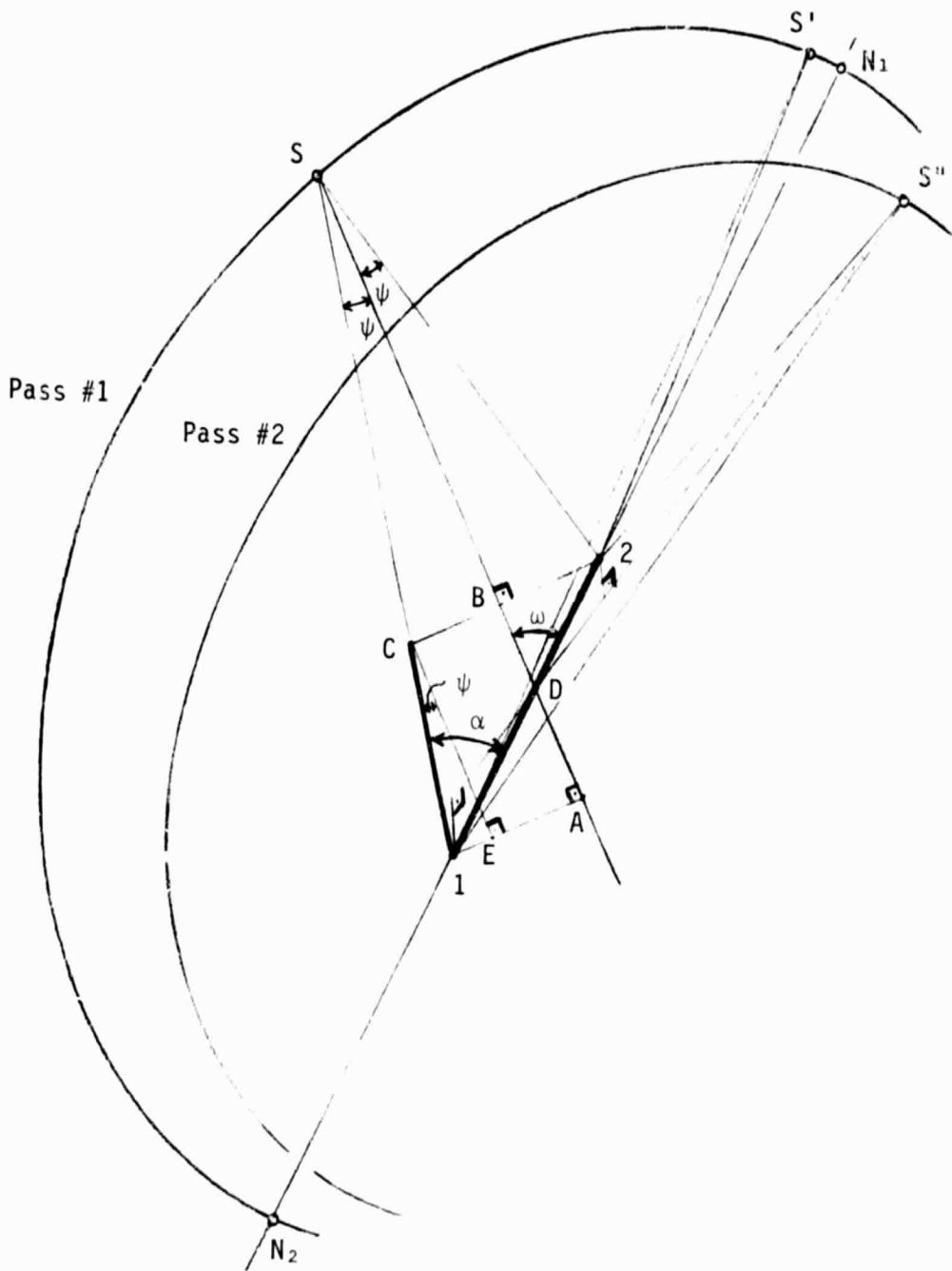


Fig. 17 Satellite pass - baseline geometry for simultaneous range-differences.

$$\delta = d \frac{\cos(\alpha + \psi)}{\cos\psi} \quad (142)$$

It becomes obvious from (142) now that if the observations were collected near the satellite point equidistant from stations 1 and 2, then their values would be near zero and the determination of  $d$  very poor. On the other hand, as  $\alpha \rightarrow 0^\circ$  or  $180^\circ$ , which happens as  $S \rightarrow N_1$  or  $N_2$  respectively, then  $\delta \rightarrow d$  and uncertainties in the values of  $\alpha$  and  $\psi$  have no effect on the determination of  $d$ . In this case we have assumed that the baseline lies on the plane of the pass; therefore its direction intersects the satellite trajectory at  $N_1$  and  $N_2$ . Although this special case illustrates to satisfaction the relationship between observables and parameters of interest, it is hardly ever possible for it to happen in practice; and even if it did, we would have no means of knowing a priori anyway. The more realistic case is that of pass number two in Fig. 17, where the orbital plane and the direction of the baseline are nearly parallel. In this case the points  $N_1$  and  $N_2$  do not exist, but the observations which are collected at low elevation angles, near the points where the horizons of the two stations intersect with the satellite trajectory, will still be the ones with the greatest amount of information about the baseline. For stations which are not too far apart (baselines of a few hundred kilometers), the laser rays will travel through almost the same atmospheric layers and any errors from an incomplete refraction model which is always a limiting factor in low elevations, will be highly correlated and therefore cancel out in the differencing. Using the SRD mode for the reduction of laser ranging data, therefore, we can make use of the low elevation observations that are normally edited from the range adjustment

and at the same time enjoy the minimization of biases due to errors in the mathematical model which this approach offers.

#### 4.5.3 Optimal design for the estimation of the motion of the pole.

Baselines are, of course, not the only parameters of interest. The coordinates of the celestial pole are equally important here as well. The former are parametric functions of the adjustment parameters, and as such we could not use the sensitivity matrix of the design to deduce the optimal experiment for their estimation. For the latter, though, this approach can be taken since they enter the adjustment directly. The goal of this investigation is to find an experimental design for SRD measurements which will result in a set of normal equations with an associated matrix being as close to a diagonal matrix as possible and with as large diagonal elements as possible. Such a normal matrix will, of course, result in small parameter variances and insignificant correlations among them. To put it in fewer words: an orthogonal design. In the case of a truly orthogonal design, the columns of the design matrix  $A$  are orthogonal, and since the normal matrix is the Gramian of those vectors, the off-diagonal elements are all zero. When exact orthogonality cannot be met, we must try to stay as close to such a design as possible.

One way to do this, and probably the most illustrative, is to examine the variations in the sensitivity of the observable with respect to the parameters as a function of its various possible realizations. In other words, compare the elements of the design matrix for each of the parameters at all possible observation points. Since each SRD observation involves two station locations and one satellite position, there are an infinite number of variations of this three-point configuration to be

examined. We have again a practically intractable problem. The pole coordinates, though, are basically two orthogonal rotations about the x- and y-axes, and one can therefore use an intuitive approach to identify a small number of configuration variations that would be enough to support the analysis. Based on the form of the sensitivity matrix elements that correspond to the (x,y) parameters and the definition of the coordinate system in which these parameters are referenced, we conclude that two absolute locations for the observing stations that could give information about our problem are those near the meridional planes on which the x and y axes lie, i.e., the  $\lambda = 0^\circ$  and  $\lambda = -90^\circ$  meridians.

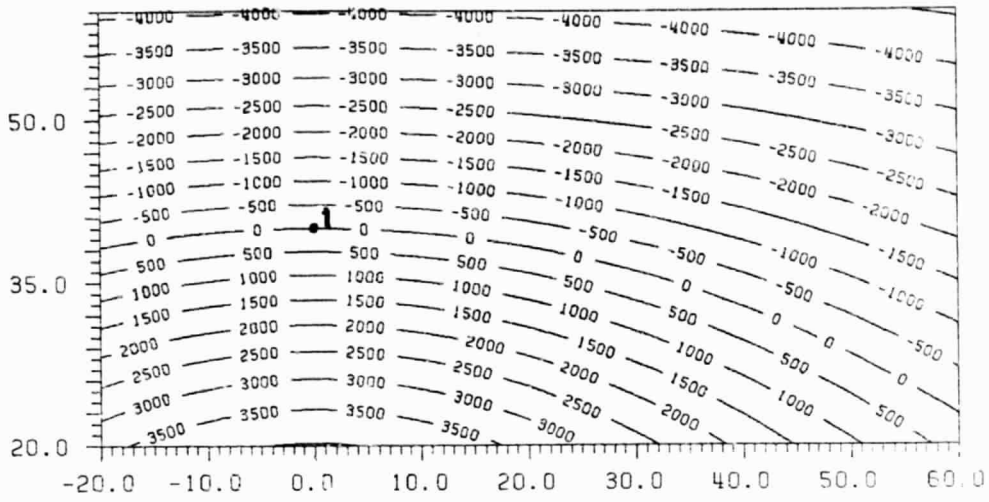
The rotations for the motion of the pole are about axes that lie on the equatorial plane, and therefore their effect on the coordinates of stations increases as the latitude of these stations increases. From the practical point of view though, we cannot expect to have laser stations in near polar latitudes, and we have therefore limited our tests to areas where most of the currently operational stations are located. This study follows very closely the setup for the bias propagation study. We have again used spherical approximations and a circular orbit at Lageos' mean altitude, and we have plotted the values of the sensitivity coefficients for each of the parameters at the intersection points of a  $1^\circ \times 1^\circ$  grid surrounding the coobserving stations. In order to examine the dependence of the observable's sensitivity on the relative positioning of the stations in the case of the SRD mode, we have used various baseline lengths and azimuths to determine the second station with respect to a fixed position of the first one. From the analytical expressions for the sensitivity coefficients, we can gather that their numerical values will

in general increase as the coordinate separation between the stations increases. This observation has been verified by the numerical tests for different baseline lengths. It has also been observed that the absolute maximum of these sensitivity curves is encountered near the midpoint of the baseline, and their gradient is minimum in a direction nearly perpendicular to the baseline at its midpoint. These observations and the fact that the simultaneity requirements constrain the actual baseline lengths to not more than about 2000 km indicate that a 1000 km separation would be the optimum for obtaining a sufficient number of observations with high enough sensitivity for a precise parameter determination. We have therefore included here only the sensitivity plots that refer to this particular case.

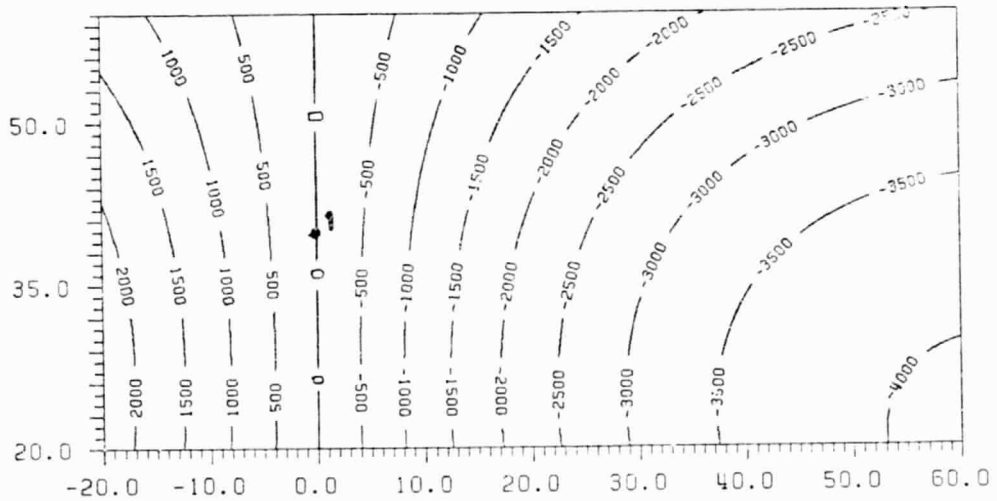
The sensitivity surfaces are shown for the range observable from a station at  $40^\circ$  N latitude in Fig. 18 for  $0^\circ$  longitude, and Fig. 19 for  $\lambda = -90^\circ$ . It can be readily verified from these plots that as the station is moved in longitude by  $90^\circ$  to the west of its original position, the sensitivity surfaces undergo a  $90^\circ$  counter-clockwise rotation about the station's geocentric radius. The end result is that the sensitivity surfaces for  $x$  and  $y$  at  $0^\circ$  longitude are identical to those of  $y$  and  $x$  at  $90^\circ$  W longitude except for a sign change in the coefficients for  $x$  at the second location and those for  $y$  in the first.

Inspection of other cases where the stations are located in between the above two meridians shows that indeed the shift in sensitivity from one parameter to the other is a smooth operation and on the  $\lambda = 45^\circ$  meridian (or  $\lambda = -45^\circ$ ) the range observable is equally sensitive to both parameters. It is also worth noting here that the sensitivity of the system





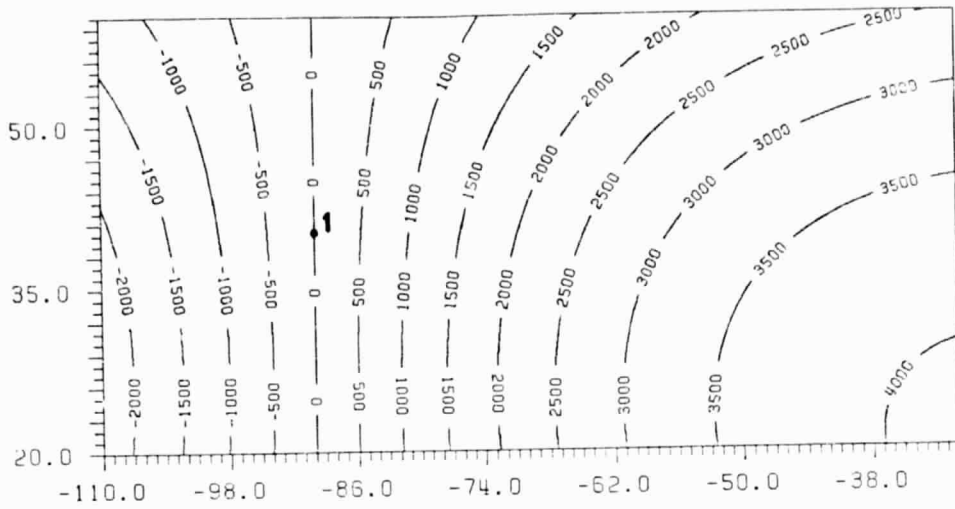
(a) x-coordinate



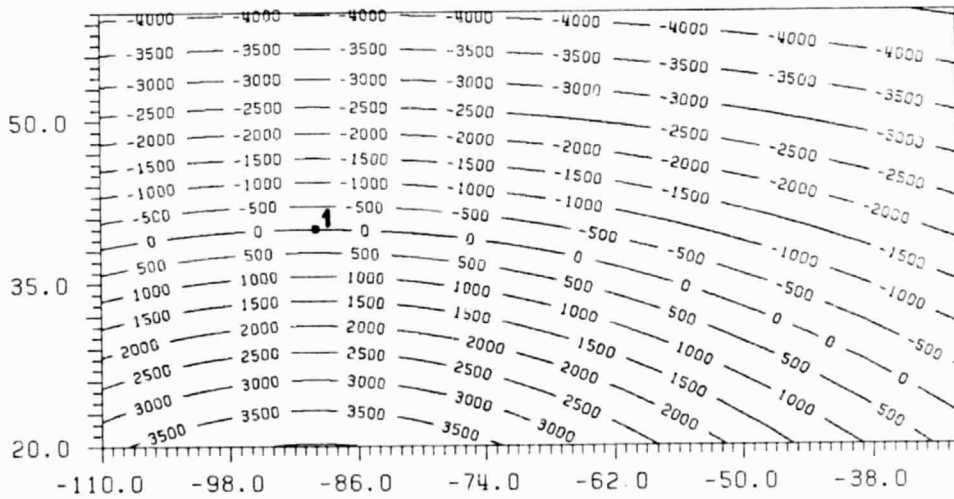
(b) y-coordinate

Fig. 18 Sensitivity surfaces for the coordinates of the pole in the case of a station at  $\lambda = 0^\circ$ ,  $\phi = 40^\circ$ .

ORIGINAL PAGE IS  
OF POOR QUALITY



(a) x-coordinate

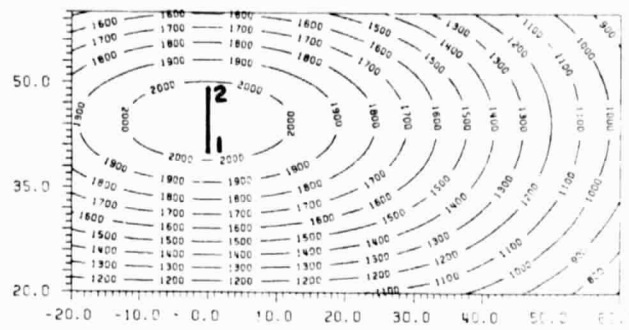


(b) y-coordinate

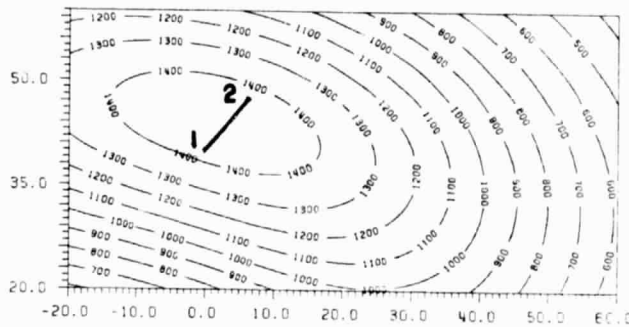
Fig. 19 Sensitivity surfaces for the coordinates of the pole in the case of a station at  $\lambda = -90^\circ$ ,  $\phi = 40^\circ$ .

is in general increased with respect to either of the parameters as the observed satellite positions are selected farther away from the station's zenith. In the case of ranging, therefore, we are in the unfortunate situation that we have to use very low elevation observations if we want to increase the sensitivity of our system with respect to the motion of the pole. As it has already been mentioned, these observations have the largest uncertainties due to incomplete modeling of the atmospheric refraction effects and since the ranging mode cannot eliminate biases as the SRD mode does, such poor quality observations are hardly ever included in the range adjustment.

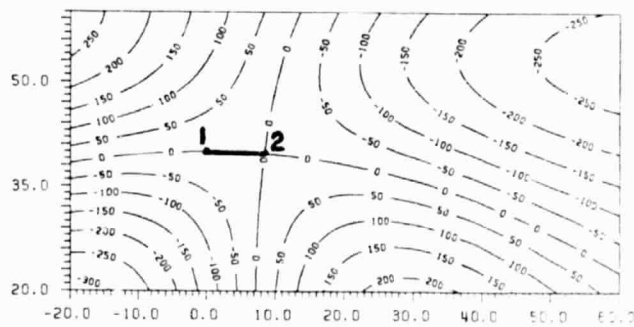
These last few observations, when first noted in the initial steps of this investigation, prompted us to examine the potential use of the SRD mode for the estimation of the coordinates of the pole. Based on the sensitivity surfaces of the previously used station pairs we computed by differencing the sensitivity surfaces for the SRD mode. From Figs. 20 and 22 we can see that for a stronger determination of the  $x$  coordinate the station pair must be in the vicinity of the  $\lambda = 0^\circ$  meridian (or  $\lambda = 180^\circ$ ), and of all possible baseline orientations, that nearest the North-South direction will result in the highest sensitivity possible. Similarly, Figs. 21 and 23 indicate that the strongest determination of the  $y$  coordinate will result from the observations at a station pair near the  $\lambda = -90^\circ$  meridian (or  $\lambda = 90^\circ$ ), and again the highest possible sensitivity will be achieved if the orientation of the baseline is in the general North-South direction. It can be verified also that baselines in the East-West direction will contribute to the sensitivity of the model too, but in a reverse manner from that of the North-South baselines. That is



(a)  $0^\circ$  azimuth

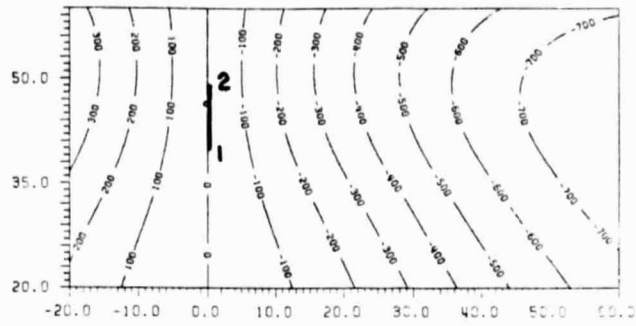


(b)  $45^\circ$  azimuth

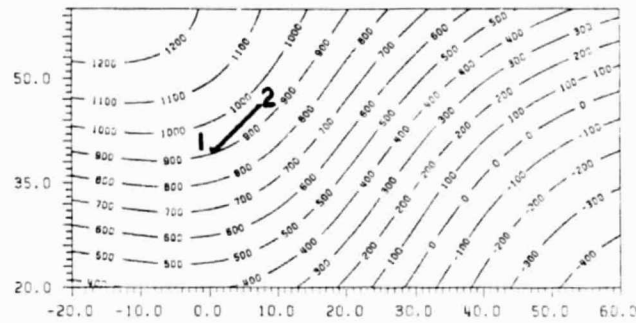


(c)  $90^\circ$  azimuth

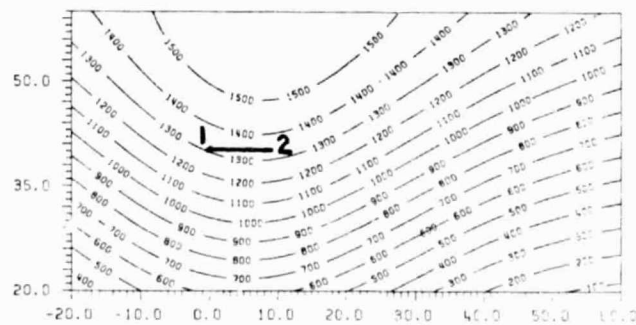
Fig. 20 Sensitivity surfaces for the x-coordinate of the pole for three 1000 km baselines near  $\lambda \approx 0^\circ$ .



(a) 0° azimuth

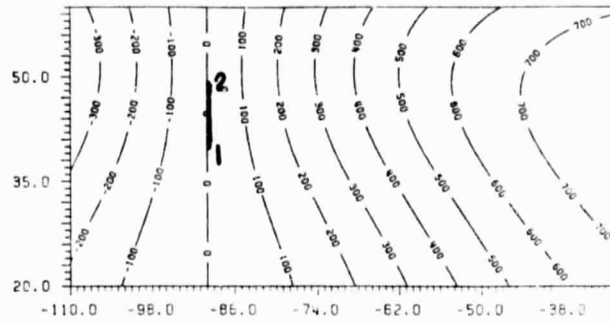


(b) 45° azimuth

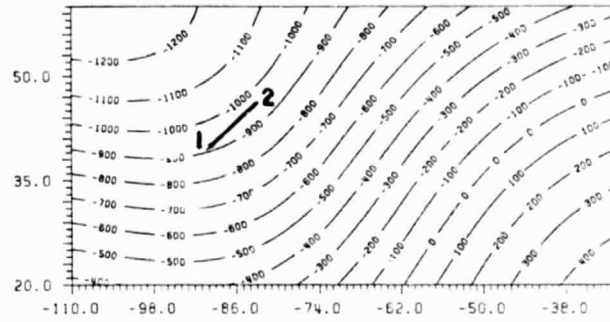


(c) 90° azimuth

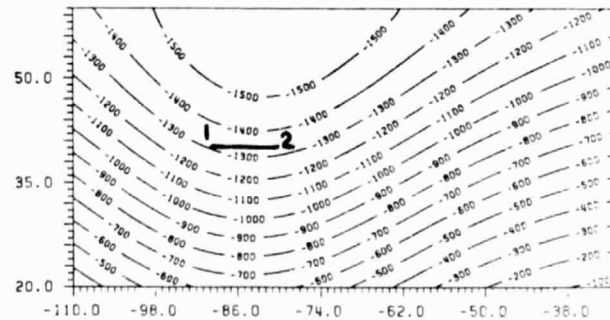
Fig. 21 Sensitivity surfaces for the y-coordinate of the pole for three 1000 km baselines near  $\lambda = 0^\circ$ .



(a) 0° azimuth

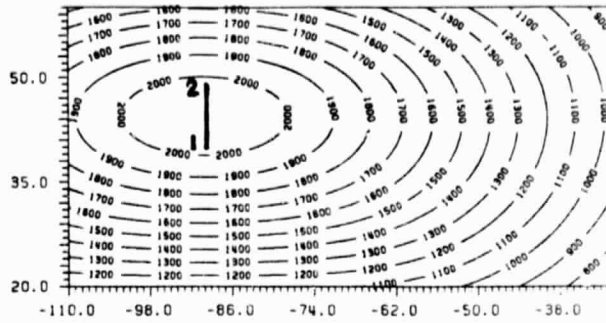


(b) 45° azimuth

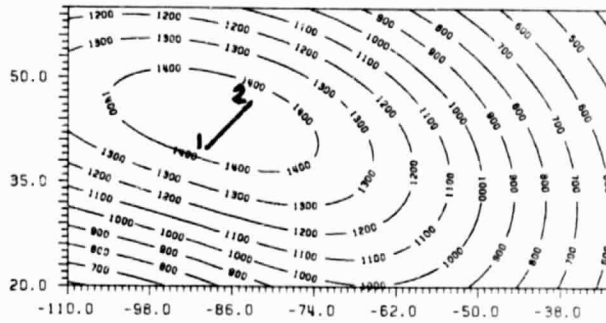


(c) 90° azimuth

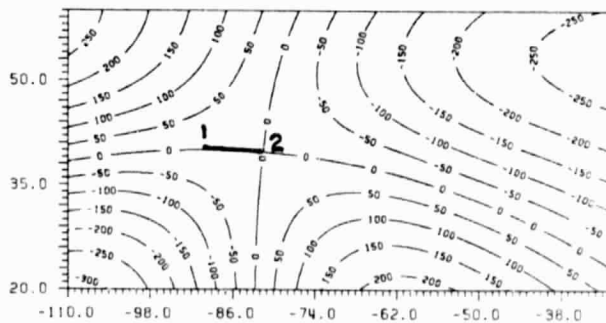
Fig. 22 Sensitivity surfaces for the x-coordinate of the pole for three 1000 km baselines near  $\lambda \approx -90^\circ$ .



(a)  $0^\circ$  azimuth



(b)  $45^\circ$  azimuth



(c)  $90^\circ$  azimuth

Fig. 23 Sensitivity surfaces for the y-coordinate of the pole for three 1000 km baselines near  $\lambda \approx -90^\circ$ .

to say, an E-W baseline near the  $\lambda = 0^\circ$  or  $180^\circ$  meridian will be sensitive to the y coordinate although almost completely insensitive to the x, as Figs. 21(c) and 20(c) show respectively. In parallel, for an E-W baseline near  $\lambda = 90^\circ$  or  $-90^\circ$ , the observable is sensitive to the x coordinate but not to y, as Figs. 22(c) and 23(c) indicate.

The conclusions which can be drawn from this study are rather obvious by now. The optimal SRD network for monitoring the motion of the pole should consist of perpendicular baseline pairs located near the two meridians on which the x and y coordinate axes lie. Some savings in the number of dedicated laser equipment can be achieved by giving these subnetworks an L-shape, one station being common for both the N-S as well as the E-W baselines. Considering now that laser ranging is a weather-dependent system and the fact that with a single Lageos target there is a six hour gap in every 24-hour period during which a typical station at about  $40^\circ$  latitude will not be able to observe due to the earth's inertial rotation, it is only logical to plan for far more stations than the mere minimum. If the additional requirement of a uniform distribution of the observations over the globe is considered, then we should also include subnetworks located in the Southern Hemisphere. In this manner we not only increase the chances of observing the target within a given time interval, but we can also minimize orbital biases coming mainly from an inaccurate geopotential model. The importance of having a uniform distribution of data in time will be further discussed in connection with the operational estimation technique for the coordinates of the pole. What should be considered though as the major advantage of this network configuration over simple ranging is the fact that the resulting design



is nearly orthogonal over the entire area surrounding each baseline. In other words, observations from each of the baselines in an L-pair are only sensitive to one of the parameters, either  $x$  or  $y$ , and estimates of these parameters will have nearly zero correlation as the normal equations matrix is almost diagonal. This cannot occur in the case of ranging except in very restricted designs where the satellite pass follows either of the two directions on which the sensitivity with respect to one of the parameters is nearly zero while it is maximum for the other one (see Fig. 18).

#### 4.6 Operational Approach for Parameter Estimation

##### 4.6.1 Estimation of baseline lengths.

The estimation of baseline lengths in a dynamic solution is based on the estimated coordinates of the observing stations. We have shown already that in a long-arc problem where the satellite is tracked over several revolutions, the coordinates of the tracking stations are separable from the initial conditions for the orbital integration (initial satellite state vector) except for an ill-conditioning in longitude caused by the peculiarities of the earth's mass distribution.

The first option that one has then is to adjust all the data collected from all stations observing the satellite in one batch adjustment with one station's longitude constrained to an adopted value. Such a solution, of course, will have to utilize a very detailed orbital model, since any unmodeled sources will progressively affect the solution more and more as the length of the arc becomes longer and longer. As the model gets more complicated, the computations become more complex and

time consuming; therefore, the cost per estimated baseline increases. In addition to the above, a requirement of the long-arc solution is the uniform distribution of the observations over the entire arc, and for this to be achieved the stations must have a global distribution. That presupposes the existence (and continuous maintenance) of a global network of stations. For various reasons, the land-sea distribution being the most obvious, the existence of such a network cannot always be guaranteed.

An alternate approach which circumvents the aforementioned problems is the semi-dynamic solution where each satellite pass over a station of interest is treated as an independent arc. In this case the length of the arc hardly ever exceeds one-third of a complete revolution, and the orbital model therefore cannot furnish the required information about the origin and orientation of the underlying coordinate system. The shorter the arc, the less the contributed information by the orbit. Such solutions have been common practice with Doppler system users, especially individual ones who have no way of observing the satellites on a global scale. The usual remedy to the problem is the constraint of the satellite orbit over each pass to some fairly accurate known values. By doing so, one hopes that the introduced bias in the recovered positions of nearby stations will be highly correlated and cancel out during the inter-station distance computation. This, however, is neither guaranteed nor does it mean that the resulting baseline estimate is bias-free by definition. The advantages of this method though are quite obvious. There are no requirements for an extensive network and the orbital arcs being very short, the orbital model can be simplified tremendously, since long

period and secular perturbations in the model have no time to build up and corrupt the solution. As a result, the cost of this mode of solution compared to the previous one (for the same amount of data) is reduced substantially, in some cases by an order of magnitude.

#### 4.6.2 Estimation of the coordinates of the pole.

The fact that the coordinates of the pole cannot be separated from those of the observing stations in a simultaneous adjustment has been shown already in Section 4.3.1. At that point some options were examined for the separation of these parameters. Because of the arguments we raised at that point, the second option seems to be the only one which can produce consistent results over a long period of time. What is even more important is the fact that this method would result in a set of pole coordinates that is compatible in sense with those currently obtained and published by the international organizations such as BIH.

Since the coordinates of the observing stations are fixed to some adopted values (which define the CTS), errors in these values will affect the resulting polar motion record. As long as we always use the same set of coordinates the effect of their errors on the polar motion record is more or less the same, and we need not concern ourselves with this item any further. The effort should be diverted in establishing the connection between the previously adopted CTS and the one used in the new techniques. In fact this has been one of the most pressing issues in recent years, and there are several suggestions on how to deal with it, the most recent and, in our opinion, the most straightforward appears in [Mueller et al., 1982].

The idea of monitoring the motion of the pole by two rigid body rotations of the station polyhedron with respect to the CIS defined by the satellite orbit seems to be in agreement with the current trends and requirements of the interested parties. There are two items which are of concern in connection with this mode of estimation--the dynamic nature of the parameters and the stability of the satellite-defined CIS. Since we do not have a rigorous mathematical model to describe polar motion, we must resort to a discretization of the problem for the estimation of the state of the process. The quality of the final result will depend on the distribution of these individual estimates in time. On the other hand, the distribution of these estimates in time is associated directly with the spectrum of the process and the capabilities of the measuring system. The already long record of observations has established the fact that there are two dominant frequencies in the spectrum, an annual one and the 14-month or Chandler frequency. From this point of view then, the determination of an appropriate interval for the computation of the state is rather simple. The complications arise from the consideration of the capabilities that the satellite system can demonstrate. It is not only important that this system is accurate enough so that the signal can be separated from the noise; we must also be able to collect a sufficiently large number of observations over the estimation interval in order to be able to produce reliable results. The laser systems, being weather dependent, will have a disadvantage in that respect since observations lost on one day cannot be made up with additional observations on the next day. That implies that a large number of optimally selected stations should be employed at all times.

Because of the fact that the station polyhedron defines the CTS, a question which must be examined very carefully is the effect of missing stations' observations in the estimates. From the theoretical point of view, deleting or adding stations (or changing their location or coordinates) results in a new CTS, and one should therefore be alert to this for the proper interpretation of discontinuities or irregular behavior in the estimates. In connection with the reference system stability, we must also examine that of the satellite CIS. It is true that Lageos, which is the favored target for geodynamics research, has a very stable orbit compared to other geodetic satellites, but nevertheless we still do not know of an orbital model which would result in a centimeter level accurate orbit over a period of a few years. For obvious reasons it is not very desirable to have even a quasi-inertial system whose definition changes so much in so little a time. The general consensus on this issue is to use the satellite system as an interpolatory one and periodically calibrate it with respect to one of the systems that exhibits long-term stability such as Lunar Laser Ranging (LLR) and Very Long Baseline Interferometry (VLBI). The application of the SRD mode, however, can considerably increase the stability of the satellite system due to the fact that the biases in the observations can be greatly reduced with proper scheduling. That not only will increase the quality of the end product, but it will also reduce the need for a frequent calibration procedure, which can be a nuisance and a source for further error.

Returning now to the data distribution question, we should point out that by the discretization process we have in essence approximated the nonlinear functions which represent the coordinates of the pole with

a step function. It is obviously desired that the values of the step function at each interval be unbiased estimates of the average value of the true function over that interval. This can hardly be achieved if the collected data are not uniformly distributed over the entire interval as Fig. 24 illustrates. Even with a large number of stations involved, we still cannot guarantee the uniformity of the data at all times because we have no control over the weather or system failures. We suggest here that in processing data for polar motion determination, a different set of coordinates of the pole should be estimated when the data set density changes abruptly, that is, each batch of observations which span a time interval no larger than that determined by the resolution of the system be used to estimate one set of x,y coordinates. Furthermore, and perhaps more important, the reference epoch for these estimates should be computed on the basis of the data distribution rather than the middle epoch of the interval, as is currently assumed. In Fig. 25 we have plotted an assumed distribution of data for the problem of Fig. 24. With the current practice, the estimates will refer to epochs  $M_1$ ,  $M_2$ , etc. With the proposed new approach, the corresponding epochs will be  $E_1$ ,  $E_2$ , etc. When these epochs are used in plotting the variation curve, it is obvious that the estimated curve will be much closer to the true curve than the dashed line of Fig. 24 which is based on the  $M_1$ , etc. epoch labeling. The fact that the new estimates are not equally spaced should not alarm the standard users of this information, for a smooth curve can be fit to these points, and thereby one can obtain estimates at regular intervals. In fact, the astrometrically determined coordinates of the pole are always smoothed by means of Vondrak's method [1977] and the published results are indeed the output of this filtering process.

ORIGINAL PAGE IS  
OF POOR QUALITY

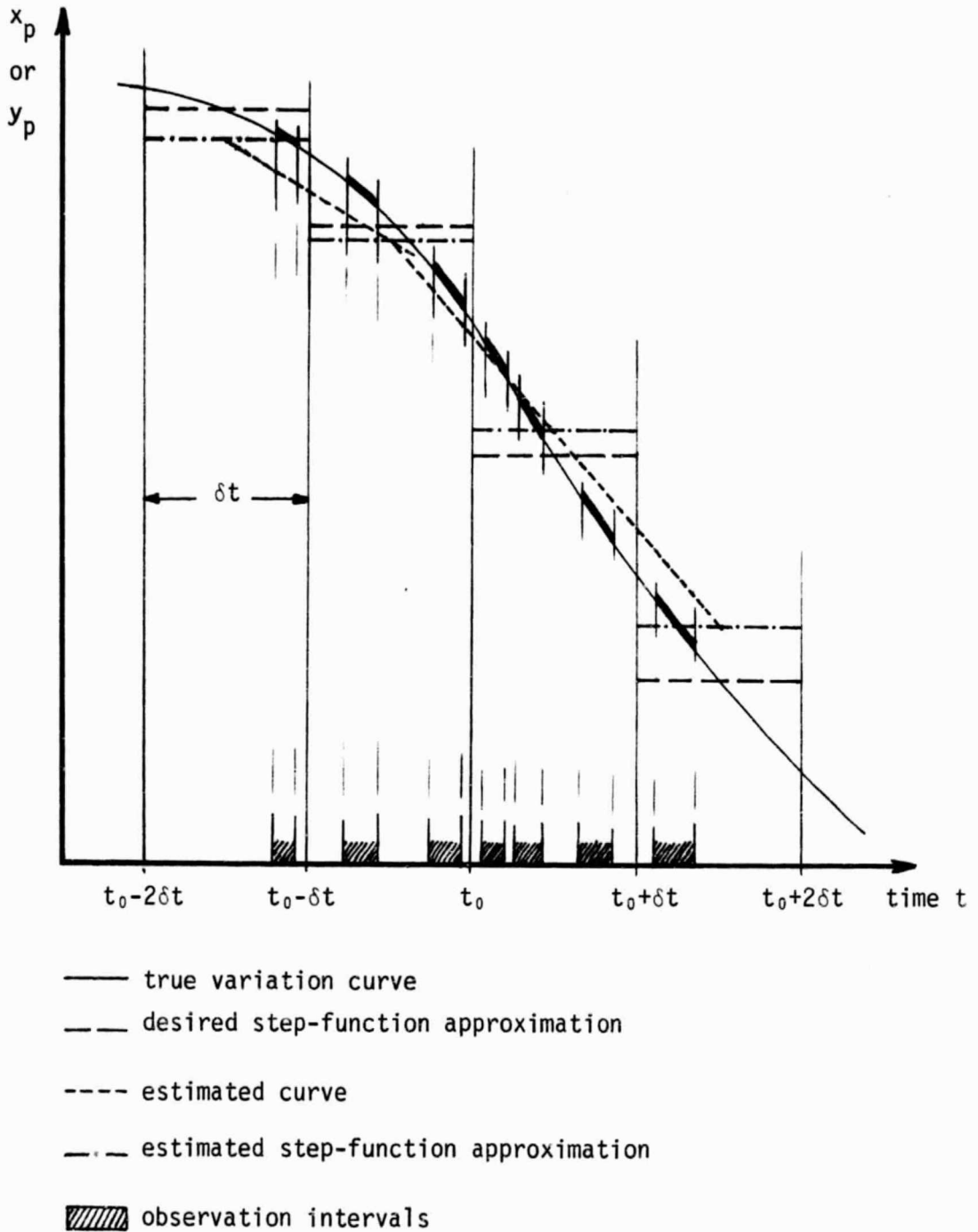
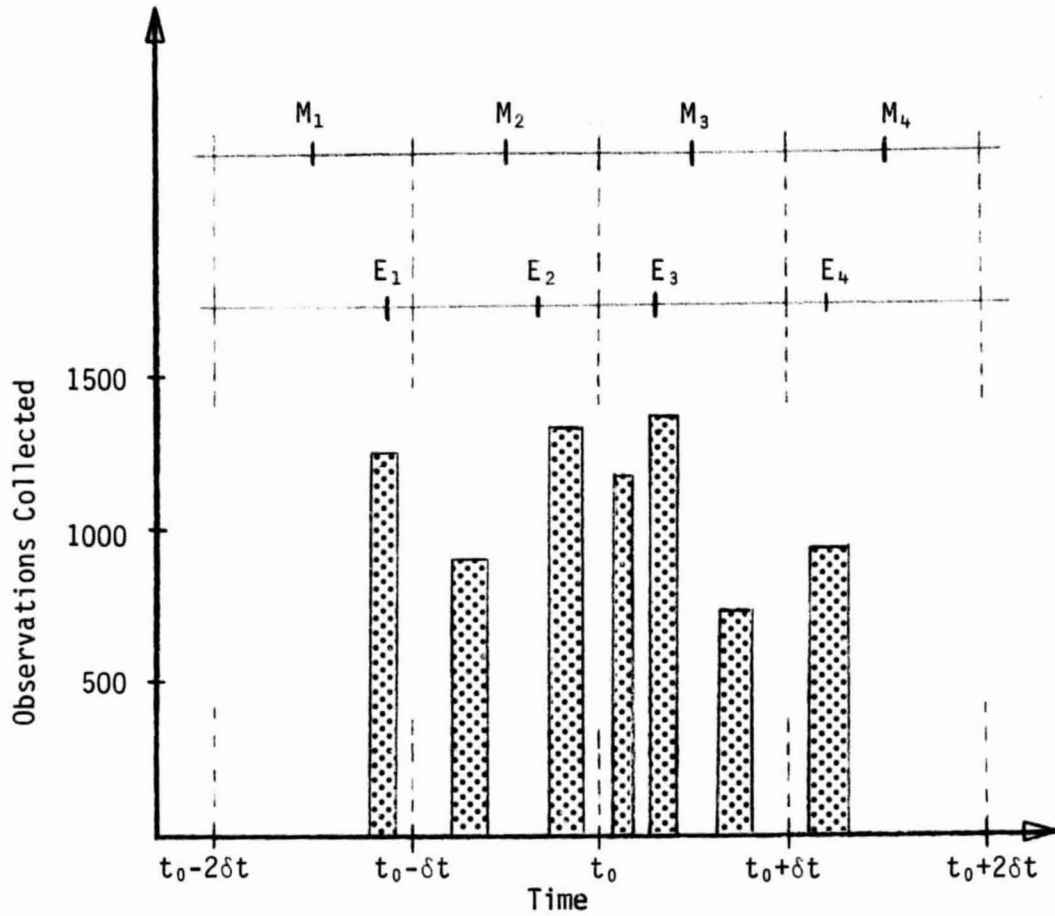


Fig. 24 The effect of nonuniform observing schedules on the estimation of the coordinates of the pole.

ORIGINAL PAGE IS  
OF POOR QUALITY



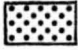
 Shaded area shows the quantity of collected observations over the indicated time interval

Fig. 25 Unbalanced data distribution effects in the estimation of time-dependent averages.



## 5. NUMERICAL EXPERIMENTS AND RESULTS

### 5.1 Simulation Studies

A number of simulation studies were performed in order to substantiate our claims about the estimation of geodetic parameters from SRD observations as opposed to the classical range observations. Simulations provide a lower bound on the accuracy of the results expected from the analysis of real data. In this case, however, this is of lesser concern to us because the main purpose of these simulations is to show the relative performance between the two approaches on the basis of identical data.

In order though that the results of these simulations reflect reality too, we have used in most cases orbital models that contain all of the major perturbation sources and station configurations that either exist or whose existence in the near future is nearly certain. What has not been accounted for in the generation of the simulated observations is the weather. It is common practice in simulation studies to adopt a certain percentage  $p$  (usually 50%), which is used as a weather factor, i.e., if  $N$  is the total number of observations which are possible, then  $pN$  of them are deleted to account for poor weather at the observing sites. Since we are interested in a relative comparison of the results, this is not an important issue. The treatment of the weather problem in the above fashion raises several questions, the most important of which is how does one apply the weather factor. It certainly makes little sense

to delete the first or last pN observations of the campaign since that only shortens its duration, and deleting pN observations at random is not very realistic either since it is equivalent to reducing the sampling rate by an appropriate factor. Modeling the weather realistically at each station, based on past weather records would certainly seem to be the most logical solution. This, however, would result in unduly increasing the complexity of the simulation process and with no major gains in the relative comparison of the results.

In connection with the distribution of the data issue, a related factor is the observational capabilities of the stations. Although currently only a few stations can observe during the day, most of the stations are undergoing upgrading to the third generation of laser instrumentation which will make it possible to observe at all times. For this reason, we have not discriminated between day and night observations in the simulations.

In the following we discuss the three most important simulation studies performed. The first one involves nine existing stations. Its purpose was to find out what amount of SRD data could be collected from these nine stations over the observational period of ten days in the second half of August, 1980, and compare it with what was actually collected over that period of time. The purpose of the second simulation was to investigate the merits of using the proposed method in analyzing data collected from a hypothetical network of 17 stations which is likely to be realizable by 1983 as proposed in [CSTG Bulletin, June 9, 1982]. The goal of this network is the establishment and maintenance of a Conventional Terrestrial Reference System by means of modern observational

techniques such as satellite laser ranging (SLR) and very long baseline interferometry (VLBI). Our study focuses on the problem of determining the baseline lengths between the observing stations of this network. In the third simulation, four nearly optimal baselines of the previous network have been singled out in order to study the capability of this sub-network in determining the coordinates of the pole.

In all three simulation studies all possible simultaneous events between pairs of stations are generated. Since the SRD data set which consists of only simultaneous events is used to create the simple range data set, the number of observations in the latter is twice that of the former. In addition to this, because SRD observations will be in practice obtained from independent range observations, assuming that the two ranges in a pair have equal noise variance  $\sigma^2$ , the resulting SRD will have a noise variance equal to  $2\sigma^2$ . This fact is also considered in the simulations.

Each of the simulated pair of data sets (one for ranges and one for SRD's) is then used in estimating the parameters of interest, whether they be baseline lengths or the coordinates of the pole. Being simulation studies, if everything is left as is, there will be no difference in the recovered results larger than the input noise level. Our interest though is to compare the two methods when there are unmodeled orbital biases in the problem which are not being accounted for in the solution parameters. To achieve this, we apply a bias in the reference orbit which is a common input and identical for both the range and the SRD adjustment. The method which is least affected by this bias is obviously the one which recovers the parameters of interest closer to their "true" values.

5.1.1 Simulations for an existing SLR network.

The fact that the simultaneity constraint reduces significantly the amount of usable ranging data in the SRD mode has been mentioned already. In anticipation of using some existing laser ranging data for testing the proposed method, we performed an initial simulation study using the same stations from which the real data had been obtained and covering a period of time during which these stations seemed to have performed extremely well in acquiring large amounts of data.

Of all stations observing during August of 1980, eight NASA stations and two SAO stations seemed to be the only ones with significant amounts of data. After a preliminary inspection of the data distribution in time, it was apparent that nine of these stations had coobserved Lageos passes with significant overlapping intervals. Table 14 gives a summary of the available real data from all ten stations and the

Table 14 Lageos Data Selection Summary

Station No.	Available Observations	Selected Observations
7090	73590	19042
7943	6068	1934
7092	4167	607
7096	4492	786
7120	18245	2749
7907	3040	207
7063	5522	1698
7115	7165	1047
7091	7522	519
7114	4130	524
<b>Totals</b>	<b>133921</b>	<b>29113</b>

corresponding amounts of data collected simultaneously by any two stations of the network. Comparing the totals in these two columns, it is obvious that less than 22% of the available data can be used in the SRD mode.

From a detailed tabulation of the selected Lageos data (per day/station), it was found that the greatest concentration is in the second half of the month for almost all stations. When the data collected in overlapping time intervals are selected, it turns out that only 38 Lageos passes had been coobserved. A listing of the data per pass for each station in a station pair is given in Table 15. From this tabulation it becomes very clear that the two stations on the Australian continent, Yaragadee (7090) and Orroral (7943), which dominate the complete data set (cf. Table 14), are also the ones with the most data in the selected (simultaneous) observations data set. The implications of these facts will become more obvious at a later stage when we will discuss the analysis of real data. From the initial 133921 available ranges, only 2431 SRD events could be generated for the following seven station pairs:

7090 - 7943	7115 - 7114	7114 - 7063
7120 - 7115	7092 - 7120	
7943 - 7096	7092 - 7943	

Following the general guidelines of our simulation process, we have generated a data set of SRD observations which are collected from a network including the above eight stations and an additional one, the SAO station 7907, located at Arequipa, Peru. The generated data span a ten-day period, August 16 - 25, 1980, and we have used a sampling rate of one range every 30 s for all stations. A total of 26253 SRD events are possible for the selected station pairs. The groundtracks of the observed

ORIGINAL PAGE IS  
OF POOR QUALITY

Table 15 Overlapping Data Distribution for Eight Station Pairs

Satellite Pass	Station No.	7090	7943	7096	7092	7120	7115	7114	7063
1		664	49						
2						669	647		
3		551	41						
4		701	76						
5						106	30		
6		836	58						
7		543	45						
8		431	31						
9			13	36					
10		149	32						
11		117	22						
12		289	34						
13		220	28						
14			6	58					
15		80	8						
16		640	80						
17		315	12						
18		513	61						
19							935	181	
20						66	12		
21						286	29		
22		131	10						
23		100	9						
24		30	6						
25							37	40	
26							32	26	
27						60	37		
28		226	32						
29		632	88						
30		176	18						
31					6	32			
32					112	115			
33			10		118				
34		1217	151						
35		149	46						
36		876	113						
37								228	598
38		55	7						

Lageos passes and the baselines defined by the selected station pairs are shown in Fig. 26. We refer to this data set as the AG80 data, since the observational period falls in the interval during which this campaign occurred.

Even if we halve the number of possible events to account for the fact that not all of the stations had day-night observational capabilities, and further take half of the remaining observations to account for poor weather, equipment breakdowns, etc., we are still left with over 6500 events. Considering that these events span only one-third of the entire month of August and, furthermore, that our sampling rate of one observation every 30 s is nearly ten times lower than the observational rate of most stations, one should realize that the actual number of possible SRD events for the entire month should be well above 50,000 with ample allowance for all factors. It therefore seems that either extremely adverse conditions in the worst possible combinations dominated the performance of these stations over that period or there was a lack of effort in obtaining all possible observations.

The data generated for the AG80 data set were subsequently used in two recovery adjustments, one for polar motion components and one for baseline lengths. Both adjustments were done in the SRD as well as in the ranging mode. To identify which of the two modes is affected more severely by orbital errors, we perturbed the reference orbit in two different ways.

Initially we used only a random error applied to each coordinate of the satellite; subsequently, though, we augmented that with a linear trend time-dependent component. The adjustments are purely geometrical,

ORIGINAL PAGE IS  
OF POOR QUALITY

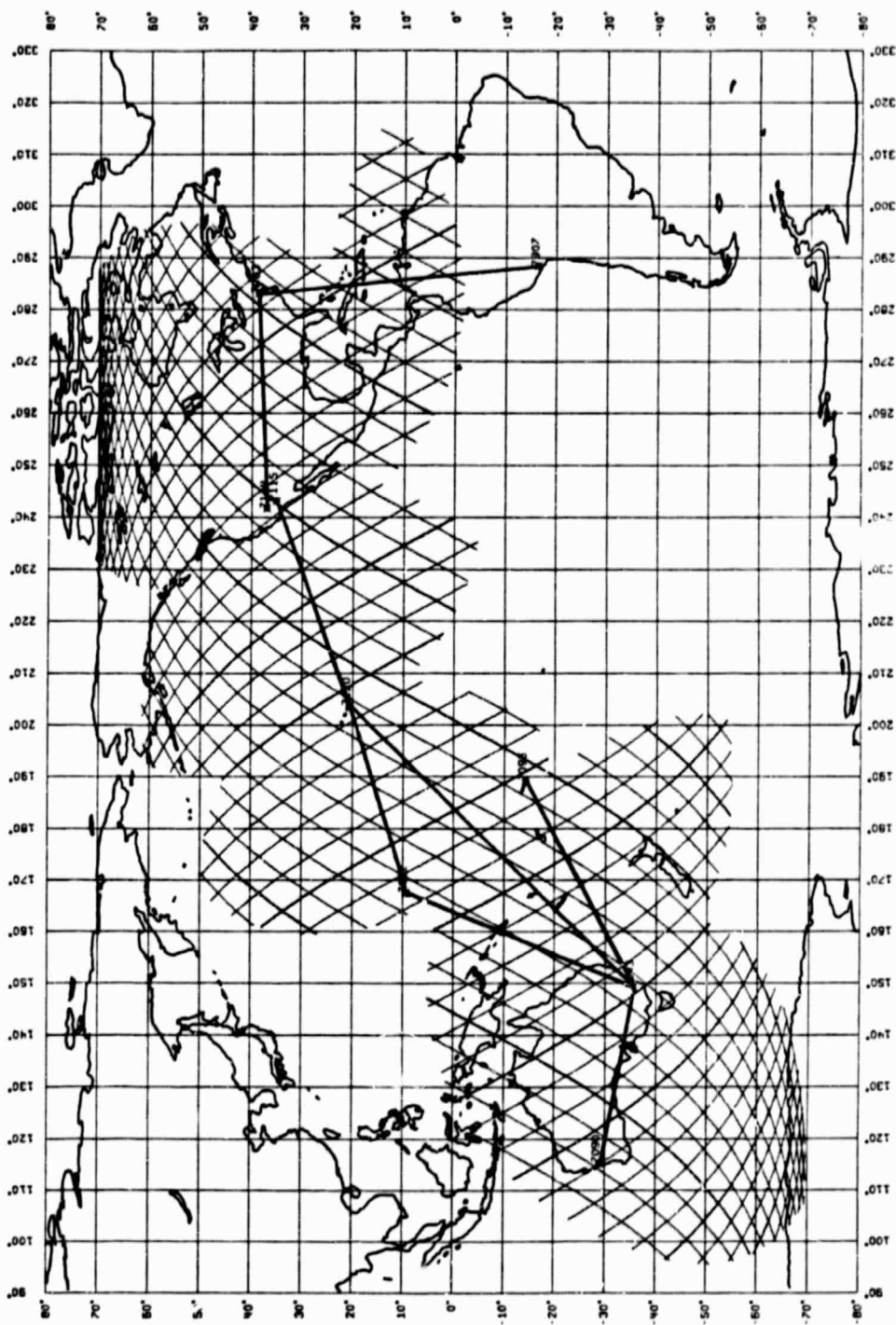


Fig. 26 Lageos groundtracks for the AG80 simulated data set.



i.e., the reference orbit is assumed perfectly known and no adjustment for it is allowed. The differences therefore between the simulated and recovered polar motion components and baselines ("recovery errors") reflect the effect of the induced orbital errors on the solved for parameters of interest.

The random error used in the first simulation has a zero mean and a 2.0 m standard deviation. The bias model of the second simulation can be analytically expressed as

$$B_i = a_i + b_i(t - t_0) + n_i \quad i = X, Y, Z \quad (144)$$

where the following (arbitrary) numerical values were used for the coefficients  $a_i$ ,  $b_i$  and the noise component  $n_i$ :

$$\begin{aligned} a_X &= -0.20 \text{ m} & b_X &= 0.01 \text{ m/day} & n_i &\sim N(0.0, 0.05) \\ a_Y &= 0.40 \text{ m} & b_Y &= -0.01 \text{ m/day} \\ a_Z &= -0.50 \text{ m} & b_Z &= 0.02 \text{ m/day} \end{aligned} \quad (145)$$

and  $t - t_0$  represents the time in days elapsed since the epoch  $t_0$  of the first day of the simulation.

The recovery of the polar motion components was done for two different averaging interval scenarios. Initially, we broke down the ten-day mission into three intervals: a four day, a five day, and a one day, in this order. Subsequently, since the data distribution permitted it, we attempted a solution for ten daily averages.

The baseline recovery simulation involved eight baselines between the same station network used for the polar motion simulation. Only the second orbit-biasing scenario was used in this simulation.

The results of the two simulations described so far have been summarized in the form of recovery errors in Table 16 for the polar motion components and Table 17 for the eight baselines. As can be seen from Table 16, the range adjustment results for the coordinates of the pole deteriorate by an order of magnitude when the orbit is perturbed by white noise (Case 1). In the case of the SRD adjustment though, the rms error increases by only 70% from its nominal value for the true orbit solution. When the errors in the orbit are of a systematic nature (equation (144)) as in Case 2, the range adjustment results exhibit a fourfold increase in the rms recovery error compared to the SRD-based results. The results of the range adjustment can be significantly improved--although still worse than the SRD results--by recovering the coordinates of the pole over shorter time intervals (Case 3). The less time the biases are allowed to accumulate, the less their effect on the estimated parameters. In this case the rms recovery error for the range adjustment dropped from 0.022 to less than 0.009 (Table 16, Case 3).

The summary of the baseline recovery adjustments are given in Table 17. Only the systematic error model was used in this simulation. The rms recovery errors were computed based on the differences of the recovered baseline lengths from the a priori (modeled) baseline lengths. They are 1.9 cm and 3.7 cm for the SRD and the range adjustment results respectively. The contrast between these results is not as impressive as in the case of the coordinates of the pole, the reason being that we are dealing here (by choice) with extremely long baselines and in most cases with rather unfavorable geometry. In fact, from Fig. 26 one can gather that except for the baseline between stations 7943 and 7092,

ORIGINAL PAGE IS  
OF POOR QUALITY

Table 16 Polar Motion Component Recovery Error Summary

Adjustment Mode	True Orbit Noise only Case	Random Orbital Error Case 1	Systematic Error Case 2	Orbital Case 3
Ranges	0.50	2.55	21.70	8.50
SRD's	0.40	0.69	6.10	6.20

Note : Table values in milliarseconds.

Table 17 Baseline Recovery Error Summary

Baselines between Stations	Adjustment with Ranges	SRD's
7053 - 7114	-0.9	-0.7
7053 - 7907	-3.2	-3.0
7090 - 7943	-1.3	1.1
7092 - 7120	-2.1	-2.5
7092 - 7943	-5.3	2.1
7096 - 7943	-3.0	2.5
7115 - 7120	0.1	0.5
7120 - 7943	-6.9	-1.3
rms recovery error (cm)	3.7	1.9

in all other cases the geometry of satellite groundtracks - baseline direction is of the type to be avoided. This strong dependence of the SRD mode on the geometry of the problem has already been pointed out in Section 4.5.2, and these results merely confirm it.

#### 5.1.2 Simulations for a proposed SLR network.

5.1.2.1 Baseline Recovery. Based on an optimal global laser station distribution (likely to be realizable by mid-1983) proposed at a recent meeting of the COTES study group [CSTG Bulletin, June 9, 1982], a simulation study for baseline recovery was performed. Except for the fact that different stations (17 total) are involved, this simulation was similar to the one previously reported for the AG80 data set. The station locations and the data distribution are given in Tables 18 and 19. Baseline estimates and their statistics were computed for both the range and the SRD adjustments. In order to assess the effect of orbital biases on the baseline recovery, the orbit used in the adjustment (range and SRD) was again biased. In this simulation, however, the bias was applied in a slightly different manner from what was done in previous simulations, by applying it in terms of a radial, an along-track, and an across-track error as follows:

radial bias	2.00 m
along-track bias	0.60 m
across track bias	-1.20 m

Two different adjustments were performed. In the first case the coordinates of all stations were obtained in a simultaneous adjustment based on the data collected from all station pairs. On the basis of this solution the baselines between all possible station combinations were

Table 18 Coordinates for the Stations Used in the Simulations

Station #	X (m)	Y (m)	Z (m)
FTDAVS 7086	-1324510.442	-5332139.932	3231791.056
WETTZE 7914	4074613.305	931963.678	4801492.271
HAWAII 7120	-5464096.683	-2402363.153	2240358.273
STALAS 7063	1130304.818	-4831721.449	3993759.624
WESTFO 7091	1492212.742	-4458121.791	4296005.489
ONSALA 7095	3392750.872	783278.257	5325906.607
HERSTM 7911	4022035.768	000000.000	4933550.635
GRAZ 7999	4130031.490	1106638.602	4716882.075
JAPAN 7935	-4121637.800	3220176.370	3637871.320
RICHMO 7069	961533.601	-5674186.968	2740519.741
QUINCY 7051	-2516274.896	-4198843.469	4075154.589
YARAGA 7090	-2389125.331	5042839.038	-3078750.728
CHILBO 7901	3844341.319	-134247.357	5070549.690
ORRORA 7943	-3912965.794	2259151.854	-4488060.975
DIONYS 7940	4728637.251	1910493.462	3817397.791
AREQUI 7907	1941330.115	-5802024.122	-1796312.986
GRASSE 7942	4550759.258	639567.505	4408096.973

Table 19 Distribution of Ranges and SRD's for Each Baseline

No.	Baseline End Stations	Length (m)	Range Obs.	SRD Obs.
1	7901 => 7914	1123487.006	7202	3601
2	7095 => 7940	2308853.694	5976	2988
3	7942 => 7999	700368.121	7460	3730
4	7095 => 7942	1484591.097	6954	3477
5	7091 => 7095	5669657.481	2594	1297
6	7063 => 7911	5708839.391	2442	1221
7	7069 => 7942	7451634.061	446	223
8	7911 => 7940	2322723.588	5884	2942
9	7901 => 7942	1239620.646	7062	3531
10	7942 => 7914	683352.290	7468	3734
11	7911 => 7095	1073641.514	7450	3725
12	7942 => 7940	1412734.544	6496	3248
13	7095 => 7999	1009482.790	7478	3739
14	7999 => 7940	1346693.532	6620	3310
15	7095 => 7914	872957.116	7612	3806
16	7091 => 7069	2044497.683	4496	2248
17	7063 => 7907	5926566.472	1024	512
18	7036 => 7907	6014011.635	994	497
19	7069 => 7907	4643137.992	1716	858
20	7069 => 7036	2363121.040	4112	2056
21	7063 => 7051	3701936.397	3944	1972
22	7051 => 7036	1848222.236	5296	2648
23	7120 => 7051	3909408.132	2950	1475
24	7120 => 7026	5167466.031	1850	925
25	7036 => 7063	2618612.747	4666	2333
26	7091 => 7036	3135345.207	4348	2174
27	7120 => 7935	5947116.046	1342	671
28	7935 => 7090	7171939.095	366	183
29	7090 => 7943	4200079.994	3226	1613
30	7935 => 7051	7603305.998	412	206

obtained along with their formal accuracies and differences with respect to their "true" values. Part of the baseline results are summarized in Table 20. Only the cases in which a station pair has coobserved have been listed. In all cases but two, one listed (7090-7943) and one not (7901-7911), the baseline lengths have been overestimated although the errors in the SRD case are about an order of magnitude smaller than the ones for the range adjustment. Since the positive radial bias results in an "expansion" of the network of satellite positions, this should come as no surprise. The stations have a global distribution and because the observations from all stations are adjusted simultaneously, their positions become interdependent and the aforementioned expansion affects all of them similarly. Fig. 27 shows the results of the two adjustments for all possible baselines.

This first solution prompted us to test the recovery of baselines from independent adjustments. In this second case the data collected from each pair of stations are adjusted independently and the estimated baselines are only the ones defined by coobserving station pairs. The results of this second type of solution are shown in Table 21. What is obvious again is that the SRD results for the baseline lengths are again superior to the range adjustment results.

The most interesting observation, though, in this solution is that on the basis of the same data the range adjustment now underestimates the baselines and the recovery errors are all negative. The reason behind this is the one-sided data distribution in this instance, as opposed to the global distribution that existed in the network adjustment case. From Fig. 26 it is obvious that we are dealing with extremely long

Table 20 Baselines Recovered from Network Adjustments

No.	Baseline End Stations	A priori Length (m)	Range Solution			SRD Solution		
			Obs.	Recovery Error (m)	Formal Sigma (m)	Obs.	Recovery Error (m)	Formal Sigma (m)
1	7901 => 7914	1123487.006	7202	0.018	0.011	3601	0.053	0.004
2	7095 => 7940	2308853.694	5976	0.230	0.009	2988	0.130	0.006
3	7942 => 7999	700368.121	7460	0.079	0.009	3730	0.033	0.003
4	7095 => 7942	1484591.097	6954	0.135	0.008	3477	0.082	0.004
5	7091 => 7095	5669657.481	2594	2.119	0.011	1297	0.257	0.015
6	7063 => 7911	5708339.391	2442	2.230	0.012	1221	0.269	0.016
7	7069 => 7942	7451634.061	446	2.713	0.011	223	0.361	0.018
8	7911 => 7940	2322728.588	5884	0.389	0.011	2942	0.117	0.006
9	7901 => 7942	1239620.646	7062	0.070	0.011	3531	0.067	0.005
10	7942 => 7914	683352.290	7468	0.075	0.009	3734	0.033	0.003
11	7911 => 7095	1073641.514	7450	0.090	0.010	3725	0.052	0.004
12	7942 => 7940	1412734.544	6496	0.151	0.009	3248	0.072	0.004
13	7095 => 7999	1009482.790	7478	0.182	0.010	3739	0.056	0.004
14	7999 => 7940	1346693.532	6620	0.043	0.010	3310	0.077	0.004
15	7095 => 7914	872957.116	7612	0.041	0.010	3806	0.051	0.004
16	7091 => 7069	2044497.683	4496	0.534	0.013	2248	0.119	0.005
17	7063 => 7907	5926566.472	1024	1.115	0.036	512	0.331	0.019
18	7086 => 7907	6014011.635	994	1.165	0.035	497	0.338	0.018
19	7069 => 7907	4643187.992	1716	0.743	0.035	858	0.256	0.016
20	7069 => 7086	2363121.040	4112	0.705	0.013	2056	0.156	0.007
21	7063 => 7051	3701986.397	3944	1.104	0.014	1972	0.218	0.009
22	7051 => 7056	1848222.236	5296	0.602	0.012	2648	0.100	0.006
23	7120 => 7051	3909408.182	2950	1.130	0.020	1475	0.246	0.011
24	7120 => 7086	5167466.031	1850	1.748	0.019	925	0.327	0.014
25	7086 => 7063	2618612.747	4666	0.622	0.013	2333	0.161	0.007
26	7091 => 7086	3185345.207	4348	0.834	0.013	2174	0.199	0.008
27	7120 => 7535	5947116.046	1342	2.147	0.045	671	0.236	0.028
28	7935 => 7090	7171939.095	366	3.100	0.031	183	0.284	0.073
29	7090 => 7943	4203079.994	3226	-0.461	0.042	1613	0.279	0.039
30	7935 => 7051	7603305.998	412	3.106	0.037	206	0.366	0.029

ORIGINAL PAGE IS  
OF POOR QUALITY

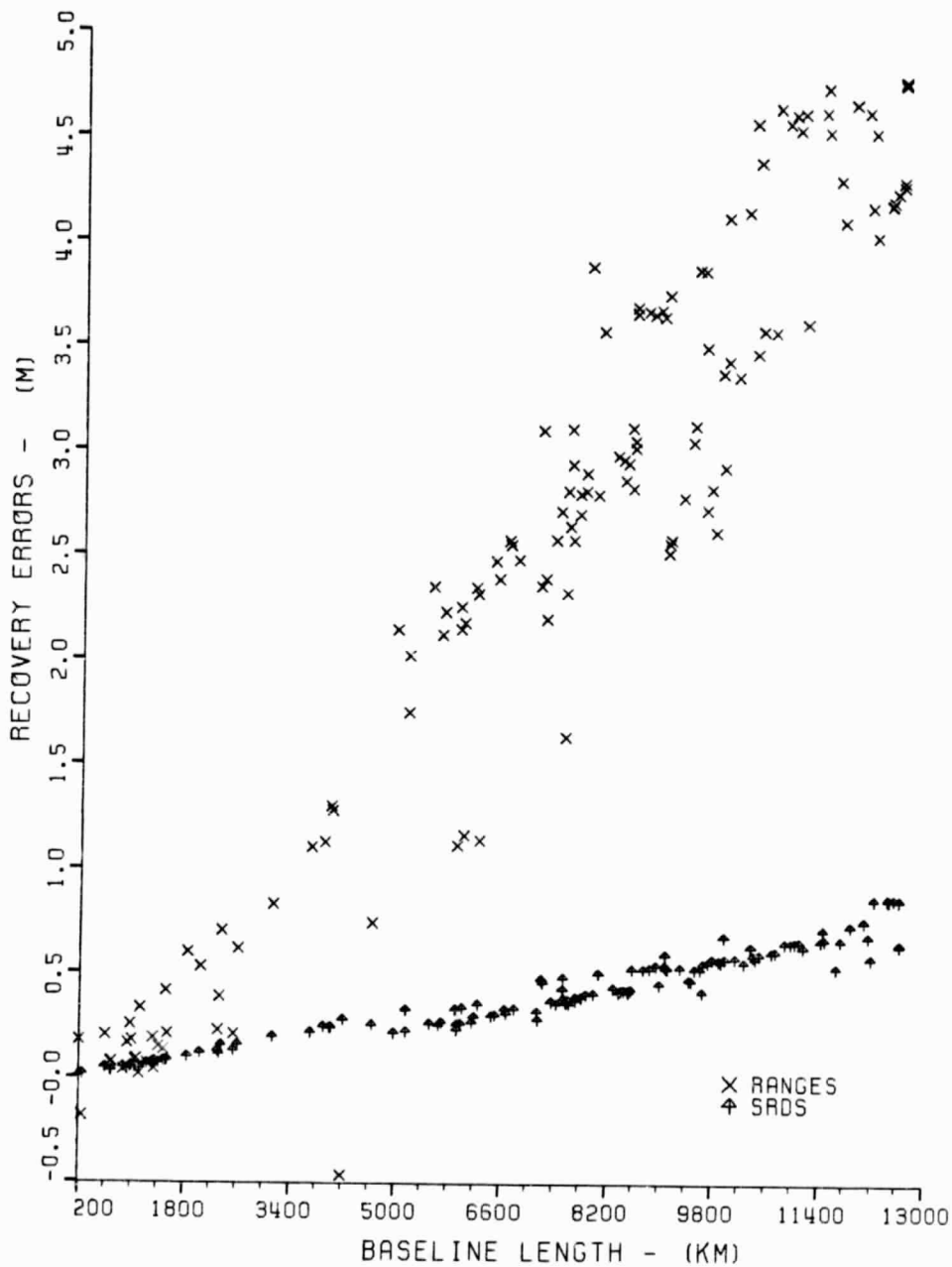




Table 21 Baselines Recovered from Independent Adjustments

No.	Baseline End Stations	A priori Length (m)	Range Solution			SRD Solution		
			Obs.	Recovery Error (m)	Formal Sigma (m)	Obs.	Recovery Error (m)	Formal Sigma (m)
1	7901 > 7914	1123487.006	7202	-0.117	0.017	3601	-0.005	0.018
2	7095 > 7940	2308853.694	5976	-0.362	0.019	2988	-0.047	0.028
3	7942 > 7999	700368.121	7460	-0.096	0.019	3730	0.010	0.016
4	7095 > 7942	1484591.097	6954	-0.228	0.020	3477	0.004	0.020
5	7091 > 7095	5669657.481	2594	-0.973	0.027	1297	0.413	0.328
6	7063 > 7911	5708839.391	2442	-1.076	0.033	1221	0.323	0.279
7	7069 > 7942	7451634.061	446	-1.397	0.165	223	0.311	5.138
8	7911 > 7940	2322728.588	5884	-0.382	0.020	2942	-0.038	0.030
9	7901 > 7942	1239620.646	7062	-0.187	0.020	3531	-0.006	0.020
10	7942 > 7914	683352.290	7468	-0.091	0.019	3734	-0.001	0.015
11	7911 > 7095	1078641.514	7450	-0.153	0.020	3725	-0.009	0.017
12	7942 > 7940	1412734.544	6496	-0.207	0.020	3248	-0.008	0.021
13	7095 > 7999	1009432.790	7478	-0.158	0.020	3739	0.002	0.017
14	7999 > 7940	1346693.532	6620	-0.194	0.019	3310	0.006	0.019
15	7095 > 7914	872937.116	7612	-0.122	0.020	3806	0.025	0.016
16	7091 > 7069	2044497.683	4496	-0.305	0.022	2248	0.010	0.029
17	7063 > 7907	5926566.472	1024	-1.165	0.057	512	0.059	0.483
18	7036 > 7907	6014011.635	994	-1.264	0.060	497	-0.083	0.627
19	7069 > 7907	4643187.992	1716	-0.864	0.037	858	0.168	0.175
20	7069 > 7036	2363121.040	4112	-0.375	0.025	2056	0.041	0.036
21	7063 > 7051	3701986.397	3944	-0.666	0.025	1972	0.038	0.069
22	7051 > 7086	1848222.236	5296	-0.308	0.023	2648	0.020	0.027
23	7120 > 7051	3909403.132	2950	-0.724	0.030	1475	-0.035	0.083
24	7120 > 7086	5167466.031	1850	-0.991	0.040	925	0.249	0.220
25	7036 > 7063	2618612.747	4666	-0.452	0.025	2333	0.090	0.039
26	7091 > 7086	3135345.207	4348	-0.569	0.026	2174	-0.041	0.050
27	7120 > 7935	5947116.046	1342	-1.211	0.052	671	-0.302	0.443
28	7935 > 7090	7171939.095	366	-1.608	0.155	183	4.760	3.401
29	7090 > 7943	4203079.994	3226	-0.811	0.029	1613	-0.069	0.090
30	7935 > 7051	7603305.998	412	-1.458	0.202	206	7.029	8.130

baselines in which case the simultaneous events are confined in the area in between the end stations. The loss of the uniform data distribution around the stations results in a one-sided biasing of the station position towards the opposite station or, better, towards the "barycenter" of the observed satellite events. Since this, as we discussed above, lies in between the two stations, thence the "shrinkage" of the estimated baselines.

For the SRD results there seems to be no bias preference, and those errors are rather randomly distributed and in almost all cases at the centimeter level. The three baselines for which the range adjustment has given better results than the SRD all have lengths in excess of 7000 km and very few observations. As it has been previously reported, the SRD mode is much more geometry dependent than the range mode, and as the results of Table 21 show it admits of its limitations very eagerly (note the formal accuracies on those baselines!). Unlike the SRD mode, the formal accuracies for the range mode give no hint whatsoever as to the real accuracy of the results. Even though the recovery errors are of the order of a few decimeters in all cases, the reported  $\hat{\sigma}$ 's are hardly ever higher than 2 cm! A pictorial presentation of the recovery errors for this solution are shown in Fig. 28.

On the basis of these simulations one can conclude that the SRD mode will in all likelihood provide more meaningful results in the presence of unmodeled orbital biases of the type considered herein than the range mode, and it will also give more reliable accuracy estimates for those results. Comparing the batch (global) solution to that of individual adjustments, the latter seems to be by far a better approach in the

ORIGINAL PAGE IS  
OF POOR QUALITY

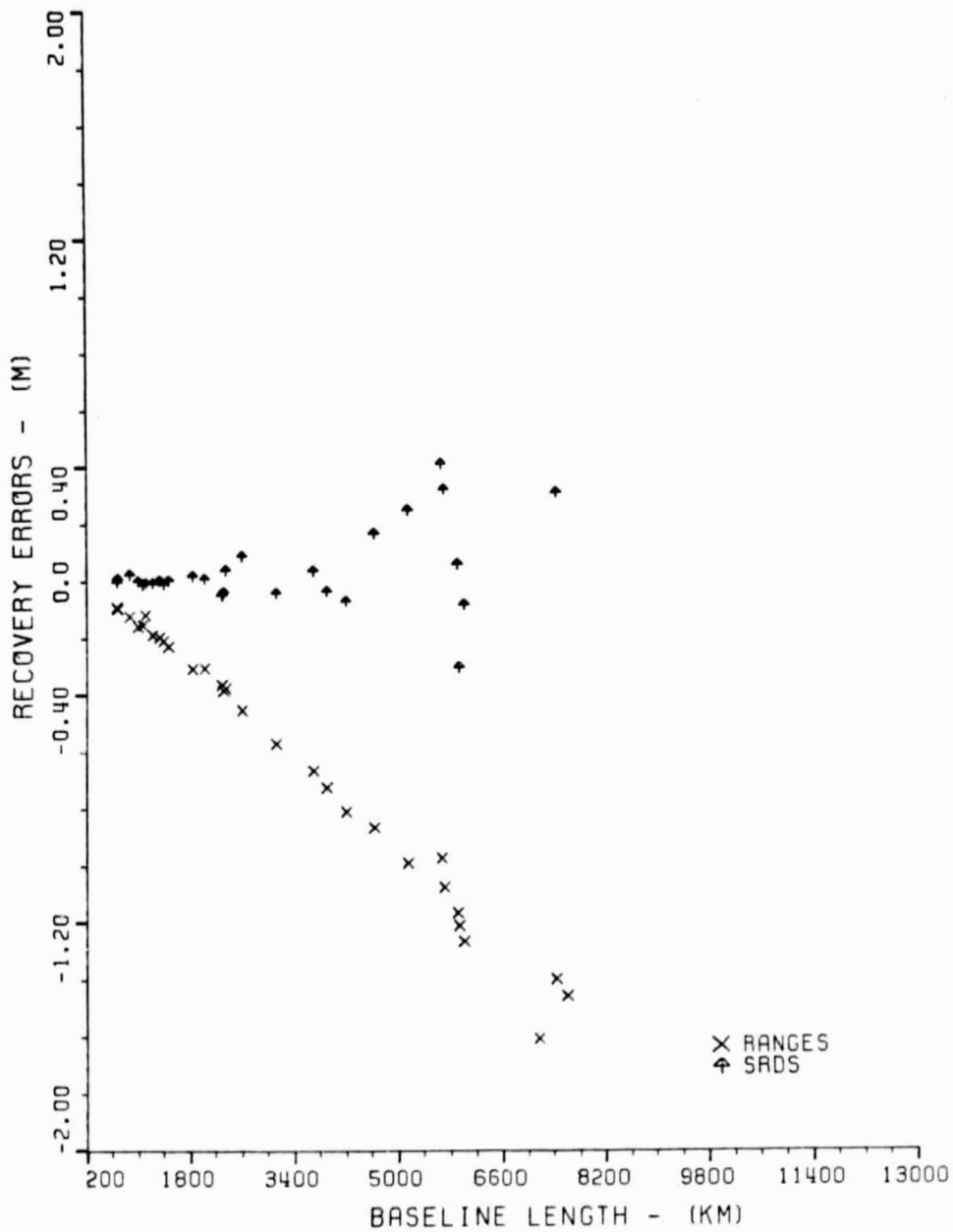


Table 22 Summary Statistics for Baseline Recovery Errors

Adjustment Mode :		Network	Independent
Statistic	Observable		
Mean Recovery Error (cm)	Ranges	89	-55
	SRD's	18	4
Mean Ratio Error/Sigma	Ranges	52	-17
	SRD's	17	0.2

case of SRD observations, although the opposite is true for the range observations. Compare, for instance, the level of recovery errors between Tables 20 and 21. This is also documented by the average values of the recovery errors displayed in Table 22 for both the ranges and the SRD's as obtained from the network as well as the independent solutions.

5.1.2.2 Polar Motion Parameter Recovery. Since the global rotations of the CTS polyhedron will be monitored by a subset of the defining stations [CSTG Bulletin, June 9, 1982], we selected four baselines out of the 136 possible between the proposed 17 stations [ibid.] to investigate the performance of such a subnetwork in estimating the coordinates of the pole.

The selected baselines were chosen in such a way that they conform as nearly as possible with the optimality criteria established in the previous chapter of this investigation with respect to polar motion estimation from SRD observations. The locations of the eight stations defining these baselines are given in Fig. 29. A set of SRD observations was

ORIGINAL PAGE IS  
OF POOR QUALITY

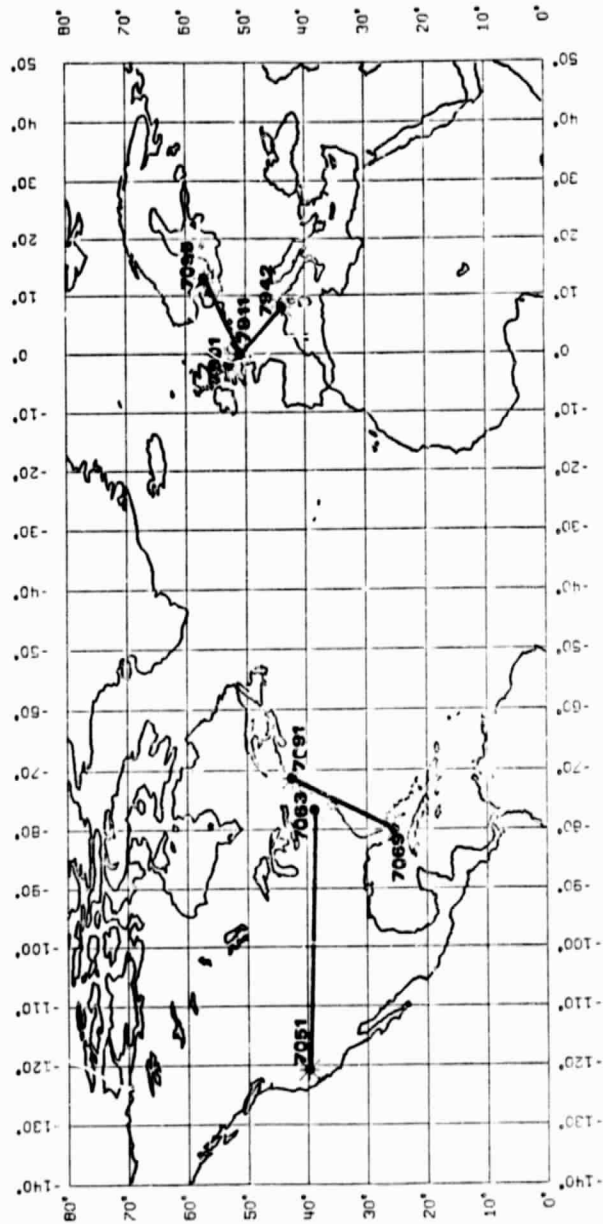


Fig. 29 Baseline network for polar motion monitoring.

generated, spanning a seven-day period, August 14 through 20, 1980. The sampling rate in this simulation was one observation per minute, and to each SRD observation was added a white noise component with a standard error of 14 cm, the equivalent of 10 cm in each range. The coordinates of the pole were specified as two-day averages; their "true" numerical values are given in Table 23. The satellite orbit was biased in the same manner as for the previous simulation, this time by the following errors:

radial bias	1.00 m
along-track bias	0.06 m
across-track bias	-0.12 m

Table 23 Polar Motion Component Values Used  
in the Simulations

Time Interval		True Values	
YYMMDD	YYMMDD	x	y
800814	- 800816	-0"020	0"310
800816	- 800818	-0"019	0"311
800818	- 800820	-0"018	0"312

The results of the two adjustments for the three two-day averages of the coordinates of the pole are shown in Table 24. The rms errors for the range adjustment are nearly an order of magnitude higher than those for the SRD adjustment. Table 25 lists the statistics of the estimated coordinates of the pole for both adjustments. Despite the comments made above as to the quality of each solution, the formal statistics give no hint at all about it, and it should once again be pointed out that they are completely unreliable in the presence of unmodeled errors.

Table 24 Polar Motion Component Recovery Results, Complete Data Set Solution

Simulated Pole Coordinates		True Values		Recovered Pole Coordinates		SRD Solution	
Time Interval	YYMMDD	x	y	Range Solution	SRD Solution	x	y
800814 - 800816		-0"020	0"310	-0"008	0"316	-0"019	0"308
800816 - 800818		-0"019	0"311	-0"004	0"317	-0"019	0"311
800818 - 800820		-0"018	0"312	-0"006	0"318	-0"017	0"311
rms recovery error				0"013	0"006	0"001	0"001

Table 25 Statistics for the Recovered Polar Motion Components Obtained from the Complete Data Set

Step	Range Solution		SRD Solution			
	Standard Deviations	Correlation	Standard Deviations	Correlation		
(i)	$\sigma_{x(i)}$ (mas)	$\sigma_{y(i)}$ (mas)	$x(i) \leftrightarrow y(i)$	$\sigma_{x(i)}$ (mas)	$\sigma_{y(i)}$ (mas)	$x(i) \leftrightarrow y(i)$
1	0.039	0.083	-0.023	0.314	0.459	-0.148
2	0.039	0.087	-0.046	0.311	0.459	-0.142
3	0.090	0.087	0.003	0.311	0.459	-0.145

It must be obvious by now that an order of magnitude improvement in the accuracy of the coordinates of the pole can be achieved by analyzing the exact same range observations in the SRD mode. One should also consider that this particular simulation is based on feasible station locations which are in no way the optimal network for polar motion determination, and additionally no effort was made to single out the optimal satellite passes for each specific baseline. Yet, the results are rather promising in view of the generally accepted requirement of 0"002-accurate pole positions over two-day intervals.

In an effort to account for the effect of loss of data we have readjusted the simulated observations only this time we restricted the

admissible observations to those with an elevation of 40° above the station's horizon. The recovered coordinates of the pole and their statistics are given in Tables 26 and 27 respectively. The SRD adjustment still recovers the parameters better than the range adjustment. What is more interesting here, however, is the indication of a downward trend in the correlations between the recovered values for the SRD case and the opposite for the range case. When we used the more restricted data set in the second simulation, we in effect forced our observations to lie within and around the two baseline stations. As we have already seen in Section 4.5.3, this is the optimal region for selecting observations which will result in the highest sensitivity with respect to one of the parameters and the lowest with respect to the other. Although the

Table 26 Polar Motion Component Recovery Results, Restricted Data Set Solution

Simulated Pole Coordinates		Recovered Pole Coordinates					
Time Interval		True Values		Range Solution		SRD Solution	
YYMMDD	YYMMDD	x	y	x	y	x	y
800214	- 800316	-0"020	0"310	0"091	0"311	-0"021	0"308
800316	- 800318	-0"019	0"311	0"095	0"305	-0"019	0"310
800318	- 800320	-0"018	0"312	0"017	0"303	-0"019	0"309
rms recovery error				0"028	0"007	0"000	0"002

Table 27 Statistics for the Polar Motion Components As Obtained from the Restricted Data Set

Step	Range Solution			SRD Solution		
	Standard Deviations	Correlation		Standard Deviations	Correlation	
(i)	$\sigma_x(i)$ (mas)	$\sigma_y(i)$ (mas)	$x(i) \leftrightarrow y(i)$	$\sigma_x(i)$ (mas)	$\sigma_y(i)$ (mas)	$x(i) \leftrightarrow y(i)$
1	0.464	0.597	0.068	1.203	1.161	-0.103
2	0.498	0.615	-0.016	1.219	1.112	-0.104
3	0.493	0.606	0.006	1.246	0.955	-0.044



original correlation of -15% is not really significant, it is only fair to point out that in the restricted second simulation it drops to -10% or less. At the same time the range adjustment results show in general a slight increase in the correlation.

Finally, we compare the formal accuracy estimates between the two solutions. The first simulation is based on 7407 SRD's, while the second on only 669, a ratio of about 11:1. Since in both cases the noise level is the same, one would expect that the increase in the formal accuracies between the two adjustment should follow the  $\sqrt{n}$  law,  $n$  being the ratio of the observations between the two solutions, or in our case we would expect roughly a threefold increase in the  $\sigma$ 's of the recovered parameters. Any deviation from this ratio on the higher side indicates that the poorer data distribution affects the solution, while on the lower side it indicates that the new geometry is superior to the former. This is exactly what happens here since the  $\sigma$ -ratio for the ranges is nearly 5.6 (compared to the expected  $\sqrt{11.07} \approx 3.3$ ), while for the SRD's it is only 2.5. The invoked data selection has not only compensated for the loss of data, but in fact it has improved the sensitivity of the system with respect to the estimated parameters.

## 5.2 Experiments with Real Data

### 5.2.1 Preliminary adjustment for data editing.

Since the purpose of this investigation is the introduction and study of a new method for the analysis of ranging observations to satellites and in particular to Lageos, knowing the quality of the data which we planned to use for testing the method was one of our primary concerns. As we have already discussed, the distributing agencies such as NASA and SAO do edit the raw data and delete most of the spurious observations.

This editing, however, is done on a pass-by-pass basis and not for the whole aggregate of the available data. To do so one has to "fit" an orbit to the data as a whole and to compare the discrepancies of each observation from that orbit. This is the primary reason for which we considered an adjustment for the complete data set as a necessity.

Secondarily, though, such an analysis of the data would also provide an indication of how well and to which level of accuracy our orbital model fit the data. The lower the rms residual of the observations, the better the orbital model deployed. The qualitative and quantitative characteristics of this model are of great interest in this investigation. We will later use this model to calculate the reference orbit with respect to which the SRD observations are adjusted.

Last but not least, since most of the data have already been analyzed by other agencies, the results of our own software (GEOSP--GEO-Satellite Positioning Program) could provide a check on the code and give us some confidence in the program. This latter is always a major problem since, as someone put it, "Every nontrivial program has at least one error."

An initial inspection of the August, 1980, Lageos data set (Section 5.1.1) had already indicated that the highest concentration of simultaneously observed Lageos passes fell in the second half of the month of August. For that reason our effort focused on the subset of data spanning the period from August 14 through 31, 1980. It turns out that the last coobserved pass occurs on August 28. Data from the ten most active stations during that period were selected in order to subsequently be used for SRD event generation. A total of 24240 range observations were selected in such a way that all stations but one (7907) have nearly the same amount of data. These data were analyzed with our computer program GEOSPP in a preliminary adjustment.

The theory behind the orbital model used in GEOSPP has been described in Section 2.2; the numerical values for some of the constants used in the program are given in Table 28. We have used the geopotential coefficients of the preliminary model PGS-L1 [Lerch and Klosko, 1981] up to degree and order twelve, since as it is reported in [ibid.] the perturbations of higher harmonics for such a short period of time (14 days) are nearly equal with the errors caused by the uncertainties in the

Table 28 Numerical Values of Constants Used by GEOSPP

Semi-axis major.....:	6378144.11	(m)
Inverse flattening.....:	298.255	---
Gravitational constant.....:	398600.4125x10 <sup>9</sup>	(m <sup>3</sup> /s <sup>2</sup> )
Rotational rate.....:	0.000072921158547	(rad/s)
Speed of light.....:	299792458.0	(m/s)
Astronomical Unit (1 AU).....:	149597870950.0	(m)
Solar pressure at 1 AU.....:	4.62576x10 <sup>-6</sup>	(N/m <sup>2</sup> )

**ORIGINAL PAGE IS  
OF POOR QUALITY**

coefficients themselves. An initial state vector for Lageos was provided by Dr. P. Dunn, although in a reference frame different from that used in GEOSPP. The state vector that we used was obtained from the former by applying to the former the nutation, precession and equinox

Table 29 Numerical Orbit Integration Information for GEOSPP

**VARIABLE ORDER-VARIABLE STEPSIZE NUMERICAL INTEGRATION :**  
=====

NOMINAL STEPSIZE.....: 140.0 SEC  
 MINIMUM STEPSIZE.....: 0.0 SEC  
 MAXIMUM STEPSIZE.....: 600.0 SEC  
 RELATIVE ACCURACY  
 EQUATIONS OF MOTION.....: 1.0D-07  
 VARIATIONAL EQUATIONS...: 1.0D-04  
 INT.MESSAGE OUTPUT UNIT : 21

**PERTURBATION MODEL :**  
=====

GEOPOTENTIAL.....: (12,12)  
 FOR VARIATIONAL EQUATIONS.....: ( 4, 4)  
 MOON.....: YES  
 SUN.....: YES  
 UNMODELED ACCELERATIONS.....: YES  
   ALONG TRACK = -0.3489D-11 (M/S2)  
   CROSS TRACK = 0.0 (M/S2)  
   RADIAL = 0.0 (M/S2)  
 SOLAR RADIATION PRESSURE.....: YES  
   SATELLITE AREA = 0.2827 (M2)  
   SATELLITE MASS = 406.9650 (KG)  
   SATELLITE REFLECTIVITY CR= 1.1729  
 SOLID EARTH TIDES.....: YES  
   LOVE NO. K2=0.2740  
   PHASE ANGLE E2=2.3300  
 LOVE NUMBER FOR RADIAL EXPANSION H2 = 0.600  
 SHIDA NUMBER FOR HORIZONTAL SHEAR L2 = 0.075

**INPUT INFORMATION FOR ARC : 7603901.01**  
=====

                                  YYMMDD HHMMSS.SSS  
 EPOCH OF ELEMENTS.....: 80 813 235930.028  
 OBSERVATIONS START AT...: 80 814 0 0 0.000  
 OBSERVATIONS END AT....: 80 829 0 0 0.000  
 REFERENCE SYSTEM EPOCH.: 80 731

**INERTIAL CARTESIAN ELEMENTS AT THE EPOCH :**  
=====

X (M)	Y (M)	Z (M)
-5998161.430	-5961700.182	-9377042.063
XDOT (M/S)	YDOT (M/S)	ZDOT (M/S)
-4720.0626632	-870.0206757	3111.3650676

ORIGINAL PAGE IS  
OF POOR QUALITY

corrections that relate the two reference frames. The result along with the other information required for the numerical integration of the orbit is given in Table 29. The orbit was allowed to adjust freely in this solution. The a priori station locations are given in Table 30. Table 31 gives the summary of the residuals' statistics for the last iteration of the solution. We have already discussed the fact that the dynamic mode is an ill-conditioned problem due to the physical

Table 30 A Priori CTS Station Coordinates

Station No.	X (m)	Y (m)	Z (m)
STALAS 7063	1130711.700	-4831371.300	3994088.700
ML0502 7090	-2389002.297	5043333.488	-3078528.544
ML0702 7091	1492450.900	-4457281.700	4296817.000
ML0802 7092	-6143448.500	1364706.900	1034164.800
ML0602 7096	-6100049.584	-996197.831	-1568978.317
ML0211 7114	-2410428.196	-4477802.221	3838688.071
ML0307 7115	-2350867.357	-4655546.092	3660999.228
ML0110 7120	-5466003.686	-2404404.305	2242228.593
ARELAS 7907	1942786.100	-5804078.900	-1796938.600
ORRLAS 7943	-4447545.681	2677137.812	-3694997.951

Table 31 Residual Summary for the Complete Lageos Range Data Set Adjustment by GEOSPP

ADJUSTMENT STATISTICS FOR ITERATION : 2  
=====

DEGREES OF FREEDOM FOR THIS ADJUSTMENT.....: 24234  
 PREVIOUS WEIGHTED SUM OF SQUARES OF THE RESIDUALS/D.F.....: 0.1760  
 CURRENT WEIGHTED SUM OF SQUARES OF THE RESIDUALS/D.F.....: 0.1760  
 IMPROVEMENT IN PERCENT (NEG.SIGN INDICATES DECREASE).....: 0  
 CONTRIBUTION FROM STATION PARAMETER CONSTRAINTS.....: 1745.D-04  
 CONTRIBUTION FROM POLAR MOTION PARAMETER CONSTRAINTS.....: 5508.D-12  
 CONTRIBUTION FROM ORBITAL PARAMETER CONSTRAINTS.....: 0.

PASS BY PASS BREAKDOWN OF ADJUSTMENT STATISTICS FOR ITERATION : 2  
=====

PASS NO.	CONSTRAINTS FROM : STATIONS	P.M.	STEPS	ORBIT	TOTAL NO.OF CONSTRAINTS	NUMBER OF OBSERVATIONS	NUMBER OF PARAMETERS
1	30	6	0		36	24240	42

WEIGHTED SS. OF RESIDUALS	DEGREES OF FREEDOM	VARIANCE COMPONENT	VTPV(1) #OBS.-6	RMS OF THE RESIDUALS	MEAN OF RESIDUALS
0.42666D+04	24234	0.1761	0.18	0.4195	-0.0009

characteristics of the earth (Section 4.3). This ill-conditioning can be alleviated in a range data solution if, for example, the longitude of one station is constrained. In this particular problem though we preferred an alternate solution which has been discussed previously in [Pavlis, 1979], that is, the "ridge estimation." By applying a very small weight in all station coordinates, we overcome the numerical singularity of the normal equation matrix and at the same time we show no preference for any single station. The weight applied in this case corresponds to a variance of  $(50 \text{ m})^2$  in each station coordinate.

As the residual summary in Table 31 shows, the data seem to be of rather good quality since they fit the orbit with an rms of 42 cm overall. The station position estimates and their statistics are given in Table 32 and the adjusted satellite state vector and its statistics in Table 33. It should be no surprise that the estimated variances for the X and Y coordinates are so much higher than those for Z. The ridge estimator has overcome the numerical singularity, but it does not separate completely the two parameters which are associated with the stations' longitude, i.e., X and Y. This should be of no immediate concern, since the relative quantities such as the baseline lengths which are of more interest to us are not affected by this peculiarity.

The estimates for the baseline lengths for all possible station pairs (45 total) are given in Table 34 along with their formal accuracies. All of these estimates show an internal consistency of 2 - 3 cm. Exceptions are the baselines which involve station 7907, primarily because that station has almost ten times less data than the average station in the solution.

Table 32 Station Coordinates and Standard Deviations Estimated by GEOSPP

Station No.	X (m)	Y (m)	Z (m)	$\sigma_X$ (m)	$\sigma_Y$ (m)	$\sigma_Z$ (m)
STALAS 7063	1130700.445	-4651371.261	3994080.935	5.728	1.341	0.040
ML0502 7090	-2389000.008	5043224.831	-3078527.612	5.979	2.833	0.035
ML0702 7091	1492448.214	-4457282.664	4296817.845	5.284	1.770	0.041
ML0802 7092	-6143448.162	1364709.118	1034163.064	1.618	7.284	0.041
ML0602 7096	-6100049.965	-996195.202	-1568977.313	1.181	7.232	0.041
ML0211 7114	-2410430.112	-4477001.286	3838688.977	5.309	2.858	0.040
ML0307 7115	-2350869.216	-4655545.167	3660999.858	5.519	2.787	0.037
ML0110 7120	-5466004.678	-2404402.080	2242229.461	2.851	6.481	0.040
ARELAS 7907	1942783.228	-5804080.205	-1796919.713	6.881	2.304	0.091
ORRLAS 7943	-4447544.472	2677140.227	-3694997.074	3.174	3.273	0.034

Table 33 Initial State Vector for Lageos As Obtained by GEOSPP from the Complete Lageos Range Data Set Adjustment

Reference System :		Mean of 800731		
P O S I T I O N		X (m)	Y (m)	Z (m)
Estimate :		-5097881.421	-5961549.913	-9377290.436
Standard Deviation :		7.068	6.044	0.042
rms position (m) :			5.369	
V E L O C I T Y		$\dot{X}$ (m/s)	$\dot{Y}$ (m/s)	$\dot{Z}$ (m/s)
Estimate :		-4720.07387	-871.25438	3111.28230
Standard Deviation :		0.00103	0.00560	0.00002
rms velocity (m/s) :			0.00329	
Reference System :		TOD 800813 235930.028		
Position (m) :		-5098243.471	-5961677.201	-9377012.675
Velocity (m/s) :		-4720.05663	-870.98060	3111.38509
Note : TOD - "True of Date"				

ORIGINAL PAGE IS  
OF POOR QUALITY

Table 34 Baseline Lengths and Standard Deviations Estimated by GEOSPP

Baseline No.	End Stations	Apriori Estimate (m)	Adjusted Value (m)	Adjusted minus Apriori	Sigma (m)
1	7063 ==> 7090	12645951.761	12645950.847	-0.914	0.018
2	7063 ==> 7091	602032.143	602032.169	0.026	0.036
3	7063 ==> 7092	10003296.515	10003295.833	-0.682	0.025
4	7063 ==> 7096	9896473.055	9896471.526	-1.528	0.022
5	7063 ==> 7114	3562138.713	3562137.442	-1.272	0.041
6	7063 ==> 7115	3501893.178	3501891.797	-1.381	0.037
7	7063 ==> 7120	7244020.742	7244019.261	-1.482	0.028
8	7063 ==> 7907	5928036.951	5928019.003	-17.948	0.085
9	7063 ==> 7943	12108539.654	12108538.064	-0.990	0.018
10	7090 ==> 7091	12638160.062	12638160.219	0.156	0.024
11	7090 ==> 7092	6674009.770	6674008.743	-1.027	0.024
12	7090 ==> 7096	7247520.432	7247520.743	0.311	0.023
13	7090 ==> 7114	11768618.014	11768618.337	0.323	0.018
14	7090 ==> 7115	11810628.856	11810629.014	0.158	0.016
15	7090 ==> 7120	9656458.579	9656458.910	0.331	0.021
16	7090 ==> 7907	11750456.119	11750458.620	2.500	0.034
17	7090 ==> 7943	3196328.733	3196328.646	-0.087	0.021
18	7091 ==> 7092	10141371.223	10141371.602	0.379	0.031
19	7091 ==> 7096	10199643.124	10199642.536	-0.587	0.025
20	7091 ==> 7114	3929728.800	3929728.019	-0.782	0.039
21	7091 ==> 7115	3900598.445	3900597.570	-0.876	0.034
22	7091 ==> 7120	7540273.824	7540273.123	-0.701	0.029
23	7091 ==> 7907	6257037.782	6257020.271	-17.511	0.088
24	7091 ==> 7943	12249596.212	12249596.272	0.059	0.022
25	7092 ==> 7096	3514556.686	3514554.371	-2.316	0.027
26	7092 ==> 7114	7479017.596	7479018.461	0.865	0.027
27	7092 ==> 7115	7584680.410	7584681.155	0.745	0.028
28	7092 ==> 7120	4015538.430	4015538.979	0.550	0.028
29	7092 ==> 7907	11171115.715	11171110.424	-5.291	0.041
30	7092 ==> 7943	5192643.026	5192640.982	-2.044	0.024
31	7096 ==> 7114	7414696.951	7414696.912	-0.040	0.023
32	7096 ==> 7115	7402692.901	7402692.731	-0.170	0.025
33	7096 ==> 7120	4112220.542	4112220.461	-0.081	0.025
34	7096 ==> 7907	9373094.052	9373093.497	-0.554	0.044
35	7096 ==> 7943	4554571.701	4554572.165	0.464	0.024
36	7114 ==> 7115	258289.958	258290.167	0.210	0.036
37	7114 ==> 7120	4022959.527	4022959.505	-0.022	0.031
38	7114 ==> 7907	7243602.178	7243588.024	-14.154	0.076
39	7114 ==> 7943	10587702.281	10587702.701	0.420	0.018
40	7115 ==> 7120	4096904.174	4096904.146	-0.027	0.031
41	7115 ==> 7907	7038726.657	7038712.246	-14.411	0.074
42	7115 ==> 7943	10595990.172	10595990.425	0.253	0.018
43	7120 ==> 7907	9097407.601	9097399.389	-8.212	0.052
44	7120 ==> 7943	7880988.899	7880989.300	0.401	0.022
45	7907 ==> 7943	10787493.058	10787496.735	3.676	0.041

The station-by-station and pass-by-pass analysis of the residuals gives some more insight into the relative performance of the stations and the relative quality of their data. Tables 42 through 51 in Appendix D give these summaries for each of the ten stations. In general, the standard deviation of the residuals in a pass is at the decimeter level,



although for some of the stations (e.g., 7063, 7907, and 7943) it is about three times higher than that or more. In addition to that, it seems that the observations from three of the stations on four particular occasions include an unreasonably high bias. These are

for station 7063: pass #4	-2.1 m	(cf. Table 42),
pass #8	-4.4 m	

for station 7114: pass #11	-4.5 m	(cf. Table 47),
----------------------------	--------	-----------------

and for station 7115: pass #4	-6.8 m	(cf. Table 48).
-------------------------------	--------	-----------------

Overall, the data seem to be of consistent quality, except for the instances cited above, and the performance of the orbital model and the computer software were satisfactory.

The data were subsequently examined to find the baselines with the most simultaneously observed passes. A computer program (OVERLAP) supplied to us by Mr. R. Kolenkiewicz of NASA/GSFC was used for this purpose. When we isolated the data falling in the overlap periods and examined their distribution by station and by time, it was realized that there were no aggregates of passes that spanned intervals of time long enough to detect polar motion with decimeter level observations. In addition to that, the number of observations per baseline was disappointingly small to attempt a baseline solution, except perhaps for the station pair 7943-7090 which had 984 observations. For these reasons we concentrated on attempting a solution in the SRD mode with data collected from the aforementioned baseline only.

5.2.2 Estimation of the 7943-7090 baseline.

The overlap range data from stations 7943 and 7090 were processed along the guidelines established in Chapter 3 for the generation of "quasi-observable" SRD's. The data distribution for the range observations from each station is given in Tables 35 and 36. Out of these nearly 7500 range observations, only 975 simultaneous events could be generated. The corresponding range data set of course contains exactly twice as many observations, i.e., 1950.

Table 35 Observation Summary for Range Data from Station 7943

Station : 7943		Passes Tracked : 32		Observations total : 3418			
Pass No.	Beginning Date YYMMDD HHMMSS.S	Ending Date YYMMDD HHMMSS.S	Pass Duration (s)	Obs.	Density Lag (s)		
1	800814 1101 0.2	800814 112015.2	1154.9	56	20.62		
2	800815 92745.0	800815 100630.3	2325.3	122	19.06		
3	800815 124959.9	800815 132145.0	1905.1	82	23.23		
4	800815 1603 7.7	800815 1641 0.0	2272.3	98	23.19		
5	800815 1945 7.6	800815 200952.4	1484.7	83	17.89		
6	800816 81544.9	800816 84152.7	1567.8	85	18.44		
7	800816 114022.8	800816 1204 7.8	1425.0	90	15.83		
8	800816 144522.7	800816 1531 7.7	2745.0	212	12.95		
9	800816 181515.0	800816 190345.0	2910.0	159	18.30		
10	800817 101652.8	800817 1049 7.7	1934.9	47	41.17		
11	800817 134030.4	800817 140545.0	1514.7	54	28.05		
12	800817 170115.0	800817 1728 0.0	1605.0	75	21.40		
13	800818 90422.7	800818 93445.2	1822.5	139	13.11		
14	800818 1217 0.2	800818 124837.7	1897.5	100	18.97		
15	800818 153015.1	800818 161930.1	2955.0	170	17.38		
16	800818 191822.5	800818 194952.5	1890.0	106	17.83		
17	800819 110015.2	800819 113215.1	1919.9	90	21.33		
18	800820 125830.2	800820 133437.7	2167.5	44	49.26		
19	800821 1507 7.7	800821 154515.2	2287.5	79	28.96		
20	800821 183030.1	800821 191159.9	2489.8	178	13.99		
21	800822 102622.7	800822 105115.2	1492.5	38	39.28		
22	800822 134252.8	800822 141745.3	2092.5	88	23.78		
23	800822 170915.1	800822 175622.4	2827.3	172	16.44		
24	800823 92930.2	800823 940 0.1	629.9	73	8.63		
25	800825 131730.2	800825 134430.1	1619.9	67	24.18		
26	800825 163237.7	800825 165937.4	1619.7	96	16.97		
27	800826 34152.6	800826 91352.5	1919.9	163	11.78		
28	800826 115522.7	800826 122837.7	1995.0	191	10.44		
29	800826 150922.7	800826 155922.5	2999.8	262	11.45		
30	800828 92537.5	800828 958 0.2	1942.7	97	20.03		
31	800828 1238 0.0	800828 131415.1	2175.1	61	35.66		
32	800828 155722.7	800828 162230.1	1507.4	41	36.77		

Table 36 Observation Summary for Range Data from Station 7090

Station : 7090		Passes Tracked : 30		Observations total : 4143		
Pass No.	Beginning Date YYMMDD HHMMSS.S	Ending Date YYMMDD HHMMSS.S	Pass Duration (s)	Obs.	Density Lag (s)	
1	800814 73524.0	800814 81120.0	2156.0	97	22.23	
2	800814 110144.0	800814 1138 6.0	2182.0	167	13.07	
3	800814 1735 8.0	800814 1817 7.0	2519.0	182	13.84	
4	800814 210657.0	800814 2148 8.0	2471.0	207	11.94	
5	800815 93831.0	800815 102222.0	2631.0	196	13.42	
6	800815 162235.0	800815 165245.0	1810.0	141	12.84	
7	800815 1941 5.0	800815 202838.0	2853.0	263	10.85	
8	800818 91445.0	800818 94842.0	2037.0	119	17.12	
9	800818 124141.0	800818 1259 1.0	1040.0	67	15.52	
10	800818 190634.0	800818 1953 1.0	2787.0	171	16.30	
11	800819 111532.0	800819 114928.0	2036.0	136	14.97	
12	800819 175015.0	800819 183136.0	2481.0	203	12.22	
13	800819 212421.0	800819 213355.0	574.0	50	11.48	
14	800820 629 6.0	800820 65033.0	1287.0	29	44.38	
15	800820 200224.0	800820 204123.0	2339.0	136	17.20	
16	800821 83132.0	800821 91537.0	2645.0	104	25.43	
17	800822 72745.0	800822 74943.0	1318.0	55	23.96	
18	800822 104041.0	800822 111838.0	2277.0	162	14.06	
19	800822 171526.0	800822 175657.0	2491.0	173	14.40	
20	800822 204756.0	800822 2128 5.0	2409.0	136	17.71	
21	800826 84746.0	800826 928 7.0	2421.0	155	15.62	
22	800826 122016.0	800826 123826.0	1090.0	41	26.59	
23	800826 1534 1.0	800826 155759.0	1438.0	88	16.34	
24	800826 1847 5.0	800826 193427.0	2842.0	233	12.20	
25	800827 105652.0	800827 112919.0	1947.0	115	16.93	
26	800827 143042.0	800827 143215.0	93.0	6	15.50	
27	800827 172746.0	800827 181144.0	2638.0	189	13.96	
28	800827 210429.0	800827 213938.0	2109.0	154	13.69	
29	800828 161247.0	800828 164735.0	2088.0	154	13.56	
30	800828 1937 5.0	800828 2022 5.0	2700.0	214	12.62	

Both data sets were adjusted using the GEOSPP program to obtain station positions with respect to a fixed orbit. The results for the station positions and the associated baseline length from the range and SRD adjustments are given in Tables 37 and 38 respectively. The two baseline estimates differ by about one meter, which considering the fact that the SRD observations are good to about 0.5 m and, taking into account the sparseness of the data used in this experiment, can hardly be used as a basis for drawing firm conclusions about the absolute quality of the two estimates.

ORIGINAL PAGE IS  
OF POOR QUALITY

Table 37 Station Coordinates and Baseline Length Estimates and Statistics Obtained from the Range Data Adjustment

Station No.	X (m)	Y (m)	Z (m)	$\sigma_X$ (m)	$\sigma_Y$ (m)	$\sigma_Z$ (m)
ML0502 7090	-2389000.233	5043334.860	-3078527.569	0.043	0.038	0.027
ORRLAS 7943	-4447544.467	2677140.178	-3694997.100	0.048	0.032	0.033
Baseline Length (m)	3196328.569					
Standard Deviation (m)	0.062					

Table 38 Station Coordinates and Baseline Length Estimates and Statistics Obtained from the SRD Data Adjustment

Station No.	X (m)	Y (m)	Z (m)	$\sigma_X$ (m)	$\sigma_Y$ (m)	$\sigma_Z$ (m)
ML0502 7090	-2389002.227	5043335.760	-3078530.595	0.744	0.560	0.669
ORRLAS 7943	-4447545.783	2677142.099	-3695000.143	0.595	0.750	0.658
Baseline Length (m)	3196327.380					
Standard Deviation (m)	0.342					

Besides that, if we consider the location of the stations on the earth and the fact that Lageos has a nominal inclination of  $109^\circ$ , we reach the conclusion that optimal passes parallel to the dominantly East-West direction of this baseline will be hard to come by for this satellite at any time. We plotted the coobserved events in Fig. 30, and as expected almost the entire set of points come from satellite passes orthogonal or nearly so to the baseline direction. The deficiency of the strongly geometry-dependent SRD mode in such a situation has already been pointed out, and it has also been confirmed through the very first simulation studies discussed in Section 5.1.1. The results in that case (Table 17) indicated that the error of recovery for the ranges would

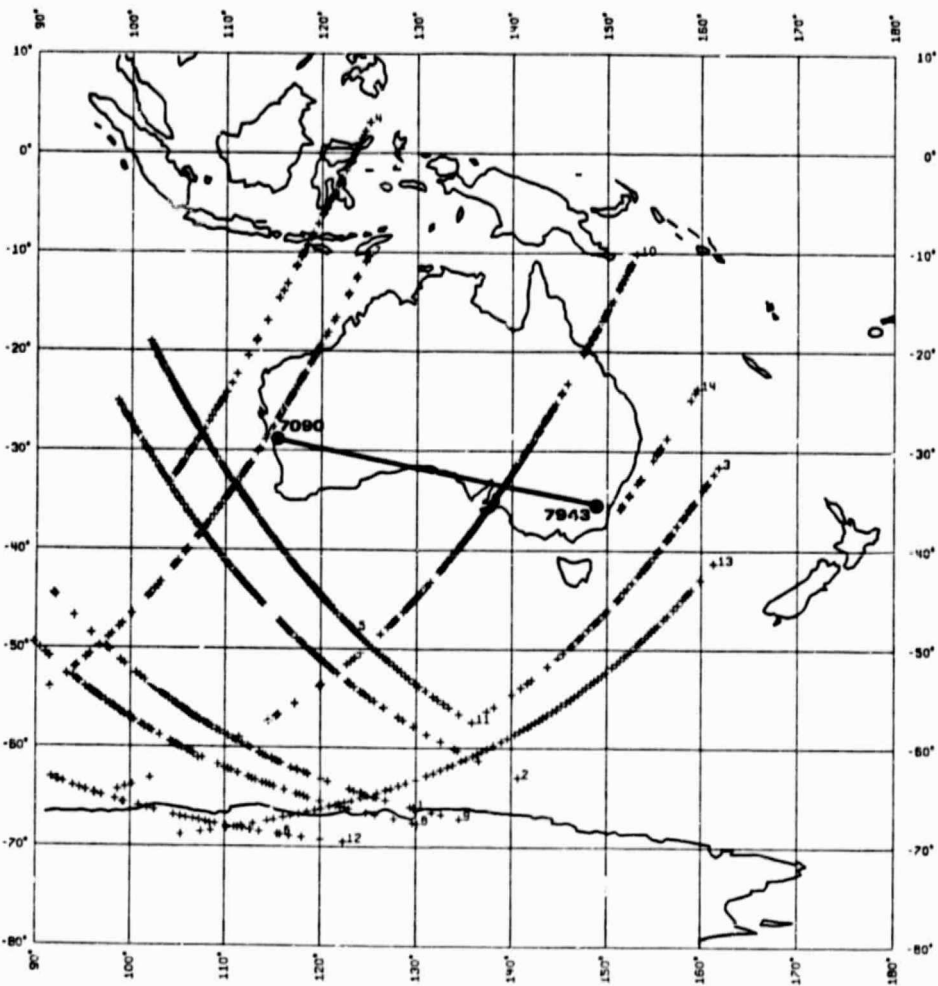


Fig. 30 Lageos SRD Event Distribution for the Data Used in Determining the 7090-7943 Baseline

only differ (be worse) by 7 mm from that for the SRD solution. If we compare this difference to the corresponding differences for some baselines with optimal location with respect to the tracked satellite passes (e.g., 7120-7943, 5.6 cm; 7092-7943, 3.2 cm), we realize that it is really of an insignificant level. It is not surprising either that the results of the second simulation study discussed in Section 5.1.2.1 also point out that this particular baseline is not the best for testing the proposed method. Even though in that case the recovery errors for the range solution are 3-4 m larger than the corresponding ones for the SRD mode, in the case of the station pair 7090-7943 the difference between the two errors is only 18 cm!--hardly significant in the presence of 10 cm noise.

The residuals' summary for each of the adjustment are given in Tables 39 and 40 for the range solution, and in Table 41 for the SRD's. Comparing the mean residual per pass between the two adjustments, we find that the SRD solution tends to fit the orbit better for passes 1, 3, 5, 6, 12, 13 and 14, which, as can be seen from the groundtrack plot in Fig. 30, are the ones better conforming with the optimality criteria for spatial data distribution in the SRD mode. Finally, a comparison of the rms residual between the two solutions shows that the SRD solution tends to have residuals with a dispersion which is dictated by the most "noisy" of the two stations collecting the observables. In the present case, we have already seen in the preliminary adjustment of the complete range data set that station 7943 has a noise level 5-10 times higher than station 7090. It is understandable then that the rms residuals in the SRD solution are almost identical to those obtained in the range adjustment for the data from station 7943.

Table 39 Pass-by-Pass Residual Summary for Adjusted Range Data from Station 7090

Pass No.	Obs.	Residual Mean (m)	rms (m)	Standard Deviation (m)	Pass Duration (s)	Minimum Residual (m)	Maximum Residual (m)	Mean Closure (m)
1	53	-0.0237	0.058	0.053	1049.92	-0.117	0.097	-0.02
2	117	0.0035	0.113	0.113	1657.67	-0.214	0.305	0.00
3	57	-0.2763	0.291	0.094	1064.96	-0.415	-0.075	-0.28
4	82	-0.1879	0.202	0.074	1462.25	-0.269	-0.059	-0.19
5	55	0.0790	0.125	0.097	1192.00	-0.175	0.235	0.08
6	22	-0.0055	0.073	0.075	399.00	-0.132	0.146	-0.01
7	105	-0.0361	1.136	1.140	1815.00	-1.384	7.648	-0.04
8	65	-0.0788	0.099	0.060	952.60	-0.173	0.059	-0.08
9	24	-0.0120	0.038	0.037	592.60	-0.109	0.036	-0.01
10	154	0.1124	1.426	1.426	2340.04	-2.939	4.611	0.11
11	121	0.1202	0.160	0.106	1554.00	-0.125	0.354	0.12
12	15	0.0835	0.105	0.065	473.00	-0.052	0.184	0.08
13	87	0.1704	0.212	0.127	1414.00	-0.203	0.405	0.17
14	18	-0.4927	0.497	0.069	495.05	-0.666	-0.440	-0.49

Table 40 Pass-by-Pass Residual Summary for Adjusted Range Data from Station 7943

Pass No.	Obs.	Residual Mean (m)	rms (m)	Standard Deviation (m)	Pass Duration (s)	Minimum Residual (m)	Maximum Residual (m)	Mean Closure (m)
1	53	-0.0133	0.437	0.441	1049.92	-1.040	0.952	-0.01
2	117	0.0868	0.315	0.304	1657.67	-0.716	0.851	0.09
3	57	0.0099	0.395	0.398	1064.96	-0.973	0.687	0.01
4	82	0.1142	0.440	0.428	1462.25	-1.194	1.277	0.11
5	55	0.0634	0.082	0.052	1192.00	-0.043	0.226	0.06
6	22	0.1807	0.244	0.168	399.00	-0.116	0.536	0.18
7	105	-0.0510	0.343	0.341	1815.00	-1.098	0.733	-0.05
8	65	0.0294	0.261	0.261	952.60	-0.642	0.704	0.03
9	24	-0.0566	0.578	0.588	592.60	-1.002	1.449	-0.06
10	154	-0.0373	0.260	0.258	2340.04	-0.678	0.611	-0.04
11	121	-0.1588	0.187	0.099	1554.00	-0.316	0.188	-0.16
12	15	0.0586	0.328	0.334	473.00	-1.078	0.339	0.06
13	87	0.1719	0.203	0.109	1414.00	-0.073	0.360	0.17
14	18	-0.0776	0.453	0.460	495.05	-1.342	0.574	-0.08

ORIGINAL PAGE IS  
OF POOR QUALITY

**ORIGINAL PAGE IS  
OF POOR QUALITY**

Table 41 Pass-by-Pass Residual Summary for Adjusted SRD Data  
from the 7090-7943 Station Pair

Pass No.	Obs.	Residual Mean (m)	rms (m)	Standard Deviation (m)	Pass Duration (s)	Minimum Residual (m)	Maximum Residual (m)	Mean Closure (m)
1	53	-0.0138	0.414	0.418	1049.92	-1.002	0.980	-0.01
2	117	-0.1076	0.313	0.295	1657.67	-0.691	0.591	-0.11
3	57	-0.1531	0.426	0.401	1064.96	-0.995	0.694	-0.15
4	82	-0.2073	0.464	0.418	1462.25	-1.363	1.047	-0.21
5	55	-0.0381	0.176	0.173	1192.00	-0.381	0.310	-0.04
6	22	0.1796	0.253	0.182	399.00	-0.171	0.480	0.18
7	105	-0.0663	1.189	1.193	1815.00	-1.680	7.513	-0.07
8	65	-0.0985	0.283	0.267	952.60	-0.714	0.545	-0.10
9	24	0.0382	0.573	0.584	592.60	-1.467	0.941	0.04
10	154	0.1218	1.420	1.419	2340.04	-3.544	4.152	0.12
11	121	-0.2444	0.276	0.129	1554.00	-0.585	0.123	-0.24
12	15	-0.0225	0.311	0.321	473.00	-1.130	0.288	-0.02
13	87	-0.0774	0.134	0.110	1414.00	-0.364	0.226	-0.08
14	18	-0.3999	0.600	0.460	495.05	-1.010	0.905	-0.40



## 6. CONCLUSIONS AND RECOMMENDATIONS

### 6.1 Conclusions

The theoretical investigations and the numerical examples presented in this study lead to a number of conclusions concerning the issues raised herein. The most important of these is the fact that the analysis of Lageos data in the SRD mode minimizes the effect of all of the considered types of systematic orbital errors on the estimated baselines and coordinates of the pole. We have refrained from attributing these errors to any particular source; it is, however, important that we discuss one of them.

It is well known that baseline lengths are independent of the underlying reference system; baseline "estimates," however, especially when determined by satellite techniques or even more generally by any non-direct measuring system, are directly dependent on the reference system. To be more specific, they depend on the stability with which this system can be maintained. This is a consequence of the fact that the estimate is obtained from the end-station coordinates which are determined on the basis of their individual observing records. If the "barycenters" of these data are considerably apart in time, then the station coordinate estimates are affected by the reference system errors accumulated in the intervening time interval. The along-track and across-track errors used in the simulation study of Section 5.1.2.1 can be analyzed in a

latitudinal and a longitudinal component, and therefore one could think of them as the errors in the coordinates of the pole used to rotate the satellite positions from the CIS to the CTS frame.

It is self-evident that when the SRD mode is invoked, the above problem is alleviated completely by virtue of the simultaneity of our observations. Even though the differencing of the simultaneous ranges is not required in this case (simply simultaneous data would be sufficient), we would recommend that in view of the significant improvements in the accuracy of the observable, the SRD mode be followed through in its entirety.

The quality of the results determined on the basis of the recovery errors shows that using this method the goal of determining baseline lengths with centimeter level accuracies and two-day averages of the coordinates of the pole to five centimeters is feasible even in the presence of over one meter biases in the orbital model. Such accuracies in the orbit are about two to three times our current capabilities in predicting the orbit of Lageos over thirty-day periods.

It is thus conceivable that the predicted Lageos orbit used in determining the observational schedules of the stations and the editing of the observations can also be used for the analysis of SRD data on a nearly real-time basis. The elimination of the satellite orbit from the parameter list simplifies the estimation process beyond expectation. Users with no access to global sets of data can still use their regional data sets in the SPD mode and suffer no loss of accuracy in their results even when their reference orbit model is incomplete or they use a fixed predicted orbit. The simpler computational procedures of this type of

analysis relaxes the expensive hardware requirements imposed by the more complicated softwares available.

The generation of the SRD data set can easily be incorporated into the data editing package of the data processing center. As we have seen from the results of tests performed on real data, the use of cubic spline interpolation is far better than the commonly (and presently) used least squares polynomial approximation. Since the latter has several advantages from the data editing point of view (which is of no concern in this study), a compromise between the two methods is probably the best solution. Data smoothing cubic splines exist [Späth, 1974], and in this case they would be the most suitable to use. It is our firm belief that the above scheme of generating SRD data will result in an insignificant increase of the overhead cost for data editing which will be well worth it considering the improvements in the accuracy of the results and the major reduction in the cost of analyzing the data.

It has been shown here through theoretical arguments as well as simulation studies that the SRD mode is very much dependent on the geometry of the station network and the coobserved Lageos passes. For the determination of baseline lengths the best results are obtained from data taken on passes which are parallel to the baseline direction. We cannot always ensure that such requirements are fulfilled, but we should consider doing so whenever we have a choice on the baselines to be determined. For all practical purposes, the systematic orbital errors propagate into the observables (SRD's) in proportion to the baseline distance separating the two coobserving stations. Having a rough estimate of the orbital accuracy and the lengths of the baselines between the stations, we can determine

the pairs for which the level of the systematic errors remaining in the observable after the range differencing will be minimum. The generation of bias-surface plots similar to those used in Section 4.4.2 can facilitate the planning stage of a campaign in the selection of the optimal station locations as well as the coobserving pairs of stations.

In the case of polar motion parameter estimation the situation is slightly more complicated. This is mainly because of the fact that not only does the station location matter in this case, but the distribution of the data in time is of concern here too. We discuss first the station location issue.

As shown in Section 4.5.3 we need two nearly perpendicular baselines in order to be able to resolve the two components of the motion of the pole. Because of the convention in the definition of these two components  $x$  and  $y$ , it turns out that the optimal locations are near the two prime meridians, i.e.,  $\lambda = 0^\circ$  or  $90^\circ$  or  $180^\circ$  or  $270^\circ$ . Considering the continuous operation of these stations, it is worth pointing out that great savings can be achieved if we limit ourselves to an L-shaped rather than a +-shaped network, thus decreasing the number of stations required to only three. The middle station can be paired with both of the outside stations for the required perpendicular baseline pair.

In an L-shaped network near  $\lambda = 0^\circ$  or  $180^\circ$ , the N-S pair is sensitive to the  $x$  component, while the E-W pair determines the  $y$  component. Exactly the opposite is true in the case of a network near  $\lambda = \pm 90^\circ$ . To avoid gravity related orbital errors affecting the estimates, it is advisable to keep observing networks in both the Northern as well as the Southern Hemispheres.

The second issue of interest here is the distribution of the data in time. The higher the density of the observation record, the higher the resolution in the x and y. In that sense, the resolution is only bounded by the accuracy of the observations. The precision of the estimates can be increased by either increasing the data density over the averaging interval or by increasing the interval itself. It should be kept in mind that the former does not affect the resolution of the parameters, while the latter does. It results in its decrease. These are issues to be resolved when a final decision is taken on the practical determination of the x and y. In any case though, it should be made certain that whatever the chosen averaging interval, there will always be enough networks with proper satellite observability schedules to collect enough well-distributed (globally) observations over the entire time interval.

The analysis of real data has not given us grounds for basing firmer conclusions, although the agreement between these results and those obtained from the simulation studies gives us a higher degree of confidence in the validity of the latter. The absence of extensive real data tests is due to the lack of suitable data. By this we do not mean to cast the blame on others, but rather to point out that as it is shown in this study, proper scheduling and a genuine effort from the field parties would have certainly resulted in a sizable amount of data.

There is indeed a striking similarity between the SRD and the purely geometric mode. However, the SRD mode requires the coobservation of the Lageos pass from only two stations, while in the geometric mode data from at least four and preferably more stations with strict simultaneity

are required. Apart from the weather factor, there should be no other excuse for not obtaining SRD data from nearby stations. The probability for two such stations coobserving Lageos is much higher than for the geometric mode (minimal) four-station network.

## 6.2 Recommendations

The results of this investigation have shown that the proposed simultaneous range-differencing approach for the analysis of laser ranging observations to Lageos is an avenue worth pursuing for improvement of our geodetic estimates. On the basis of these results we would recommend that

(a) An effort be made during one of the upcoming observational campaigns (the 1983 MERIT campaign, for instance) to coobserve as many Lageos passes as possible.

(b) Continue the research effort in optimizing the network configurations that will allow uninterrupted monitoring of the motion of the pole within the internationally agreed limits.

(c) Further research is warranted in the direction of SRD data generation. As the field instrumentation is upgraded and the stations become capable of obtaining more than one observation per second, the amount of incoming data will grow out of proportion. It is therefore suggested that further improvement and standardization of the SRD generation technique is needed. The possibility of integrating this procedure in the raw data preprocessing at the data gathering centers should be given serious consideration.

(d) The scheduling of mobile or highly mobile laser ranging equipment deployment should be re-examined, and if feasible advantage should be taken of this method of analysis by collecting suitable observations.

(e) As the time for the establishment of a new Conventional Terrestrial System nears, the role of the proposed method must be reaffirmed through further simulation studies and if possible the analysis of real data in contributing optimal estimates for the fundamental polyhedron's side lengths.

(f) A study should be initiated to investigate the merits of the proposed method in determining the variations in the rotation rate of the earth.

(g) Finally, the application of this method to other ranging or pseudo-ranging satellite systems such as the GPS is a research topic worth pursuing.

## REFERENCES

- Aardoom, L., A. Girnius and G. Veis (1967), "Determination of the Absolute Space Directions Between Baker-Nunn Camera Stations," The Use of Artificial Satellites for Geodesy, Vol. II, G. Veis, ed., National Technical University, Athens.
- Baker, R.M.L., Jr. (1967), Astrodynamics, Applications and Advanced Topics, Academic Press, New York.
- Blaaha, G. (1971), "Investigations of Critical Configurations for Fundamental Range Networks," Dept. of Geodetic Science Rep. 150, Ohio State Univ., Columbus.
- Bock, Y. (1982), "The Use of Baseline Measurements and Geophysical Models for the Estimation of Crustal Deformations and the Terrestrial Reference System," Dept. of Geodetic Science and Surveying Rep. 337, Ohio State Univ., Columbus.
- Bose, R.C. (1947), "The Design of Experiments," Presidential Address to Statistics Section, Proc. of 34th Session of The Indian Science Congress Association.
- Brown, D.C. (1976), "Doppler Positioning by the Short Arc Method," Proc. International Geodetic Symp. on Satellite Doppler Positioning, Physical Sciences Lab., New Mexico State Univ., Las Cruces.
- Cappellari, J.O., C.E. Velez, and A.J. Fuchs, eds. (1976), "Mathematical Theory of the Goddard Trajectory Determination System," NASA/Goddard Space Flight Center, NASA X-582-76-77, NTIS N76-24291 - N76-24302.
- Carpenter, L. (1978), "Goddard Laser Tracking Data," Geodynamics Branch, NASA/Goddard Space Flight Center, Greenbelt, Maryland.
- Chamberlain, J.N. (1978), Theory of Planetary Atmospheres, Academic Press, New York.
- Christodoulidis, D.C. and D.E. Smith (1981), "Prospects for TLRs Baseline Accuracies in the Western USA Using Lageos," NASA Technical Memorandum 82133, Goddard Space Flight Center, Greenbelt, Maryland.
- CSTG Bulletin (1982), "Reference Frame Requirements and the MERIT Campaign--Proposal for Extra Observations," June 9, Dept. of Geodetic Science and Surveying, Ohio State Univ., Columbus.



- Dahlquist, G. and A. Björck (1974), Numerical Methods, trans. by N. Anderson, Prentice, Hall, Englewood Cliffs, New Jersey.
- Davis, P.J. (1975), Interpolation and Approximation, Dover Publications, New York.
- Doodson, A.E. (1921), "The Harmonic Development of the Tide-Generating Potential," Proc. Roy. Soc. A 100, 305-329.
- Dunn, P.J. (1982), "Lageos Orbital Elements for 1982," pres. IAG General Meeting, Tokyo, May 7-20, (avail. EG&G Washington Analytical Services Center, Riverdale, Maryland).
- Eisenhart, C. (1962), "Realistic Evaluation of the Precision and Accuracy of Instrument Calibration Systems," J. of Res. of the National Bureau of Standards, 67C, No. 2, April-June.
- Fitzmaurice, M.W., P.O. Minott, J.B. Abshire and H.E. Rowe (1977), "Pre-launch Testing of the Laser Geodynamic Satellite (LAGEOS)," NASA TP-1062, Goddard Space Flight Center, Greenbelt, Maryland.
- Forsythe, G. and C.B. Moler (1967), Computer Solution of Linear Algebraic Systems, Prentice-Hall, Englewood Cliffs, New Jersey.
- Gaposchkin, E.M. (1981), "Determining Geophysical Phenomena: A Geophysical Analysis of Satellite Laser Data," AFGL-TR-81-0023, Air Force Geophysics Lab., Hanscom AFB, Massachusetts.
- Grafarend, E. and K. Heinz (1978), "Rank Defect Analysis of Satellite Geodetic Networks II--Dynamic Mode," manuscripta geodaetica, 3, No. 2/3, 135-156.
- Grafarend, E. and E. Livieratos (1978), "Rank Defect Analysis of Satellite Geodetic Networks I--Geometric and Semi-dynamic Mode," manuscripta geodaetica, 3, No. 2/3, 107-134.
- Hamilton, W.C. (1964), Statistics in Physical Science, Ronald Press, New York.
- Heiskanen, W.A. and H. Moritz (1967), Physical Geodesy, W.H. Freeman, San Francisco.
- Johnson, C.W., C.A. Lundquist and J.L. Zurasky (1976), "The Lageos Satellite," pres. XXVII Congress International Astronautical Federation, Anaheim, California, Oct. 10-16 (avail. Superintendent of Documents, Washington, D.C.)
- Kaplan, G.H. (1981), "The IAU Resolutions on Astronomical Constants, Time Scales, and the Fundamental Reference Frame," U.S. Naval Observatory Circular No. 163, Washington, D.C.

- Kleusberg, A. (1980), "The Similarity Transformation of the Gravitational Potential," manuscripta geodaetica, 5, No. 4, 241-256.
- Kouba, J. (1979), "Geodetic Satellite Doppler Positioning and Application to Canadian Test Adjustments," Collected Papers, Geodetic Survey, 1978, Geodetic Survey, Surveys and Mapping Branch, EMR, Ottawa.
- Kovalevsky, J. and I.I. Mueller (1981), "Comments on Conventional Terrestrial and Quasi-Inertial Reference Systems," Reference Coordinate Systems for Earth Dynamics, E.M. Gaposchkin and B. Kołaczek, eds., D. Reidel.
- Krogh, F.T. (1969), "A Variable Step Variable Order Multistep Method for the Numerical Solution of Ordinary Differential Equations," Information Processing 68, North-Holland Publ. Co., Amsterdam.
- Krogh, F.T. (1970), "VODQ/SVDQ/DVDQ, Variable Order Integrators for the Numerical Solutions of Ordinary Differential Equations," Technology Utilization Document No. CP-2308, Jet Propulsion Laboratory, Pasadena, California.
- Lambeck, K. (1980), The Earth's Variable Rotation: Geophysical Causes and Consequences, Cambridge Univ. Press, New York.
- Latimer, J.H. and E.M. Gaposchkin (1977), "Scalar Translocation Using Laser Range Data," Smithsonian Astrophysical Observatory, Center for Astrophysics Preprint Series 750, Cambridge, Massachusetts.
- Leick, A. (1978), "The Observability of the Celestial Pole and Its Nutations," Dept. of Geodetic Science Rep. 262, Ohio State Univ., Columbus.
- Lerch, F.J. and S.M. Klosko (1981), "Gravity Model Improvement Using Laser Data: Progress Report," pres. at 1st Crustal Dynamics Working Group, Sept. 1-3, Goddard Space Flight Center, Greenbelt, Maryland.
- Lerch, F.J. and S.M. Klosko (1982), "Gravity Model Improvement for Lageos (GEM-L1)," pres. at 4th Annual Conf. on the NASA Geodynamics Program, Jan. 26-29, Goddard Space Flight Center, Greenbelt, Maryland.
- Lieske, J.H. (1979), "Precession Matrix Based on IAU (1976) System of Astronomical Constants," Astronomy and Astrophysics, 73, 282-284.
- Love, A.E.H. (1911), Some Problems of Geodynamics, Dover Publications, New York (Dover edition, 1967).
- McClure, P. (1973), "Diurnal Polar Motion," GSFC X-592-73-259, NASA/Goddard Space Flight Center, Greenbelt, Maryland.

- Marini, J.W. and C.W. Murray (1973), "Correction of Laser Range Tracking Data for Atmospheric Refraction at Elevations Above 10 Degrees," Preprint X-591-73-351, NASA/Goddard Space Flight Center, Greenbelt, Maryland.
- Melchior, P. (1978), The Tides of the Planet Earth, Pergamon Press, New York.
- Minkowski, H. (1908), "Space and Time," The Principles of Relativity, Dover Publications, 1952 reprint.
- Moritz, H. (1979), "Concepts in Geodetic Reference Frames," Dept. of Geodetic Science Rep. 294, Ohio State Univ., Columbus.
- Moyer, T.D. (1971), "Mathematical Formulation of the Double-Precision Orbit Determination Program (DPODP)," TR-32-1527, Jet Propulsion Laboratory, Pasadena, California.
- Moyer, T.D. (1981a) "Transformation from Proper Time on Earth to Coordinate Time in Solar System Barycentric Space-Time Frame of Reference, Part 1," Celestial Mechanics 23, 33-56, Reidel.
- Moyer, T.D. (1981b) "Transformation from Proper Time on Earth to Coordinate Time in Solar System Barycentric Space-Time Frame of Reference, Part 2," Celestial Mechanics 23, 57-68.
- Mueller, I.I. (1969), Spherical and Practical Astronomy As Applied to Geodesy, Ungar Publ. Co., New York.
- Mueller, I.I., M. Kuznar and T. Soler (1973), "Free Geometric Adjustment of the SECOR Equatorial Network (Solution SECOR-27), Dept. of Geodetic Science Rep. 195, Ohio State Univ., Columbus.
- Mueller, I.I. (1980), "Reference Coordinate Systems for Earth Dynamics: A Preview," Dept. of Geodetic Science Rep. 302, Ohio State Univ., Columbus.
- Mueller, I.I., S.Y. Zhu and Y. Bock (1982), "Reference Frame Requirements and the MERIT Campaign," Dept. of Geodetic Science and Surveying Rep. 329, Ohio State Univ., Columbus.
- Musen, P. (1973), "A Semi-analytical Method of Computation of Oceanic Tidal Perturbations in the Motion of Artificial Satellites," X-590-73-190, NASA/Goddard Space Flight Center, Greenbelt, Maryland.
- Nagel, E. (1976), "Die Bezugssysteme der Satellitengeodäsie," Deutsche Geodätische Kommission, Reihe C, Heft 223, Munich.
- NASA (1980), "Laser Ranging System Development for Crustal Dynamics Applications," Resource Observation Div., Office of Space and Terrestrial Applications, Goddard Space Flight Center, Greenbelt, Maryland.

- Newcomb, S. (1898), "Tables of the Sun," Astronomical Papers prepared for the use of the American Ephemeris and Nautical Almanac, Vol. VI, U.S. Nautical Almanac Office, Washington, D.C.
- Pavlis, E.C. (1979), "Error Analysis for a Spaceborne Laser Ranging System," Dept. of Geodetic Science Rep. 290, Ohio State Univ., Columbus.
- Pearlman, M.R., J.M. Thorp, D.A. Arhold and F.O. Vonbun (1976), "Lageos Orbital Acquisition and Initial Assessment," Smithsonian Astrophysical Observatory, Center for Astrophysics Preprint Series No. 563, Cambridge, Massachusetts.
- Pollard, J.H., (1977), A Handbook of Numerical and Statistical Techniques, Cambridge Univ. Press, Cambridge, England.
- Pope, A.J. (1972), "Some Pitfalls to Be Avoided in the Iterative Adjustment of Nonlinear Problems," Proc. of the 38th Annual Meeting of the American Society of Photogrammetry, Falls Church, Va.
- Pope, A.J. (1974), "Modern Trends in Adjustment Calculus," Canadian Surveyor, 28, No. 5.
- Putney, B. (1980), "Lageos Binary Format," document distributed to Lageos Project Investigators, NASA/Goddard Space Flight Center, Greenbelt, Maryland.
- Rao, C.R. (1973), Linear Statistical Inference and Its Applications, 2nd ed., John Wiley & Sons, New York.
- Reigber, C. (1981), "Representation of Orbital Element Variations and Force Function with Respect to Various Reference Systems," Bulletin Geodesique, 55, No. 2.
- Rubincam, D.P. (1980), "Atmospheric Drag As the Cause of the Secular Decrease in the Semimajor Axis of Lageos's Orbit," Geophysical Research Letters, 7, No. 6.
- Scheffé, H. (1959), The Analysis of Variance, John Wiley & Sons, New York.
- Schmid, H.H. (1974), "Worldwide Geometric Satellite Triangulation," J. of Geophysical Research, 79.
- SGRS Workshop Report (1979), "The Report from the Workshop on the Spaceborne Geodynamics Ranging System," Institute for Advanced Study in Orbital Mechanics, Univ. of Texas at Austin.
- Silverberg, E.C. and I.A. Malevich (1978), "Multi-stop Timing Electronics for High Altitude Satellite Ranging," Proc. 3rd International Laser Ranging Workshop, Lagonissi, Greece, May, National Technical Univ. Athens.

- Silverberg, E.C. (1981), "The Feedback Calibration of the TLRs Ranging System," Proc. of the 4th International Workshop on Laser Ranging Instrumentation, IASOM TR79-2, Univ. of Texas, Austin.
- Smith, D.E. and P.J. Dunn (1980), "Long Term Evolution of the Lageos Orbit," Geophysical Research Letters, 7, No. 6.
- Smith, D.E., P.J. Dunn, D. Christodoulidis and M. Torrence (1982), "Global Baselines from Laser Ranging," pres. 4th Annual Conf. on the NASA Geodynamics Program, Goddard Space Flight Center, Greenbelt, Maryland, Jan. 26-29.
- Snyder, M.A. (1966), Chebyshev Methods in Numerical Approximation, Prentice-Hall, Englewood Cliffs, New Jersey.
- Späth, H. (1974), Splines Algorithms for Curves and Surfaces, translated from the German by W.D. Hoskins and H.W. Sager, Utilitas Mathematica Publ., Winnipeg, Canada.
- Szebehely, V. (1981), "Analysis of Lageos' Altitude Decrease," Satellite Perturbations and Orbital Determination, P. Lala, ed., Pergamon Press, New York.
- Tapley, B.D. (1982), "Polar Motion and Earth Rotation from Lageos Laser Ranging," High-Precision Earth Rotation and Earth-Moon Dynamics, O. Calame, ed., D. Reidel, Boston.
- Tsimis, E. (1973), "Critical Configurations (Determinantal Loci) for Range and Range-Difference Satellite Networks," Dept. of Geodetic Science Rep. 191, Ohio State Univ., Columbus.
- Uotila, U.A. (1967), "Introduction to Adjustment Computations with Matrices," lecture notes, Dept. of Geodetic Science, Ohio State Univ., Columbus.
- Uotila, U.A. (1973), "Useful Statistics for Land Surveyors," Surveying and Mapping, XXXIII, No. 1, 67-77.
- Uotila, U.A. (1975), "Statistical Tests As Guidelines in Analysis of Adjustment of Control Nets," Surveying and Mapping, XXXV, No. 1, 47-52.
- Van Gelder, B.H.W. (1978), "Estimability and Simple Dynamical Analysis of Range (Range-Rate and Range-Difference) Observations to Artificial Satellites," Dept. of Geodetic Science Rep. 284, Ohio State Univ., Columbus.
- Veis, G. (1967), "Results from Geometric Methods," Space Research VII, R.L. Smith-Rose, S.A. Bowhill and J.W. King, eds., North-Holland Publ., Amsterdam.

Vondrak, J. (1977), "Problem of Smoothing Observational Data," Bull. Astron. Inst. Czech., 28.

Wahr, J.M. (1981), "The Forced Nutations of an Elliptical, Rotating, Elastic and Oceanless Earth," Geophys. J.R. astr. Soc. 64, 705-727.

APPENDIX A

DERIVATION OF THE VARIATIONAL EQUATION OF STATE FOR THE  
CASE OF TIDAL ACCELERATIONS

Equation (29) (Section 2.2.5) gives the perturbing acceleration on a satellite due to the tidal effects of a perturbing body b. On the basis of this equation we will derive here equation (30) which gives the contribution of the above acceleration in the variation of the satellite position vector. For clarity we repeat equation (29):

$$\ddot{\bar{R}}_{TD_b} = \frac{3}{2} k_2 \frac{\mu_b}{|\bar{R}_b|^3} \frac{a_E^5}{|\bar{R}|^4} ([1 - 5(\bar{u}_b \cdot \bar{u})^2] \bar{u} + 2(\bar{u}_b \cdot \bar{u}) \bar{u}_b) \quad (A.1)$$

where

$$\bar{u} = \frac{\bar{R}}{|\bar{R}|} \quad (A.2)$$

and

$$\bar{u}_b = \frac{\bar{R}_b}{|\bar{R}_b|} \quad (A.3)$$

To obtain the expression for  $\left[ \frac{\partial \ddot{\bar{R}}_{TD_b}}{\partial \bar{R}} \right]$ , we differentiate each of the terms in (A.1) individually  $\left[ \frac{\partial \ddot{\bar{R}}_{TD_b}}{\partial \bar{R}} \right]$  with respect to  $\bar{R}$ :

$$\begin{aligned} \frac{\partial}{\partial \bar{R}} \left\{ \frac{[1 - 5(\bar{u}_b \cdot \bar{u})^2] \bar{u}}{|\bar{R}|^4} \right\} &= \frac{\partial}{\partial \bar{R}} \left\{ \left[ 1 - 5 \frac{(\bar{R}_b^T \bar{R})^2}{|\bar{R}_b|^2 |\bar{R}|^2} \right] \frac{\bar{R}}{|\bar{R}|^5} \right\} \\ &= \frac{\left[ 1 - 5 \frac{(\bar{R}_b^T \bar{R})^2}{|\bar{R}_b|^2 |\bar{R}|^2} \right] \frac{\partial \bar{R}}{\partial \bar{R}}}{|\bar{R}|^5} + \left[ 1 - 5 \frac{(\bar{R}_b^T \bar{R})^2}{|\bar{R}_b|^2 |\bar{R}|^2} \right] \bar{R} \frac{\partial |\bar{R}|^{-5}}{\partial \bar{R}} + \end{aligned}$$

$$\begin{aligned}
 & + \frac{\bar{R}}{|\bar{R}|^5} \frac{\partial}{\partial \bar{R}} \left\{ 1 - 5 \frac{(\bar{R}_b^T \bar{R})^2}{|\bar{R}_b|^2 |\bar{R}|^2} \right\} \\
 & = \frac{[1 - 5(\bar{u}_b \cdot \bar{u})^2]}{|\bar{R}|^5} \mathbf{I} + [1 - 5(u_b \cdot u)^2] \bar{R} \left( -5 \frac{\bar{R}^T}{|\bar{R}|^7} \right) + \\
 & + \frac{\bar{R}}{|\bar{R}|^5} \left\{ -5 \frac{2(\bar{R}_b^T \bar{R})}{|\bar{R}_b|^2 |\bar{R}|^2} \bar{R}_b^T - 5 \frac{(\bar{R}_b^T \bar{R}^T)^2}{|\bar{R}_b|^2} \left( -2 \frac{\bar{R}^T}{|\bar{R}|^4} \right) \right\} = \\
 & = \frac{[1 - 5(\bar{u}_b \cdot \bar{u})^2]}{|\bar{R}|^5} \mathbf{I} - 5 \frac{\bar{u} \bar{u}^T}{|\bar{R}|^5} + 25 \frac{(\bar{u}_b \cdot \bar{u})^2}{|\bar{R}|^5} \bar{u} \bar{u}^T \\
 & - 10 \frac{(\bar{u}_b \cdot \bar{u})}{|\bar{R}|^5} \bar{u} \bar{u}_b^T + 10 \frac{(\bar{u}_b \cdot \bar{u})^2}{|\bar{R}|^5} \bar{u} \bar{u}^T \\
 & = \frac{1}{|\bar{R}|^5} \{ [1 - 5(\bar{u}_b \cdot \bar{u})^2] \mathbf{I} - 5 \bar{u} \bar{u}^T + 35 (\bar{u}_b \cdot \bar{u})^2 \bar{u} \bar{u}^T \\
 & \quad - 10 (\bar{u}_b \cdot \bar{u}) \bar{u} \bar{u}_b^T \} \tag{A.4}
 \end{aligned}$$

$$\begin{aligned}
 \frac{\partial}{\partial \bar{R}} \left\{ \frac{2(\bar{u}_b \cdot \bar{u}) \bar{u}_b}{|\bar{R}|^4} \right\} & = \frac{\partial}{\partial \bar{R}} \left\{ 2 \left( \frac{\bar{R}_b^T \bar{R}}{|\bar{R}_b| |\bar{R}|} \right) \frac{\bar{R}_b}{|\bar{R}_b|^5} \right\} = \\
 & = 2 \frac{\bar{R}_b \bar{R}_b^T}{|\bar{R}_b|^2 |\bar{R}|^5} + 2 \frac{(\bar{R}_b^T \bar{R})}{|\bar{R}_b|^2} \bar{R}_b \left( -5 |\bar{R}|^{-6} \frac{\bar{R}^T}{|\bar{R}|} \right) \\
 & = \frac{1}{|\bar{R}|^5} \{ 2(\bar{u}_b \bar{u}_b^T) - 10(\bar{u}_b \cdot \bar{u}) \bar{u}_b \bar{u}^T \} \tag{A.5}
 \end{aligned}$$

Collecting terms in the combination of (A.4) and (A.5), we obtain:



$$(A.4) + (A.5) = \frac{1}{|\bar{R}|^5} \{ [1 - 5(\bar{u}_b \cdot \bar{u})^2] I + [35(\bar{u}_b \cdot \bar{u})^2 - 5] \bar{u} \bar{u}^T - 10(\bar{u}_b \cdot \bar{u}) [\bar{u} \bar{u}_b^T + \bar{u}_b \bar{u}^T] + 2(\bar{u}_b \bar{u}_b^T) \}$$

which when multiplied by the constant terms in (A.1):

$$\frac{3}{2} k_2 \frac{\mu_b}{|\bar{R}_b|^3} a_b^5$$

results in expression (30).

ORIGINAL PAGE IS  
OF POOR QUALITY

APPENDIX B  
SYSTEMATIC CORRECTIONS APPLIED TO THE OBSERVATIONS

B.1 Correction for Geometrodynamical Effects.

The observed and interpolated ranges are required to compute the correction to the SRD's due to signal retardation by gravitation or, better, by the curvature of the space [Shapiro et al., 1971; Shapiro, 1980]. Since the satellite position is also required to compute this correction, it seems logical to defer its computation until this position is automatically available during the DOC step.

The determination of the geometrodynamical correction is based on the formula that relates TDB and TAI ( $\ell$ ) as obtained by Moyer [1981b] and the retardation correction for light signals as given in [Shapiro, 1980].

Moyer's expression for  $\Delta T_A = [\text{TDB} - \text{TAI}(\ell)]$  can be used to convert the measured time interval at the station from a proper time interval to a coordinate one, provided we know the epochs that are associated with the transmission, reflection and reception of the laser pulse. Since though in the case of laser ranging to artificial satellites the whole interval rarely exceeds 80 ms, the change of the correction over this short time can be obtained from differentiation of  $\Delta T_A$  and retention of only those terms which are significant. From Moyer's expression for  $\Delta T_A$  we find that only the second and fourth terms are significant. For a

station with cylindrical coordinates  $(u, \lambda, z)$ ,  $u$  and  $z$  in kilometers, we can then write:

$$\begin{aligned} \frac{d(\text{TDB} - \text{TAI}(\ell))}{dt} &\cong 1.658 \times 10^{-3} \cos E \frac{dE}{dt} + \\ &+ 3.17679 \times 10^{-10} u \cos(\text{UT1} + \lambda) \frac{d \text{UT1}}{dt} \end{aligned} \quad (\text{B.1})$$

with

$$\frac{dE}{dt} = (1 + e \cos M)n \quad (\text{B.2})$$

and

$$\frac{d \text{UT1}}{dt} \cong \omega \quad (\text{B.3})$$

where  $E$ ,  $M$  and  $n$  are the eccentric anomaly, mean anomaly and the mean motion of the earth-moon barycenter's heliocentric orbit respectively, and  $\omega$  is the spin rate of the earth. Substitution in (B.1) results in

$$\begin{aligned} \frac{d(\text{TDB} - \text{TAI}(\ell))}{dt} &\cong 1.658 \times 10^{-3} n \cos E (1 + e \cos M) \\ &+ 3.17679 \times 10^{-10} \omega u \cos (\text{UT1} + \lambda) \end{aligned} \quad (\text{B.4})$$

From [Moyer, 1981b]

$$n = \frac{dM}{dt} \cong 1.99096871 \times 10^{-7} \text{ rad/s} \quad (\text{B.5})$$

and using the adopted value of  $\omega$  for GRS80 [Moritz, 1980]

$$\omega = 7192\ 115 \times 10^{-11} \text{ rad/s},$$

equation (B.4) yields

$$\begin{aligned} \frac{d(\text{TDB} - \text{TAI}(\ell))}{dt} &\cong 3.3010261 \times 10^{-10} \cos E(1 + e \cos M) \\ &+ 2.3165518 \times 10^{-17} u \cos (\text{UT1} + \lambda) \end{aligned} \quad (\text{B.6})$$

where we have changed the units of  $u$  to meters, the final result given in seconds. This equation can now be used for the time interval conversion using the finite observed time interval  $\delta t$ :

$$\delta(\delta t) \cong \frac{d(\text{TDB} - \text{TAI}(\lambda))}{dt} \delta t \quad (\text{B.7})$$

or upon multiplication of the above with  $c$ , the speed of light, the equivalent correction for the range is

$$\delta \rho_t \cong \frac{d(\text{TDB} - \text{TAI}(\lambda))}{dt} c \delta t \quad (\text{B.8})$$

Since  $c \delta t = \rho_0$ , the range prior to the correction, we finally obtain

$$\begin{aligned} \delta \rho_t \cong & [3.3010261 \times 10^{-10} \cos E (1 + e \cos M) \\ & + 2.3165518 \times 10^{-17} u \cos (UT1 + \lambda)] \rho_0 \end{aligned} \quad (\text{B.9})$$

The remaining retardation correction is computed from

$$\delta \rho_r \cong \frac{\mu_s}{c^2} 2 \ln \left[ \frac{|\bar{R}_E| + |\bar{R}_L| + |\bar{R}_E - \bar{R}_L|}{|\bar{R}_E| + |\bar{R}_L| - |\bar{R}_E - \bar{R}_L|} \right] \quad (\text{B.10})$$

where  $\bar{R}_E$  and  $\bar{R}_L$  are the solar system barycentric coordinates of the earth and the satellite respectively. The final range now can be computed as

$$\rho_c = \rho_0 + \delta \rho_r - \delta \rho_t \quad (\text{B.11})$$

the last term being subtracted since it compensates for a retardation. With each range in a SRD pair corrected, we can now determine the SRD by their difference

$$\delta \rho_c = \rho_{c_2} - \rho_{c_1} \quad (\text{B.12})$$

or using (B.11)

$$\delta \rho_c = \rho_{0_2} + \delta \rho_{r_2} - \delta \rho_{t_2} - \rho_{0_1} - \delta \rho_{r_1} + \delta \rho_{t_1} \quad (\text{B.13})$$

It can be observed though from (B.10) that  $\delta \rho_r$  is independent of the station position, and it is the same for both ranges in the SRD pair; it therefore cancels in the computation of  $\delta \rho_c$ . Some further savings can be achieved from a close examination of the  $\delta \rho_t$  terms also. From

(B.9) it can be seen that the second term depends on the station position through  $u$ ,  $\lambda$  and  $\rho_0$ , while the first only on  $\rho_0$ . With some reasonable values for these quantities, the maximal value that  $\delta\rho_t$  can reach in the case Lageos is only about  $\pm 0.007$  m. Upon differencing, therefore, in (B.13), the maximum correction for the SRD  $\delta\rho$  is at most  $\pm 0.014$  m, below the measuring accuracy of most available instruments in the field. Since the correction has a periodic nature [Moyer, 1981b], we can safely eliminate it from the computation of  $\delta\rho_C$ . Equation (B.13) therefore takes the simple form

$$\delta\rho_C = \rho_{02} - \rho_{01} \quad (\text{B.14})$$

which is used for the determination of the simultaneous range differences in this investigation.

## B.2 Systematic Corrections Due to Tidal Motions of the Observing Stations

The effects of the lunisolar tides on points located on the surface of the earth are theoretically rather well studied [Melchior, 1978]. If these temporal variations in the location of the observing stations with respect to the center of mass of the earth are not accounted for in the observations, the committed error can reach an amplitude of about 0.5 m.

The traditional way of correcting for these effects is to compute the temporal changes in the coordinates of the observing station rather than the effect on the measurement directly. In the present study only the effect of the solid earth tides was considered mainly due to the fact that the remaining effects of the ocean and atmospheric tides are much smaller and not yet as well understood or modeled [Lambeck, 1980]. The nonrigidity of the earth is accounted for by the Love number for

radial expansion  $h_2$  and the Shida number  $\ell_2$  for horizontal shear. The values used in our experiments are those used by the NASA/GSFC scientists [Chin et al., 1972]:

$$h_2 = 0.600$$

$$\ell_2 = 0.075$$

The mathematical formulation for the station coordinate corrections based on the tidal potential from equation (27) is derived in [Diamante and Williamson, 1972]. The accuracy of this formulation can hardly match the observation accuracy level today, and it is well known that for best results, the local tidal motions should be obtained from direct in situ observation rather than from the model. This has not been the case so far for almost all operational SLR stations.

## REFERENCES

- Chin, M.M., C.C. Goad and T.V. Martin (1972), "GEODYN System Description, Vol. I," Wolf Research and Development Corp., Riverdale, Maryland.
- Diamante, J. and R. Williamson (1972), "Error Models for Solid Earth and Ocean Tidal Effects in Satellite Systems Analysis," Wolf Research and Development Corp., Greenbelt, Maryland.
- Lambeck, K. (1980), The Earth's Variable Rotation: Geophysical Causes and Consequences, Cambridge University Press, New York.
- Melchior, P. (1978), The Tides of the Planet Earth, Pergamon Press, New York.
- Moritz, H. (1980), "Geodetic Reference System 1980," The Geodesist's Handbook 1980, Bulletin Geodesique, 54, No. 3.
- Moyer, T.D. (1981) "Transformation from Proper Time on Earth to Coordinate Time in Solar System Barycentric Space-Time Frame of Reference, Part 2," Celestial Mechanics 23, 57-68.
- Shapiro, I.I. (1980), "Experimental Challenges Posed by the General Theory of Relativity," Some Strangeness in the Proportion: A Centennial Symposium to Celebrate the Achievements of Albert Einstein, H. Wolf, ed., Addison-Wesley Publ. Co., Reading, Massachusetts.
- Shapiro, I.I., M.E. Ash, R.P. Ingalls, W.B. Smith, D.B. Campbell, R.B. Dyce, R.F. Jurgens and G.H. Pettengill (1971), "Fourth Test of General Relativity: New Radar Result," Physical Review Letters, 26, 1132-1135.

APPENDIX C

FURTHER DEVELOPMENT OF THE DIFFERENTIAL ERROR EQUATIONS

C.1 Station Coordinates

From the discussion in Section 4.2 of the range differential  $d\rho_{ij}$ , we can use equations (99), (100), and (101) to write

$$d\rho_{ij} = \frac{1}{\rho_{ij}} \bar{T}_{ij}^T (-[C\theta]^T) d\bar{U}_j \quad (C.1)$$

with

$$\bar{T}_{ij}^T = \bar{S}_i^T - \bar{G}_j^T = \bar{S}_i^T - \bar{U}_j^T [C\theta] \quad (C.2)$$

Substituting (C.2) in (C.1) we obtain

$$\begin{aligned} d\rho_{ij} &= -\frac{1}{\rho_{ij}} [\bar{S}_i^T - \bar{U}_j^T [C\theta]] [C\theta]^T d\bar{U}_j = \\ &= -\frac{1}{\rho_{ij}} [\bar{S}_i^T [C\theta]^T - \bar{U}_j^T [C\theta][C\theta]^T] d\bar{U}_j \end{aligned} \quad (C.3)$$

From the well-known property of orthogonal matrices  $R^T = R^{-1}$  [Mueller, 1969], we have

$$[C\theta][C\theta]^T = {}_3I_3 \quad (C.4)$$

and (C.3) becomes therefore

$$d\rho_{ij} = \frac{-1}{\rho_{ij}} [\bar{S}_i^T [C\theta]^T - \bar{U}_j^T] d\bar{U}_j \quad (C.5)$$

Considering now that by (93),

$$\bar{S}_i^T = \bar{R}_i^T [NP]^T \quad (C.6)$$

we finally obtain



$$d\rho_{ij} = -\frac{1}{\rho_{ij}} [(\text{CO NP}) \bar{R}_i - \bar{U}_j]^T d\bar{U}_j \quad (\text{C.7})$$

Note that the first vector in the brackets is the satellite position vector in the CTS frame. The differential relationship for the SRD observable  $d\delta\rho_i$  from stations  $j,k$  is obtained by substitution of (C.7) in (108).

### C.2 Satellite State-Vector

The set of equations (99), (100), (102), (103) and (104) yields the following range differential relationship:

$$d\rho_{ij} = \frac{1}{\rho_{ij}} \bar{T}_{ij}^T [\text{NP}] [Y] d \begin{bmatrix} \bar{R}_0 \\ \dot{\bar{R}}_0 \end{bmatrix} \quad (\text{C.8})$$

Using some of the derivations given in (C.1) and (C.8), we can write:

$$\begin{aligned} d\rho_{ij} &= \frac{1}{\rho_{ij}} [\bar{S}_i^T - \bar{U}_i^T [\text{CO}]] [\text{NP}] [Y] d \begin{bmatrix} \bar{R}_0 \\ \dot{\bar{R}}_0 \end{bmatrix} \\ &= \frac{1}{\rho_{ij}} [[\text{NP}] \bar{R}_i - [\text{CO}]^T \bar{U}_j]^T [\text{NPY}] d \begin{bmatrix} \bar{R}_0 \\ \dot{\bar{R}}_0 \end{bmatrix} \end{aligned} \quad (\text{C.9})$$

Using again the property of orthogonal matrices  $[\text{CO}]^T [\text{CO}] = I$ , we can insert this product between the first and second bracket in (C.9) which, upon multiplication, results in

$$d\rho_{ij} = \frac{1}{\rho_{ij}} [(\text{CO NP}) \bar{R}_i - \bar{U}_j]^T [(\text{CO NP}) Y] d \begin{bmatrix} \bar{R}_0 \\ \dot{\bar{R}}_0 \end{bmatrix} \quad (\text{C.10})$$

The second bracket in (C.10) is the transitional matrix in the CTS frame. The corresponding differential  $d\delta\rho_i$  for the SRD observations is obtained again by differencing (C.10) written for each of the observing stations.

### C.3 Polar Motion Parameters

Equations (99), (100), (105), (106) and (107) can be used to write the differential relationship between the observed range and the polar motion parameters  $x$  and  $y$

$$d\rho_{ij} = -\frac{1}{\rho_{ij}} [(C^\theta NP) \bar{R}_i - \bar{U}_j]^T [C^\theta] \begin{bmatrix} -U_{j3} \cos\theta & -U_{j3} \sin\theta \\ -U_{j3} \sin\theta & U_{j3} \cos\theta \\ U_{j1} & -U_{j2} \end{bmatrix} d \begin{bmatrix} x \\ y \end{bmatrix} \quad (C.11)$$

where we have used some of the substitutions derived in (C.1) and (C.2).

Multiplying the second with the third matrix we find

$$[C^\theta] \begin{bmatrix} -U_{j3} \cos\theta & -U_{j3} \sin\theta \\ -U_{j3} \sin\theta & U_{j3} \cos\theta \\ U_{j1} & -U_{j2} \end{bmatrix} =$$

$$\begin{bmatrix} -U_{j3}(\cos^2\theta + \sin^2\theta) + x U_{j1} \\ U_{j3}(\cos\theta \sin\theta - \sin\theta \cos\theta) - y U_{j1} \\ U_{j3}(x \cos^2\theta + y \sin\theta \cos\theta + x \sin^2\theta - y \sin\theta \cos\theta) + U_{j1} \\ -U_{j3}(\cos\theta \sin\theta - \sin\theta \cos\theta) - x U_{j2} \\ U_{j3}(\sin^2\theta + \cos^2\theta) + y U_{j2} \\ U_{j3}(x \cos\theta \sin\theta + y \sin^2\theta - x \sin\theta \cos\theta + y \cos^2\theta) - U_{j2} \end{bmatrix} =$$

$$= \begin{bmatrix} -U_{j3} + x U_{j1} & -x U_{j2} \\ -y U_{j1} & U_{j3} + y U_{j2} \\ U_{j1} + x U_{j3} & -U_{j2} + y U_{j3} \end{bmatrix} \cong \begin{bmatrix} -U_{j3} & 0 \\ 0 & U_{j3} \\ U_{j1} & -U_{j2} \end{bmatrix} \quad (C.12)$$

The last approximation in (C.12) is justified in the case of simulation studies, even in actual solutions indeed, since the  $x, y$  parameters

are of the order of  $10^{-8}$  radians and the stations are confined on the earth's surface. Therefore,

$$|U_{j\ell}| \sim 0 \quad (10^6) \quad (C.13)$$

To obtain the differential  $d\delta\rho_j$  for the SRD observation, we must evaluate (C.11) for the two coobserving stations and subtract the resulting expressions.

#### REFERENCE

Mueller, I.I. (1969), Spherical and Practical Astronomy As Applied to Geodesy, Ungar Publ. Co., New York.

APPENDIX D

RESIDUAL SUMMARIES FOR TEN SLR STATIONS FOR  
THE AUGUST, 1980, LAGEOS DATA

Table 42 Residual Summary for Station 7063

CONSOLIDATED STATISTICS FOR STATION : 7063								
PASS	OBSERV	RESID MEAN	RMS	DEVIATION	LENGTH	MIN RESD	MAX RESD	MEAN CLCS
1	4	-0.9288	5.383	6.123	1292.00	-8.493	5.007	-0.93
2	477	0.1070	0.237	0.212	1641.00	-2.866	0.398	0.11
3	202	0.1237	0.643	0.632	1494.00	-6.840	5.480	0.12
4	6	-2.0976	3.459	3.012	1689.00	-5.903	1.408	-2.10
5	859	0.1242	0.225	0.187	2358.00	-2.436	0.473	0.12
6	1	0.0458	0.046	0.0	0.0	0.046	0.046	0.05
7	1550	0.0139	0.322	0.321	2810.00	-4.383	8.987	0.01
8	4	-4.4022	5.625	4.043	1503.00	-9.652	-1.045	-4.40
9	14	-0.4982	2.473	2.514	2550.00	-4.545	5.946	-0.50
10	1167	-0.1706	0.464	0.432	2484.00	-6.694	7.124	-0.17

Table 43 Residual Summary for Station 7090

CONSOLIDATED STATISTICS FOR STATION : 7090								
PASS	OBSERV	RESID MEAN	RMS	DEVIATION	LENGTH	MIN RESD	MAX RESD	MEAN CLOS
1	97	0.0882	0.130	0.095	2156.00	-0.221	0.344	0.09
2	167	-0.0325	0.104	0.099	2182.00	-0.337	0.177	-0.03
3	182	-0.0892	0.131	0.096	2519.00	-0.513	0.131	-0.09
4	207	0.0322	0.109	0.105	2471.00	-0.282	0.264	0.03
5	196	0.0335	0.140	0.137	2631.00	-0.433	0.448	0.03
6	141	-0.0832	0.142	0.116	1810.00	-0.386	0.192	-0.08
7	263	-0.0764	0.119	0.091	2853.00	-0.427	0.177	-0.08
8	119	0.0891	0.138	0.106	2037.01	-0.153	0.384	0.09
9	67	-0.0531	0.093	0.078	1040.00	-0.235	0.145	-0.05
10	171	-0.0780	0.122	0.094	2787.00	-0.471	0.181	-0.08
11	136	-0.0981	0.138	0.097	2036.00	-0.451	0.101	-0.10
12	203	-0.0640	0.112	0.092	2481.00	-0.526	0.145	-0.06
13	50	0.0123	0.080	0.079	574.00	-0.157	0.216	0.01
14	29	0.0674	0.143	0.128	1287.00	-0.219	0.286	0.07
15	136	-0.0940	0.124	0.081	2339.00	-0.347	0.092	-0.09
16	104	0.1106	0.435	0.422	2645.00	-3.875	0.378	0.11
17	55	0.1305	0.233	0.194	1318.01	-0.282	0.690	0.13
18	162	-0.1606	0.204	0.126	2277.00	-0.472	0.071	-0.16
19	173	0.0735	0.136	0.114	2491.00	-0.272	0.326	0.07
20	136	-0.1598	0.212	0.140	2409.00	-0.567	0.111	-0.16
21	155	0.0943	0.185	0.159	2421.00	-0.323	0.378	0.09
22	41	0.0313	0.069	0.062	1090.00	-0.113	0.143	0.03
23	88	0.1992	0.218	0.088	1438.00	-0.102	0.348	0.20
24	233	-0.0433	0.112	0.104	2842.00	-0.597	0.195	-0.04
25	115	0.1264	0.156	0.092	1947.00	-0.168	0.345	0.13
26	6	0.1595	0.172	0.073	93.00	0.071	0.280	0.16
27	189	0.0197	0.128	0.126	2638.00	-0.289	0.294	0.02
28	154	0.0887	0.123	0.085	2109.00	-0.164	0.328	0.09
29	154	-0.0249	0.223	0.223	2088.00	-0.567	0.398	-0.02
30	214	0.0598	0.128	0.114	2700.00	-0.379	0.292	0.06

Table 44 Residual Summary for Station 7091

CONSOLIDATED STATISTICS FOR STATION : 7091								
PASS	OBSERV	RESID MEAN	RMS	DEVIATION	LENGTH	MIN RESD	MAX RESD	MEAN CLCS
1	137	0.0824	0.271	0.259	1145.00	-0.750	0.683	0.08
2	352	-0.0646	0.182	0.171	1718.00	-1.040	0.346	-0.06
3	240	0.0505	0.169	0.162	1879.00	-0.545	0.450	0.05
4	439	-0.0202	0.314	0.313	1965.01	-1.142	4.742	-0.02

Table 45 Residual Summary for Station 7092

CONSOLIDATED STATISTICS FOR STATION : 7092								
PASS	OBSERV	RESID MEAN	RMS	DEVIATION	LENGTH	MIN RESD	MAX RESD	MEAN CLCS
1	322	0.2185	0.268	0.156	1761.01	-0.258	0.527	0.22
2	286	-0.1712	0.268	0.206	1153.00	-0.845	0.666	-0.17
3	1273	-0.0004	0.239	0.239	2380.00	-1.234	0.986	-0.00
4	363	-0.0324	0.304	0.303	2271.00	-1.293	0.734	-0.03
5	9	0.0926	0.331	0.337	174.00	-0.367	0.726	0.09

Table 46 Residual Summary for Station 7096

CONSOLIDATED STATISTICS FOR STATION : 7096								
PASS	OBSERV	RESID MEAN	RMS	DEVIATION	LENGTH	MIN RESD	MAX RESD	MEAN CLCS
1	969	0.0078	0.189	0.189	2389.00	-0.583	0.546	0.01
2	461	0.0359	0.150	0.146	2008.99	-0.731	0.331	0.04
3	268	-0.1355	0.257	0.219	1109.01	-0.931	0.313	-0.14
4	91	-0.3075	0.391	0.244	652.00	-0.953	0.122	-0.31
5	45	0.0547	0.166	0.158	924.00	-0.451	0.356	0.06
6	616	0.0351	0.213	0.210	1368.01	-1.019	0.531	0.04

Table 47 Residual Summary for Station 7114

CONSOLIDATED STATISTICS FOR STATION : 7114								
PASS	OBSERV	RESID MEAN	RMS	DEVIATION	LENGTH	MIN RESD	MAX RESD	MEAN CLCS
1	182	-0.0405	0.176	0.172	1181.99	-0.458	1.003	-0.04
2	17	-0.1346	1.475	1.514	1136.00	-4.979	2.632	-0.13
3	855	0.0155	0.263	0.262	2535.00	-3.965	1.966	0.02
4	9	1.1201	2.490	2.358	1367.00	-1.729	5.392	1.12
5	161	0.0939	0.155	0.124	1009.99	-0.310	0.465	0.09
6	390	-0.0036	0.129	0.129	2102.99	-0.387	0.968	-0.00
7	6	-0.7358	3.655	3.922	887.00	-4.838	6.072	-0.74
8	228	-0.0292	0.350	0.349	1045.00	-0.384	4.296	-0.03
9	7	0.0771	0.111	0.086	676.00	0.001	0.236	0.08
10	7	0.4243	0.703	0.606	1080.00	0.099	1.779	0.42
11	4	-4.5052	5.795	4.208	400.00	-8.096	3.651	-4.51

Table 48 Residual Summary for Station 7115

CONSOLIDATED STATISTICS FOR STATION : 7115								
PASS	OBSERV	RESID MEAN	RMS	DEVIATION	LENGTH	MIN RESD	MAX RESD	MEAN CLOS
1	264	0.0850	0.131	0.099	1224.01	-0.178	0.379	0.08
2	29	0.2660	0.280	0.088	711.00	0.077	0.410	0.27
3	384	-0.0730	1.057	1.056	2001.00	-6.960	0.595	-0.07
4	27	-6.7929	6.793	0.090	1021.00	-6.969	-6.617	-6.79
5	500	0.0934	0.151	0.119	2271.00	-0.422	1.167	0.09
6	38	0.3169	0.328	0.088	1313.00	0.120	0.488	0.32
7	172	0.3589	0.511	0.364	1346.00	-0.525	4.824	0.36
8	63	-0.0468	0.145	0.138	889.00	-0.346	0.257	-0.05
9	119	-0.2538	0.312	0.181	1913.00	-0.739	0.504	-0.25
10	588	0.1708	0.213	0.128	2727.00	-0.255	1.811	0.17
11	37	0.1305	0.165	0.102	1608.00	-0.075	0.363	0.13
12	44	0.2436	0.286	0.151	652.00	-0.040	0.949	0.24

Table 49 Residual Summary for Station 7120

CONSOLIDATED STATISTICS FOR STATION : 7120								
PASS	OBSERV	RESID MEAN	RMS	DEVIATION	LENGTH	MIN RESD	MAX RESD	MEAN CLOS
1	225	-0.1213	0.142	0.073	1964.00	-0.380	0.120	-0.12
2	44	-0.0037	0.157	0.159	829.00	-0.772	0.180	-0.00
3	160	0.0996	0.140	0.098	1297.00	-0.225	0.313	0.10
4	42	-0.0689	0.108	0.084	618.00	-0.218	0.098	-0.07
5	187	0.0268	0.133	0.131	2614.00	-0.337	0.857	0.03
6	346	-0.0766	0.114	0.085	2759.00	-0.348	0.247	-0.09
7	401	0.0931	0.138	0.102	2573.00	-0.259	0.298	0.09
8	50	-0.2583	0.294	0.141	865.00	-0.511	0.034	-0.26
9	121	-0.1879	0.216	0.107	1655.00	-0.380	0.104	-0.19
10	328	0.1102	0.163	0.120	2417.00	-0.221	0.409	0.11

Table 50 Residual Summary for Station 7907

CONSOLIDATED STATISTICS FOR STATION : 7907								
PASS	OBSERV	RESID MEAN	RMS	DEVIATION	LENGTH	MIN RESD	MAX RESD	MEAN CLOS
1	12	0.1231	0.366	0.360	292.40	-0.408	0.939	0.12
2	41	-0.0135	0.604	0.611	1132.95	-1.520	0.761	-0.01
3	51	0.0917	0.509	0.505	862.51	-1.291	0.803	0.09
4	19	-0.0486	0.335	0.341	1027.76	-0.767	0.561	-0.05
5	5	-0.0084	0.596	0.666	360.15	-1.164	0.446	-0.01
6	52	0.1667	0.521	0.498	892.90	-0.951	2.032	0.17
7	24	0.0601	0.401	0.405	660.27	-0.925	0.724	0.06
8	19	-0.2028	0.393	0.346	607.64	-0.868	0.360	-0.20
9	35	0.0493	0.288	0.287	1162.58	-0.648	0.640	0.05
10	53	-0.0616	0.408	0.408	914.95	-1.008	0.881	-0.06
11	34	-0.0226	0.396	0.403	967.53	-1.199	0.697	-0.02
12	5	0.2501	0.257	0.065	360.10	0.169	0.303	0.25
13	24	-0.5918	1.005	0.830	1110.02	-2.043	0.962	-0.59
14	17	0.0004	0.813	0.838	689.98	-1.536	1.569	0.00
15	8	0.2717	0.528	0.484	420.00	-0.434	1.126	0.27
16	9	-0.1124	0.568	0.590	465.05	-1.312	0.452	-0.11
17	22	-0.1859	0.744	0.737	847.96	-1.970	1.863	-0.19
18	28	0.2387	0.405	0.333	1012.50	-0.646	0.796	0.24
19	2	-0.3987	0.425	0.207	90.00	-0.545	-0.252	-0.40
20	29	0.0272	0.411	0.417	779.97	-0.855	0.698	0.03

Table 51 Residual Summary for Station 7943

CONSOLIDATED STATISTICS FOR STATION : 7943								
PASS	OBSEKV	RESID MEAN	RMS	DEVIATION	LENGTH	MIN RESD	MAX RESD	MEAN CLOS
1	56	0.0012	0.433	0.437	1154.92	-1.039	0.959	0.00
2	122	0.0426	0.338	0.336	2325.29	-1.432	0.815	0.04
3	82	-0.0668	0.439	0.437	1905.10	-1.252	1.074	-0.07
4	98	-0.0301	0.408	0.409	2272.34	-0.970	0.715	-0.03
5	83	0.0633	0.426	0.424	1484.75	-1.229	1.222	0.06
6	85	0.0516	0.337	0.335	1567.79	-0.917	0.872	0.05
7	90	0.1375	0.292	0.259	1424.99	-0.489	0.991	0.14
8	212	-0.0796	0.318	0.309	2744.95	-0.864	0.679	-0.08
9	159	0.0983	0.344	0.330	2910.00	-0.720	0.861	0.10
10	47	-0.0243	0.511	0.516	1934.86	-1.052	1.198	-0.02
11	54	0.0337	0.429	0.432	1514.65	-1.193	1.353	0.03
12	75	-0.1024	0.552	0.546	1605.00	-1.306	0.974	-0.10
13	139	0.0414	0.239	0.236	1822.48	-0.681	0.594	0.04
14	100	-0.0034	0.375	0.377	1897.49	-0.853	1.041	-0.00
15	170	-0.0420	0.414	0.413	2955.00	-1.097	1.295	-0.04
16	106	-0.0837	0.347	0.338	1890.00	-1.137	0.715	-0.08
17	90	-0.0132	0.280	0.281	1919.92	-0.878	0.702	-0.01
18	44	-0.0889	0.470	0.467	2167.47	-1.129	0.643	-0.09
19	79	0.1667	0.424	0.392	2287.55	-0.943	0.899	0.17
20	178	0.0212	0.282	0.282	2489.80	-0.607	1.253	0.02
21	38	-0.1376	0.625	0.617	1492.55	-1.638	1.460	-0.14
22	88	-0.0665	0.485	0.483	2092.54	-1.147	1.249	-0.07
23	172	-0.0355	0.263	0.261	2827.32	-0.671	0.611	-0.04
24	73	-0.3053	0.399	0.259	629.94	-0.896	0.119	-0.31
25	67	0.0351	0.448	0.450	1619.87	-1.124	0.798	0.04
26	96	-0.0945	0.596	0.592	1619.69	-1.605	1.349	-0.09
27	163	-0.1419	0.279	0.241	1919.90	-0.771	0.511	-0.14
28	191	0.1105	0.330	0.312	1994.97	-0.727	0.898	0.11
29	262	0.1799	0.365	0.318	2999.78	-0.819	0.837	0.18
30	97	0.1417	0.282	0.245	1942.65	-0.673	0.703	0.14
31	61	0.1398	0.466	0.448	2175.10	-0.953	0.875	0.14
32	41	-0.0845	0.485	0.483	1507.44	-1.351	0.607	-0.09